This is to certify that the
dissertation entitled

MONITORING AND CONTROL OF CRYSTALLIZATION PROCESSES USING ON-LINE SPECTROSCOPIC METHODS

presented by

Lili Feng

has been accepted towards fulfillment
of the requirements for the

| Ph.D. | degree in | Chemistry and Chemical Engineering & Materials Science |
|---|---|---|

Major Professor's Signature

15 July 2004

Date

# MONITORING AND CONTROL OF CRYSTALLIZATION PROCESSES USING ON-LINE SPECTROSCOPIC METHODS

By

Lili Feng

A DISSERTATION

Submitted to
Michigan State University
in partial fulfillment of the requirements
for the degree of

DOCTOR OF PHILOSOPHY

Department of Chemistry
and
Department of Chemical Engineering & Materials Science

2004

# ABSTRACT

# MONITORING AND CONTROL OF CRYSTALLIZATION PROCESSES USING ON-LINE SPECTROSCOPIC METHODS

BY

Lili Feng

Proper control is needed for crystallization processes in order to produce crystalline products with desired properties such as particle size distribution, shape or solid-state modification. Coupled with on line sampling techniques, spectroscopic methods offer great advantages in crystallization process monitoring and control. This work focuses on simplifying crystallization process monitoring and control, and gaining fundamental insights to the crystallization kinetics using Raman, ATR-FTIR and fluorescence spectroscopic techniques.

Raman spectroscopy was used for *in situ* characterization of the polymorph form of acetaminophen and for monitoring of the transformation process in a crystallization slurry. Thermal history was identified as the controlling parameter for crystallization of the metastable polymorph forms. Polymorph transformation kinetics were also obtained conveniently by on line measurements using Raman spectroscopy combined with multivariate curve resolution and using ATR-FTIR. Under the conditions studied, acetaminophen polymorph transformation is limited by the crystallization rate of the more stable phase, specifically by the crystal growth rate of form II for the form T to II transformation, and by nucleation rate of form I for the form II to I transformation.

The temperature profile applied during batch cooling crystallization affects the supersaturation level, which in turn affects the crystal size distribution. ATR-FTIR interfaced to a LABMAX® automatic reactor system was used in a feedback mode to control the cooling rate to maintain low supersaturation during crystallization. The resulting temperature profile corresponds to the optimal operating conditions for the maximum in the mean crystal size. This approach is a simple and easy alternative to traditional control based on kinetic models.

Fluorescence and Raman spectroscopic techniques were applied to probe the thermodynamic and kinetic properties of highly concentrated sucrose solutions with fructose and glucose as impurities. Such properties include water activity, viscosity and molecular conformation in local environment of crystallization. The results suggest that fructose and glucose inhibit crystallization of sucrose by different mechanisms. Viscosity is not the controlling factor in sucrose crystallization inhibition by glucose and fructose in highly concentrated sucrose solutions. It was also demonstrated that fluorescence and Raman spectroscopic techniques can be adapted to monitor and control industrial sucrose crystallizations at high concentration and high temperature.

# ACKNOWLEDGMENTS

I am very grateful to my advisor, Dr. Kris A. Berglund for his patient and most valuable guidance, which helped me to fulfill all the requirements for a dual degree in chemistry and chemical engineering. I also benefited very much from other unique opportunities he has presented to me.

I wish to express my appreciation to my committee members, Dr. Babak Borhan, Dr. Gary Blanchard and Dr. Ramani Narayan. Thank you for all your time and support.

I could not have gone this far without the help and support I got along the way. Every single member of Berglund group I worked with has helped me one way or another. Some of the cheering conversations I will never forget. My internship supervisors Dr. David am Ende at Pfizer and Dr. Ruairi Omedhra at Eastman Chemical Company guided my first steps into the industrial world with valuable advice and generous encouragement. Special thanks to all my friends, especially Wei, Hua, Barry and Bonnie, for the joy and comfort you brought me and for the confidence you gave me. Thank you for brightening the gloomy days.

I cannot say thank you enough to my family. My parents and sisters have always been the source for strength and comfort that pull me through every difficulty. My husband, Dehua, I thank you for standing by me and sharing both the exciting and depressing moments along this journey.

# TABLE OF CONTENTS

## LIST OF TABLES

## LIST OF FIGURES

# Chapter 1

# INTRODUCTION

Crystallization is not only a widely observed phenomenon but also an important separation and purification unit operation in the food, pharmaceutical, agrochemical and specialty chemical industries. Control of the crystallization process is often needed to produce a crystalline product with desired properties such as particle size distribution, shape or solid-state modification. These goals can only be achieved successfully by adequate knowledge of the thermodynamic and kinetic properties of the crystallization system combined with efficient process monitoring and control. Coupled with fiber optics and employing chemometrics software, on line spectroscopic methods offer great advantages in crystallization process control, from non–invasive sampling and fast turnaround to the possibility of process control based on chemical information.

The goal of this work is to demonstrate the application of a variety of spectroscopic methods for the monitoring and control of crystallization processes. The emphases are on the simplification of method development procedures and the fundamental insights to the crystallization kinetics that can be gained by these spectroscopic studies.

## 1.1 Crystallization

Crystallization is a phase separation process where molecules aggregate together to form a crystalline phase. The process is governed by both thermodynamic and kinetic

properties of the crystallization system. Control of operational parameters must be based on proper information of the system, such as the solubility, supersaturation level and desupersaturation rate and pathway[1-4].

### *1.1.1 Supersaturation*

A supersaturated solution has a greater chemical potential than the corresponding saturated solution at equilibrium at the same temperature. This difference in chemical potential is the driving force for crystallization. Supersaturation level and desupersaturation rate affect the kinetics of nucleation and crystal growth, thus control the crystallization outcomes. Theoretically, supersaturation is defined as[1,2]

$$S = \Delta\mu / RT = \ln \frac{a}{a^*} \qquad (1.1)$$

Where $\Delta\mu$ is the chemical potential difference between the supersaturated solution and the saturated solution at a given temperature, $a$ is activity of the supersaturated solution and $a^*$ is the activity of the saturated solution. For practical applications, activity can often be approximated by concentration, thus equation 1.1 becomes

$$S = \ln \frac{c}{c^*} \qquad (1.2)$$

where $C$ is the concentration of the crystallization species in the supersaturated solution and $C^*$ is the solubility. As IR absorbance is proportional to concentration, it is possible to use IR spectroscopy with special sampling configurations to obtain the supersaturation information during crystallization[5].

Superaturation can be generated by a number of methods such as cooling, evaporating the solvent, adding anti-solvent or chemical reaction. The purpose is to reduce the solubility of the system, thus creating the supersaturation.

### *1.1.2 Nucleation*

Crystallization does not necessarily happen in a supersaturated solution. For crystallization to occur, molecules have to aggregate together and form stable nuclei. Such step is called nucleation, which is the beginning point of phase separation. Controlling nucleation step is of practical importance in many crystallization processes, as it can affect product qualities in terms particle size distribution or solid phase modification.

Generally, nucleation is categorized as homogeneous or heterogeneous nucleation. Homogeneous nucleation occurs without the presence of any particles in solution, while foreign particles (in the case of primary nucleation) or crystals of the crystallizing solute (in the case of secondary nucleation) can induce heterogeneous nucleation. Even though nucleation is rarely truly homogeneous, it still has theoretical significance in understanding the thermodynamic correlation with nucleation kinetics. On the other hand, heterogeneous nucleation is of fundamental and practical importance in many crystallization systems. Seeding is a case of heterogeneous nucleation and is a common practice in industry. By introducing particles of the crystallizing solute, nucleation can be promoted to happen at a much lower supersaturation level than the corresponding homogeneous nucleation, thus the nucleation kinetics is significantly altered. In other cases, the presence of one solid-state modification of a substance may facilitate the

nucleation of another more stable modification, thus promote polymorph transformation. An empirical power law model best describes nucleation rate[2].

$$B = k_N' W^i M_T^j (\Delta C^n) \tag{1.3}$$

Where $B$ is the nucleation rate, $K'_N$ is the nucleation rate constant, $W$ is the agitation rate, $M_T$ is the suspension density, and $\Delta C$ is supersaturation level. It is clearly shown that nucleation kinetics are affected by many process parameters. In order to obtain desired crystalline product properties, it is necessary to monitor and control relevant operational conditions to control nucleation kinetics. The study on acetaminophen polymorph crystallization in this work is a good example of controlling crystal solid-state modification by controlling the nucleation conditions.

### *1.1.3 Crystal Growth*

Once stable nuclei are formed by nucleation, molecules will continue to integrate into the nuclei and form bigger particles. This is the crystal growth step. The crystal growth rate depends on the nature and strength of the interaction between the crystal surface and solute molecules in the solution. A number of models have been proposed to describe crystal growth kinetics[1,2]. For example, continuous or normal growth models apply to growth on the kink sites of the crystal edges, while screw dislocation and two-dimensional nucleation models apply to growth at a very smooth crystal surface. Operational parameters such as temperature, supersaturation level, solvent and impurity etc al all affect nucleation rate by affecting the interactions at the solid-liquid interface.

## 1.2 Significance of Control in Crystallization

As both nucleation and crystal growth are kinetic processes that regulate the solid-state product properties such as particle size distribution and solid phase modification, process monitoring and control by robust analytical methods is often critical for desired product quality.

### *1.2.1 Polymorphism*

Polymorphism is a phenomenon wherein a substance with the same chemical identity can crystallize into different crystal structures. It is an important issue because different polymorphs have different physical properties such as thermodynamic stability, solubility, density, melting point, reactivity and other mechanical properties[6-10]. Carbon is a good example of polymorphism. Both graphite and diamond are made of carbon, but carbon atoms are arranged differently in the solid state. Carbon atoms are in sheets of six member rings in graphite, while they are in tetrahedral cubes in diamond (Figure 1.1). As a result, they exhibit very different appearances, hardnesses and are used for different purposes.

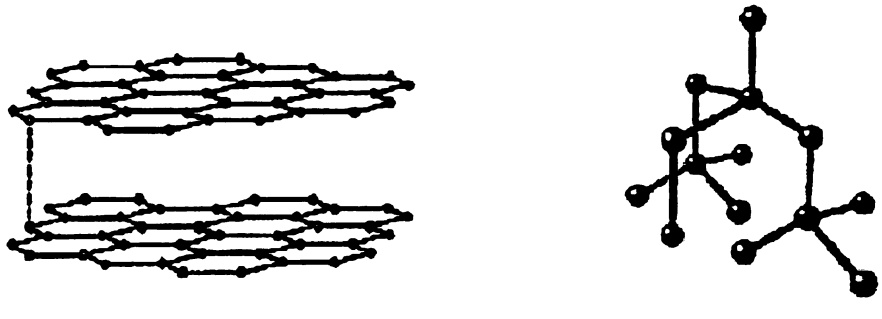

*Figure 1.1 Polymorph of carbon: graphite (left) and Diamond (right)*

Because different polymorphs have different stabilities, transformation from one polymorph to another may occur depending on the manufacturing or storage conditions. This transformation could be beneficial or deleterious depending on the application of the polymorphic material. Polymorphic materials can often be encountered in many industries including food, pharmaceutical and chemical, and many examples have shown that crystallization procedure determines the polymorph form. Efficient control of desired polymorph forms by controlling the crystallization process is of great importance. Any successful control would rely on accurate characterization of polymorph forms. The traditional characterization methods are off line[11-13], including powder X-ray diffraction (XRD), differential scanning calorimetry (DSC) or solid state NMR, and thus have problems with sample transfer and preparation. On line vibrational spectroscopic techniques can detect the different vibration states due to different molecular arrangement in polymorph material, thus offering the possibility of characterizing and control polymorph form during crystallization process.

### *1.2.2 Particle Size Distribution*

Another important property of a crystalline product is particle size. For example, small particles are often desirable for active pharmaceutical ingredients, because they have a faster dissolution rate and can be distributed into tablets more evenly. But as intermediates during manufacturing process, bigger particles may be preferred to facilitate down stream process efficiency such as during filtration and drying.

As both nucleation and crystal growth will consume solute molecules in the solution phase, their relative rates affect the resulting particle size distribution: higher nucleation

over crystal growth rate results in a large amount of small particles, while higher crystal growth over nucleation rate results in fewer, larger. Both nucleation and crystal growth kinetics are very complicated in practice and very hard if not impossible to be accurately modeled for real industrial batch crystallization processes[1,2]. Operational conditions such as cooling rates or impurity level may vary from batch to batch. Even within the same batch, factors controlling nucleation and crystal growth kinetics are constantly changing non-linearly. The diagram in figure 1.2 represents the complex crystallization events and their interactions. In general, higher supersaturation favors nucleation more than it does crystal growth, thus particle size distribution can be adjusted by controlling the supersaturation level throughout the crystallization process.

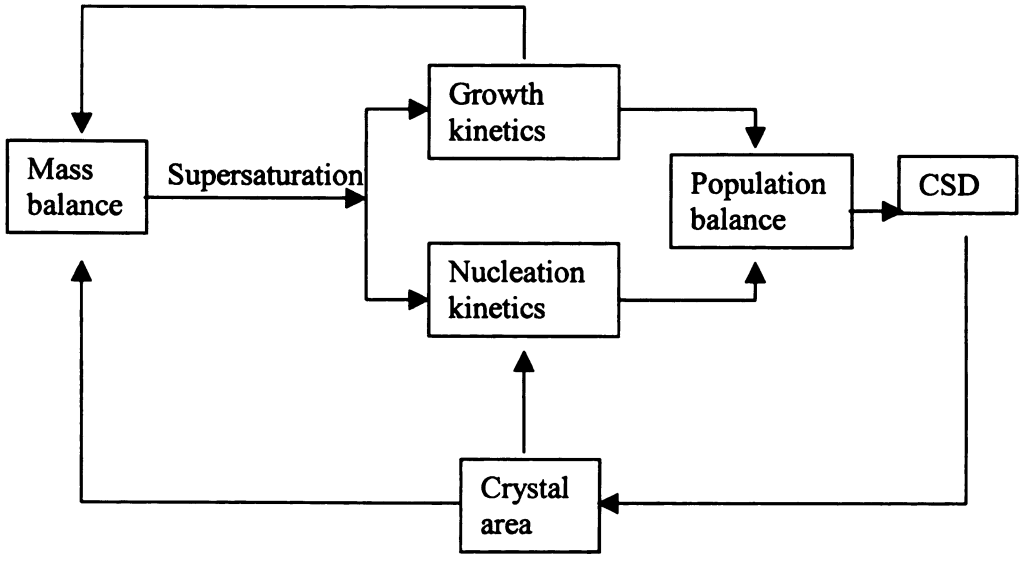


*Figure 1.2 Interrelationships of mass balance, nucleation kinetics, crystal growth kinetics, and crystal size distribution (CSD) during batch crystallization*

### *1.2.3 Inhibition of Crystallization by Impurity*

Impurities are widely known to influence crystallization from solutions for virtually all compounds. Impurities can affect both nucleation and crystal growth either thermodynamically or kinetically[1,2]. Under thermodynamic control, impurities are believed to affect the solubility of the target compound (e.g., the common ion effect). When solubility of the crystallization species is increased by addition of impurity, supersaturation level is reduced, and crystallization will be hindered or completely inhibited. Under kinetic control, impurities can inhibit crystallization through different mechanisms. They can increase solution viscosity significantly and slow crystallization by slowing mass transfer. They can also disrupt the formation of solution aggregates that are the basis for nucleation by assuming molecular conformations different than the one in crystalline form. Impurity molecules can also be absorbed to the target molecule as "tailor made" impurities and disrupt the crystal growth process. It is also possible that more than one of the aforementioned mechanisms can be operative simultaneously[1,2].

## 1.3 Spectroscopic Methods for Crystallization Monitoring and Control

The need for process monitor and control by robust analytical methods in pharmaceutical industry has recently been emphasized by the Process Analytical Technology (PAT) initiative by FDA[14], which proposes the use of non-invasive, on-line techniques to measure physicochemical properties of drug materials during processing.

Process measurement tools based on spectroscopic techniques such as IR, Raman fluorescence and NIR offer obvious advantages[15-17]. With advances in instrumentation, modern spectroscopic techniques are compact, versatile and fast. New sampling

technology allows *in situ*, on line detection. Not only chemical information can be inferred from the spectroscopic measurement, physical information may also be obtained, which is particularly valuable in characterization of manufacturing processes and for reliable prediction of end product properties early in the manufacturing processes. The development, acceptance and ready access to chemometric data processing techniques also justifies the application of on line spectroscopic techniques.

Although the scientific base for PAT is not new, the application of PAT techniques to crystallization process monitor and control has only received great interest in recent years. There are still concerns regarding to method simplicity, robustness and relevant information that can be extracted from spectroscopic measurement. This work aims to provide some practical examples where process spectroscopic techniques can contribute to the crystallization process development and control.

### *1.3.1 Raman Spectroscopy for On Line Polymorph Characterization*

As a vibrational spectroscopic technique, Raman spectroscopy is useful for determining the chemical composition and certain physical properties of samples in both qualitative and quantitative ways. Because Raman scattering and IR absorbance are different physical processes (Figure 1.3), they have different selection rules for vibrational modes in a molecule, thus Raman can often provide complimentary information to what IR provides[18]. Although IR is widely used in process applications such as monitoring reaction kinetics or quality control of reaction materials, Raman has only recently been introduced to industrial process applications thanks to the improvement in optical filtering design, detector sensitivity, readily available laser source, and most of all, the

fiber optic sampling probes. The use of fiber optic probes is very desirable for crystallization process monitoring and control, since analysis of the solid phase property can be measured on line and *in situ* without the need of filtration. Since Raman spectroscopy contains rich molecular structure information in the fingerprint region, it can be used for the characterization and quantitative analysis of polymorph materials on line[19,20].

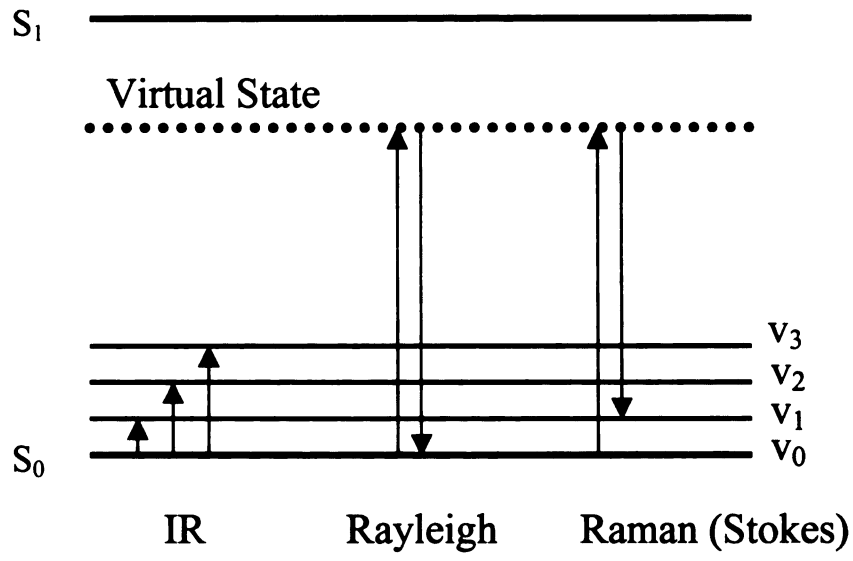


*Figure 1.3 Energy level diagram of IR absorbance, Raman scattering (Stokes) and Rayleigh scattering. Anti-Stokes lines are not shown as their intensities are usually much less than that of the Stokes lines. $S_0$ and $S_1$ are the ground electronic state and the first excited electronic state respectively. $V_0$ to $V_3$ represent different vibrational and rotational levels of a molecule.*

### *1.3.2 ATR-FTIR Spectroscopy for On Line Concentration Measurement*

Infrared spectroscopy can measure compositions in solids, liquids, gases and many hetero-phase systems because almost all chemical substances show characteristic patterns of absorption of infrared light. IR has long been used in process monitoring and is continually finding applications in expanding fields. Attenuated total reflection (ATR) is a very useful sampling technique, which brings the measurement to the sample instead of transferring the sample to the instrument[21]. Figure 1.4 shows the schematic of an ATR device.

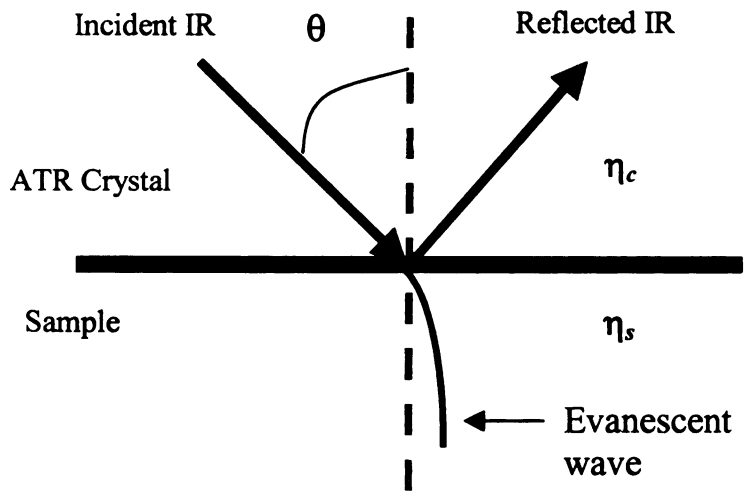


*Figure 1.4 Schematic of attenuated total reflection. ATR crystal has a much higher refractive index than that of the sample, thus allow total internal reflection. θ is the incident angle.*

The infrared radiation is transferred through the ATR crystal - a transmitting medium with high refractive index. By controlling the incident angle θ above the critical angle, total reflection occurs within the ATR crystal. When the ATR is in direct contact with a sample, the electric field of the infrared radiation (the evanescent wave) penetrates a short distance into the sample beyond the ATR surface. This electric field interacts with the absorbing sample and the reflected radiation is attenuated at wavenumbers that are characteristic to the sample. The effective 'pathlength' depends on the penetration depth *d*

$$d = \frac{\lambda}{(2\pi\eta_1(\sin^2\theta - (\eta_2/\eta_1)^2)^{1/2}} \qquad (1.4)$$

Where λ is the wavelength of the infrared radiation, η1 and η2 are the refractive indices of the ATR crystal and sample, respectively, θ is the incidence angle. This pathlength is intrinsically small, and multiple sample-contact reflections are commonly used to increase the observed absorbance due to stronger attenuation.

The small pathlength has proven to be advantageous to monitoring crystallization. Because the particles in crystallization slurry cannot get into the micron level pathlength, it is possible to sample the solution phase concentration *in situ* without the interference from the solid crystals[5].

### *1.3.3 Probing the Microscopic Properties of Crystallization Solution by Fluorescence*

Fluorescence is an emission process in which molecules are excited by absorbing UV or visible light and then relax to the ground state, releasing the excess energy as photons (Figure 1.5). Intensity change or peak shift in fluorescence spectroscopy can be correlated to environment change such as pH, temperature and solvent effects. Polarization anisotropy measurement can also be used to probe the mobility of the fluorescence species and microscopic viscosity in solution.

The fluorescence spectrometer used in this study was not configured for on line measurement. Nonetheless, it is the purpose of this study to show the type of insight that can be possibly gained in crystallization inhibition. The approach can be modified easily to on line application with commercially available fiber optic probes.

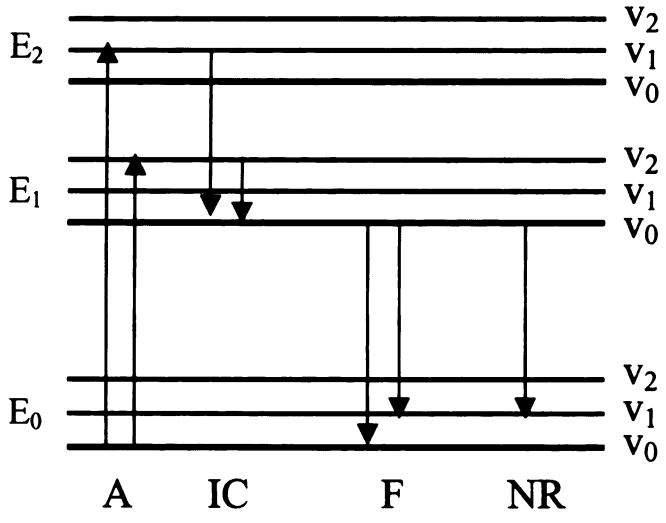


*Figure 1.5 Energy level diagram of fluorescence. $E_0$ to $E_2$ are the different electronic states. Three vibrational states are also shown at each electronic state. A:Absorption; IC:Internal conversion; F:Fluorescence; NR:Non-radiative route.*

### *1.3.4 Chemometrics Data Analysis*

One of the key advantages of process spectroscopy is its rich information about the fundamental chemistry of the process. But this could lead to information overload without proper data analysis, because spectra data tend to have high degree of redundancy. Besides, due to a lack of selectivity in the spectrum, it is often hard to find a single parameter to best predict concentration or composition. Chemometric techniques such as PCA (principal component analysis) or PLS (partial least square) are well suited for improving the effectiveness of on line spectroscopic methods[17,22]. They can be used for extracting information to develop multivariate calibration, process control, data visualization and clustering patterns. The monitoring of polymorph transformations in this study demonstrated the substantial capability of chemometrics-enhanced Raman spectroscopic method in the industrial crystallization environment.

## 1.4 Overview of This Work

The next four chapters will cover the application examples of spectroscopic techniques to the characterization, monitoring and control of crystallization process. Chapter 2 and 3 mainly focus on the application of Raman spectroscopy for polymorph crystallization and transformation monitoring and control, using acetaminophen as the model compound. Chapter 4 demonstrates the use of ATR-FTIR for particle size control during crystallization with an emphasis on developing a simple, non-model based control strategy. Chapter 5 deals with the critical insights into sucrose crystallization inhibition by non-sucrose sugars using fluorescence and Raman techniques.

## 1.5 References


(1) Mullin, J. W. *Crystallization*; Butterworth-Heinemann Ltd.: Oxford, **1993.**

(2) Myerson, A. S., *Handbook of Industrial Crystallization*, 2nd Ed. Myerson, A. S, Butterworth-Heinemann, Boston, **2002.**

(3) Tavare, N. S., *Industrial Crystallization*, Plenum Press, New York and London, **1995.**

(4) Sohnel, O.; Garside, J. *Precipitation: Basic Principles and Industrial Applications*; Butterworth-Heinemann Ltd: Oxford, **1992.**

(5) Dunuwila, D.D.; Berglund, K.A, *J. Cryst. Growth*, **1997**, 179, 185.

(6) McCrone, W. C., *Polymorphism In Physics and Chemistry of the Organic Solid State*, Fox, D.; Labes, M.M.; Weissberger, A., Eds., Interscience, New York, **1965**, Vol II, 726-767.

(7) Byrn, S.R.; Pfeiffer, R.R.; Stowell, J.G., *Solid-State Chemistry of Drugs*, 2nd ed., SCCI, Inc., West Lafayette, **1999**.

(8) Byrn, Stephen; Pfeiffer, Ralph; Ganey, Michael; Hoiberg, Charles; Poochikian, Guirag, *Pharmaceutical Research*, **1995**, 12(7), 945-54.

(9) Dunitz, Jack D.; Bernstein, Joel, *Accounts of Chemical Research*, 1995, 28(4), 193-200.

(10) Gavezzotti, A.; Filippini, G., *Journal of the American Chemical Society*, **1995**, 117(49), 12299-305.

(11) Giron, D., *Thermochimica Acta*, **1995**, 248, 1-59.

(12) Yu, Lian; Reutzel, Susan M.; Stephenson, Gregory A., *Pharmaceutical Science & Technology Today*, **1998**, 1(3), 118-127.

(13) Threlfall, Terence L., *Analyst*, **1995**, 120(10), 2435-60.

(14) U.S. FDA, *Draft Guidance for Industry, PAT A Framework for Innovative Pharmaceutical Manufacturing and Quality Assurance*, August **2003**.

(15) Taylor, Lynne S., *American Pharmaceutical Review*, 2001, 4(4), 60,62-64,66-67.

(16) Adar, Fran; Geiger, Ruth; Noonan, Jon., *Applied Spectroscopy Reviews*, **1997**, 32(1 & 2), 45-101.

(17) Chalmers, J.M., *Spectroscopy in Process Analysis*, CRC Press, **2000**.

(18) Colthup, N.B.; Daly, L.H.; Wiberly, S.E., *Introduction to Infrared and Raman Spectroscopy.* 3rd ed., Academic Press, Boston, **1990**.

(19) Wang, F., Watcher, J.A.; Antosz, F.J.; Berglund, K. A., *Org. Process R & D.* **2000**, 4 (5), 391-395.

(20) Starbuck, C.; Spartalis, A.; Wai, L.; Wang, J.; Fernandez, P.; Lindemann, C. M.; Zhou, G.X.; Ge, Z., *Crystal Growth & Design*, **2002**, 2 (6), 515-522.

(21) Mirabella, F.M., *Internal Reflection Spectroscopy, Theory and Applications*, Mercel Dekker, Inc.: New York, **1993**.

(22) Miller, C.E., *Journal of Chemometrics*, **2000**, 14, 513-528.

# Chapter 2

## CONTROL OF CRYSTALLIZATION OF ACETAMINOPHEN POLYMORPHS USING RAMAN SPECTROSCOPY

It is well known that process parameters can affect the nucleation kinetics, which in turn can affect the polymorph form during batch crystallization. It is critical to identify the controlling parameters in order to reproducibly crystallize the desired polymorph form. Acetaminophen is chosen as the model compound for current study. Thermal history, which often is neglected in organic species crystallization, is found to play a significant role in the outcome of polymorph forms during crystallization of acetaminophen. Two metastable forms of acetaminophen can crystallize out after the solution is subjected to high temperature for a prolonged time. High temperature may have changed the solution structure prior to crystallization thus changed the nucleation kinetics of different polymorphs. A Raman spectrometer was used on line and *in situ* to characterize the polymorph forms and monitor the transformation process

### 2.1 Introduction

Acetaminophen is a common antipyretic and analgesic pharmaceutical ingredient. It has three polymorphs and a number of pseudopolymorphs[7]. The three polymorphs are monoclinic form I, orthorhombic form II and monoclinic form III. Form I is the thermodynamically stable form at room temperature and is the form crystallized from solution phase without any control. Form III has only been crystallized from melted form

I, and it is highly unstable- it has only been stabilized at room temperature in a binary mixture containing a tablet binder hydroxypropylmethylcellulose[1]. Form II has been reported to undergo plastic deformation upon compression, thus it may facilitate the tabletting process[2]. Acetaminophen has also been found to form solvates and adducts with hydrogen bond acceptors[3-9]. Fachaux et al.[3, 4] prepared a dioxane hemisolvate which shows an improved compaction property after desolvation to monoclinic form. Recent studies[8,9] found a trihydrate form T can lose water upon drying and become self-micronized, which may be used to produce small particles of acetaminophen without milling.

The orthorhombic form II and the trihydrate form T are of particular interest because of their possible processing advantages over the monoclinic form I. Recently there have been some studies on the crystallization of the metastable forms from solution[8-12], which is the more desirable process than melt crystallization. Yet the processes still need to be optimized to better control the crystallization of the desired polymorphs. Form II was crystallized from ethanol using form II seed that was prepared from melt crystallization[11,12]. It was found that the purity of form II from seeded crystallization highly depends on the quality of the seed, and it is not always easy to obtain a seed with 100% form II. The yield from this procedure is relatively low because limited amounts of material can be dissolved in solution prior to crystallization in order to ensure form II. Form T was only crystallized at small scale (~10ml), and it requires the pre-filtration of the solution before crystallization is carried out. The yield for form T was also low, partially due to the low solubility of acetaminophen in $H_2O$ at high temperature, partially

due to the low success rate in controlling the crystallization of form T (only 5 out of 40 attempts gave form T).

The goal of current study is to optimize the solution crystallization processes for acetaminophen form II and form T without the need for seeding or pre-filtration of solution. More importantly, we can identify process parameters that are important to the crystallization of different polymorph forms by studying the solution crystallization of acetaminophen using on line Raman spectroscopy. This would improve the general knowledge of and add one more dimension of control to polymorph crystallization.

## 2.2 Experimental Section

Acetaminophen (98% pure) was obtained from Aldrich and used as received. Solvents used during crystallization were reagent grade ethanol and distilled, deionized water. Crystallization experiments were carried out in a 1L jacketed crystallizer, equipped with a condenser, a thermocouple and an anchor-type glass stirrer (Figure 2.1). Stirring speed was 500rpm. Two circulators were used to provide heating and cooling fluids, respectively. At the end of heating period, the crystallizer was disconnected from the heating circulator and the heating fluid was emptied out. The crystallizer was then connected with the cooling circulator.

A Hololab 5000 Raman spectrometer from Kaiser Optic Systems was used for *in situ* monitoring the crystallization and transformation process, as well as the solid-state characterization of different polymorphs. The spectrometer is equipped with a 785nm laser and coupled with an immersion probe through fiber optic cables.

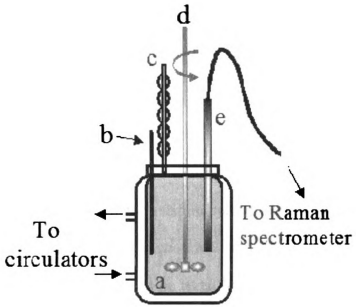


*Figure 2.1. Schematic of experimental setup for solution crystallization of acetaminophen. a) Jacketed crystallizer connected with two circulators; b) Thermal couple; c) Condenser; d) Glass stirrer; e) Raman probe coupled with fiber optic cable.*

### *2.2.1 Solubility Measurement of Different Polymorphs*

The solubility of acetaminophen polymorph I was determined by gravimetric analysis. Mixtures of ethanol and water were used as solvents. The slurry was stirred at equilibrium for 30 minutes before a small sample of the solution was drawn from the slurry using a fritted pipette. The wet sample was accurately weighed before it was dried in the oven to evaporate the solvent, then the dried sample was weighed again and the solubility was calculated.

To evaluate the relative stability, the solubilities of acetaminophen form I, II and trihydrate were also determined in the mixture solvent of ethanol:water ratio of 1:3 (based on weight). A small sample of solution was drawn from the slurry at equilibrium using a fritted pipette. Three samples were taken for each polymorph at –10°C, -5°C, 0°C, 5°C and 10°C. The samples were weighed and dried in oven overnight and then analyzed by HPLC. Due to the fast transformation of trihydrate polymorph to monoclinic polymorph at high temperature, no sample was taken for trihydrate at 10°C.

### *2.2.2 Polymorph Crystallization of Acetaminophen by Cooling*

The crystallization of acetaminophen was carried out in pure water and in mixtures of ethanol and water. The concentration range of acetaminophen solutions studied were: 1-3 g/100g water in water, 7-28g/100g solvent in 25% aqueous ethanol solvent and 20-80g/100g solvent in 50% aqueous ethanol solvent. Crystallization with an initial concentration higher than the upper limit would result in very thick slurries after nucleation, thus prevent an efficient mixing even at high stirring rate.

Solutions with different initial concentrations were subjected to three different preheating procedures prior to rapid cooling using the coolant at 0°C (Figure 2.2): a) Low overheating profile: Solution was heated at 40°C (water as solvent) or 50°C (ethanol and water mixture as solvent) for 30minutes before cooling; b) Solution was vigorously refluxed at boiling point for 30 minutes and then rapidly cooled to 0°C at about 6°C/minute; c) Solution was vigorously refluxed at boiling point for 30 minutes and then cooled to 0°C at about 2°C/minute. The onset of nucleation was detected both visually and by the Raman spectrometer. The polymorphic form of acetaminophen was also identified using Raman spectroscopy in the crystallization slurry.

### *2.2.3 Transformation of Acetaminophen Form T in Slurry*

The slurry of acetaminophen trihydrate in 25% aqueous ethanol solvent was monitored at 0°C using an immersion Raman probe. The resulting spectra were analyzed by Principal Component Analysis (PCA) within HoloReact software from Kaiser Optical Systems to extract the transformation profile.

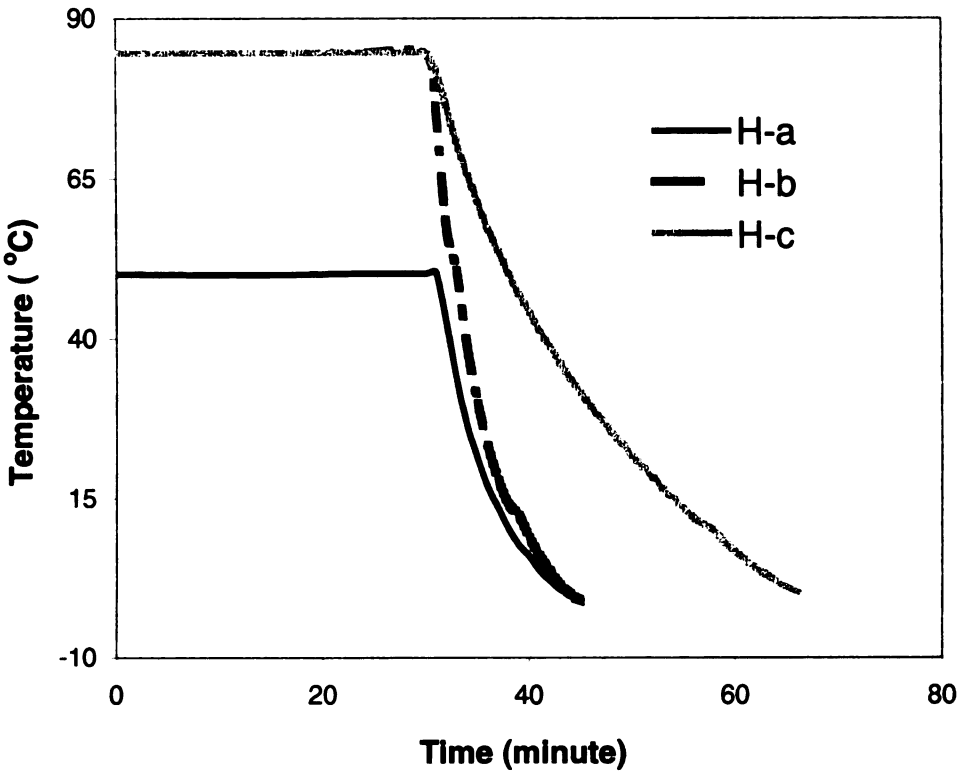


*Figure 2.2. Different heating and cooling profiles applied to the acetaminophen solution prior to crystallization. H-a: Low heating at40 ~50 ℃ followed by rapid cooling to 0 ℃; H-b: High heating at boiling point of solution followed by rapid cooling to 0 ℃; H-c: High heating at boiling point of solution followed by slower cooling to 0 ℃.*

## 2.3 Results and Discussion

### *2.3 1 Characterization of Acetaminophen Polymorphs*

Form I, form II and form T were obtained from solution crystallization. The characterization has been previously reported using offline analytical techniques such as DSC and XRD[8-15]. While DSC can differentiate different forms of acetaminophen from melt crystallization, it often times fails to tell the difference between form I and form II from solution crystallization[11]. Moreover, forms II and T from solution crystallization tend to transform to stable form I rapidly at room temperature, especially when there is solvent residue left on the crystal. Thus, extra care has to be taken to prevent transformation during sampling and subsequent sample preparation such as filtration, drying and sample mounting, which makes it inconvenient to use the offline characterization methods as routine characterization tools.

Raman spectroscopy with an immersion probe can be conveniently used to identify the polymorph form of acetaminophen in the crystallization slurry without any sampling procedure. Raman spectra for solid samples of different acetaminophen polymorphs are shown in Figure 2.3.

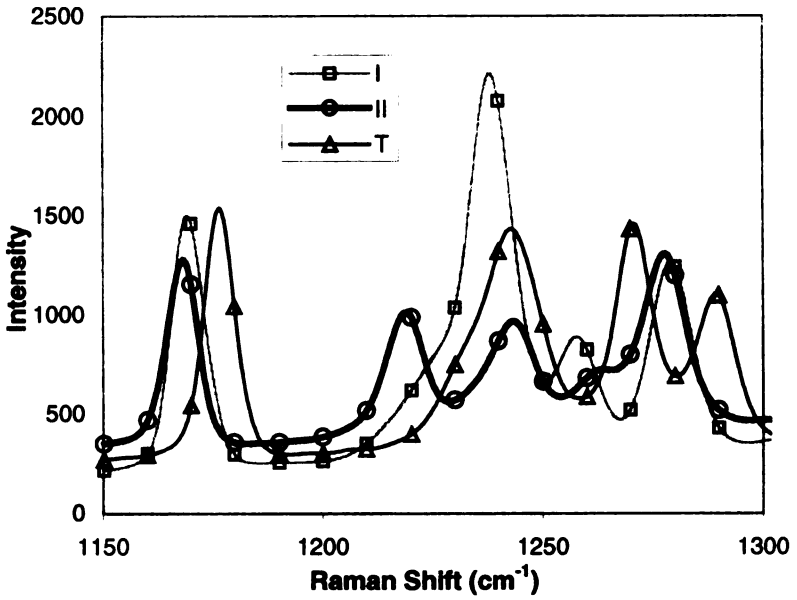


(a)

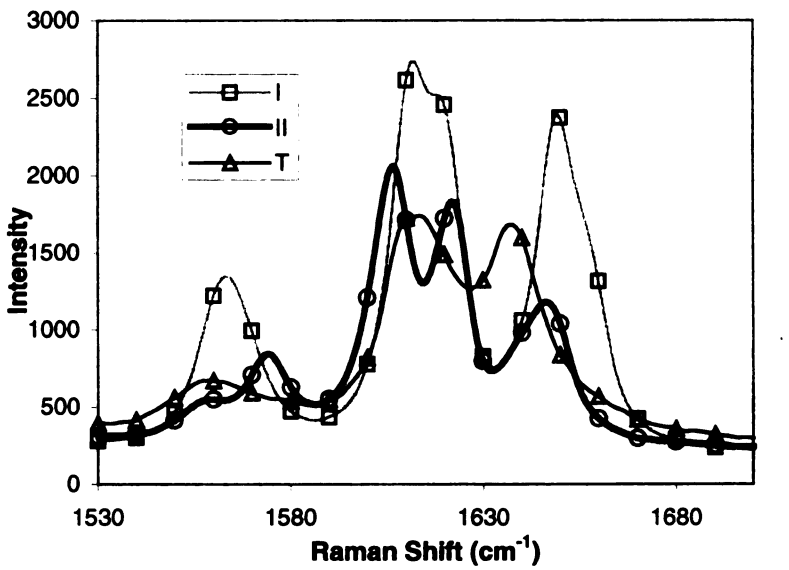


(b)

*Figure 2.3. Raman spectra for solid sample of acetaminophen polymorph within ranges of 1150 ~ 1300cm$^{-1}$ (a) and 1530 ~ 1700cm$^{-1}$ (b)*

Significant differences can be observed within the ranges of 1150 ~1300cm-1 and 1530 ~ 1700cm-1. These differences in Raman characteristics reflect different configurations of acetaminophen molecules in the crystalline state caused by intermolecular hydrogen bonding. The slurry of different acetaminophen polymorphs in ethanol and water showed similar spectroscopic characteristics to those of the corresponding solid sample, thus different polymorph was identified in the crystallization slurry using Raman spectroscopy.

The three polymorphs of acetaminophen also exhibit different morphologies (Figure 2.4). Thus, optical microscopy was used as a complimentary technique to confirm the polymorph form of acetaminophen, although it should not be used as the sole technique for identification purpose. The same polymorph can present different morphologies depending on the solvent system and other crystallization conditions applied, different polymorphs can adopt the same morphology as well. Besides, microscopy does not give quantitative information for a sample of mixed polymorphs.

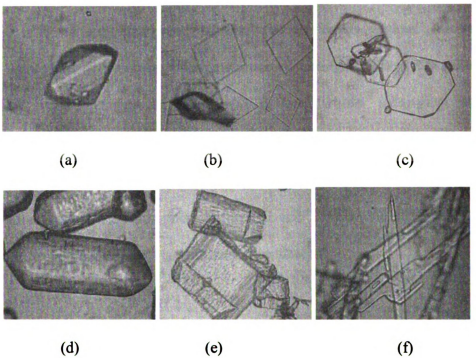


*Figure 2.4. Different morphologies observed during solution crystallization of acetaminophen polymorphs: (a) Form I from ethanol; (b) Form I from ethanol/water; (c) Form I from water; (d) Form II from ethanol/water; (e) Form II from ethanol/water; (f) Form T from ethanol/water.*

### *2.3.2 Solubility of Acetaminophen Polymorphs*

Acetaminophen has only limited solubility in water even at high temperature (Figure 2.5), thus water is not a good recrystallization solvent for acetaminophen. Its solubility increases with ethanol percentage, with a maximum solubility in 75% of ethanol in water. Twenty-five percent ethanol in water was chosen for the subsequent solubility measurements for different polymorphs because acetaminophen has relatively high solubility at high temperature and low solubility at about 0°C. More importantly, all three modifications of acetaminophen, forms I, II and T were able to crystallize out in this solvent by applying different crystallization conditions.

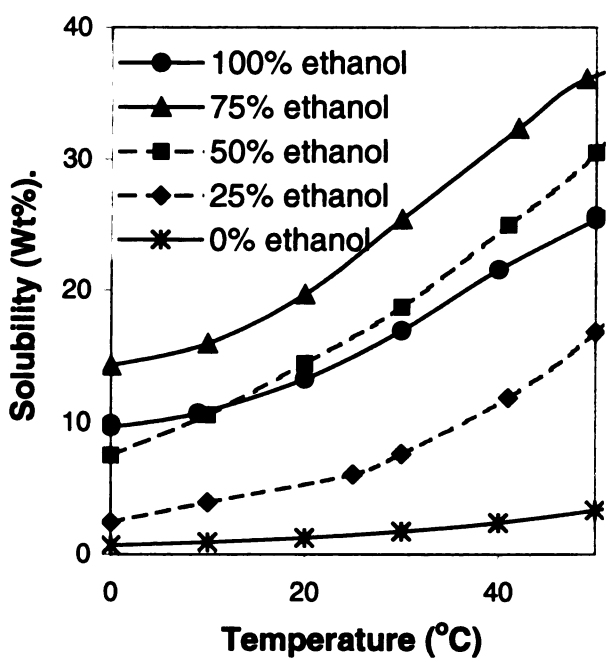


*Figure 2.5. Solubility curve of acetaminophen form I in ethanol/H2O mixture solvent.*

The solubility of acetaminophen polymorphs in 25% aqueous ethanol can be used to evaluate their relative thermodynamic stability. During sampling, modifications II and T were stirred in slurry at low temperature for 10 ~ 30 minutes before transforming to polymorph I. In addition, the solubility and the differences in solubility of I, II and T modification are large enough to allow accurate sampling and subsequent analysis by HPLC.

As discussed by Terry Threlfall[16] and Wolf Beckmann[17], the relative stability of true polymorphs observed through solubility measurement is independent of the solvent system used. True polymorphs are the ones with exactly the same chemical identity, e.g, form I and form II of acetaminophen. Thus, the thermodynamic stability of acetaminophen form I and form II can be derived from their solubility diagram as shown in Figure 2.6. The monoclinic polymorph I is less soluble than the orthorhombic form II, thus it is the more stable modification within the temperature range of –10°C to 10°C. While solvates and adducts are considered pseudopolymorphs, their relative solubility can change depending on the solvent system used, and the stability assessment based on solubility diagram should be carried out in the desired solvent system. In 25% of ethanol in water, the trihydrate modification T is most soluble, thus least stable above 0°C, but its solubility decreases rapidly below 0°C and it is enantiotropic with respect to polymorph II. The transition temperature is estimated to be about -9°C. The stability of polymorph T is greatly increased at low temperature. Slurry samples of polymorph T in ethanol and water can be stored at –10°C for weeks without inducing transformation. These current observations agree with the results of the study of the trihydrate form in water by Peterson et al.

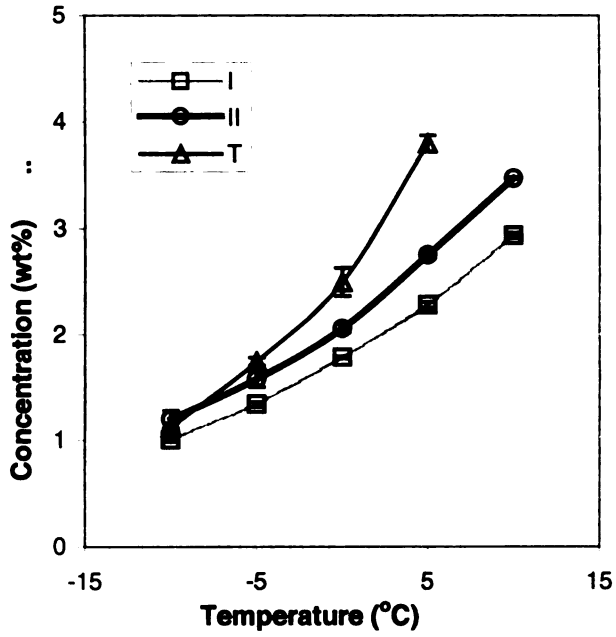


*Figure 2.6. Solubility curve of acetaminophen polymorphs in ethanol:H2O ratio of 1:3.*

As the solubility difference between the metastable polymorph and the stable polymorph decreases with temperature, the driving force of transformation is significantly reduced at temperatures close to 0°C and the metastable polymorphs are more likely to remain in slurry before transformation occurs. In other words, a low nucleation temperature will favor the crystallization of the metastable polymorph. Later crystallization experiments proved the chance of obtaining polymorph II or T is greatly increased when the onset of crystallization is controlled to occur at temperatures below 10°C. As nucleation is a kinetically controlled process, in order to crystallize the metastable polymorphs, it is necessary to adjust the process parameters such as solvent composition and to control the nucleation temperature to change the nucleation kinetics of different polymorphs of acetaminophen.

### *2.3.3 Effect of Thermal History on Acetaminophen Polymorph Crystallization*

The crystallization conditions for obtaining different polymorphs of acetaminophen are summarized in Table 2.1. Among all the operational parameters studied for the unseeded batch crystallization of acetaminophen in mixed solvent of ethanol and water, thermal history of the solution is found to be the most significant factor in determining which polymorph can be crystallized. The three heating and cooling profiles described in the experimental section are represented as H-a, H-b and H-c. Compared to the solutions heated at temperature much lower than boiling point, solutions that were heated at boiling point prior to cooling showed a significantly lower nucleation temperature or metastable point temperature. As this nucleation temperature extends below 5°C, the metastable modifications II and T have a much better chance to crystallize than polymorph I.

**Table 2.1**. Effect of thermal history and solvent composition on polymorph of acetaminophen obtained from unseeded batch crystallization. H-a, H-b and H-c represent different heating and cooling profiles.

| **Solvent Composition Ethanol:$H_2O$** | **Initial concentration of solution (g/100g solvent)** | **Acetaminophen Polymorph** | | |
|---|---|---|---|---|
| | | **H-a** | **H-b** | **H-c** |
| **1:1** | **20-80** | **I** | **II** | **II** |
| **1:3** | **7-28** | **I** | **T** | **II** |
| **0:1** | **1-3** | **I** | **T** | **T** |

Similar effects were observed for solution crystallization of vanillin by Hussain etc[18], which showed "high overheating" increases the metastable zone width (MZW) and leads to the precipitation of metastable form. Although the effect of thermal history on MZW has been known to aqueous solution crystallization of inorganic substances, vanillin crystallization has been the only case reported for the effect of thermal history on polymorph crystallization of organic substances. The mechanism causing this effect is not known yet. One possible explanation is extensive heating changes the pre-nucleation solution structure, although no difference in Raman or NMR spectroscopy were observed for acetaminophen solutions subjected to different heating profiles. Another explanation might be the solid heterogeneous particles in the solution are deactivated or destroyed, thus the solution becomes more homogenous, which increases the activation energy for nucleation and the onset of nucleation is "delayed" to the region of high supersaturation. As high supersaturation favors metastable polymorph formation, there is a better chance for metastable polymorphs to crystallize out of solution. While the mechanism for this effect still needs to be investigated, it is worth to note that thermal history might be a very important parameter to be considered in high throughput polymorph crystallization, especially for systems with water as the solvent.

Cooling rate also affects the outcome of polymorph for acetaminophen crystallization in a 25% aqueous ethanol solvent. For a solution heated to the boiling point, fast cooling results in the less stable trihydrate polymorph while slower cooling results in more stable polymorph B even when nucleation occurs at the same temperature in both cases. This might be caused by changes in solvent and solute molecular interactions during cooling,

fast cooling preserves the interactions at high temperature, while the same type of interactions may have changed during the course of slow cooling.

### *2.3.4 Effect of Solvent Composition on Acetaminophen Polymorph Crystallization*

It is well known that solvent plays an important role in crystallization of polymorphs. As Threlfall[17] pointed out, when crystallization occurs at a temperature far away from the transition point temperature, polymorph crystallization is under thermodynamic control, where only the thermodynamically stable polymorph will be crystallized out regardless of the solvent used. But when crystallization occurs at a temperature close to the transition point temperature, the solvent can affect the polymorph formed by changing the crystallization kinetics of each polymorph.

The effects of solvent composition on crystallization of acetaminophen polymorphs are also included in Table 2.1. For solutions that are not heated to the boiling point, nucleation tends to occur at temperatures well above 10°C where crystallization is under thermodynamic control and only the stable polymorph is obtained. While for solutions that are heated to the boiling point, nucleation can be controlled to occur at temperatures close to the transition point temperature of polymorph T and II where the composition of solvent affects which polymorph can be crystallized out. As the percentage of water is increased from 50% to 100%, the trihydrate polymorph becomes easier to crystallize than polymorph II. The low solubility of acetaminophen in water reduces the transformation rate from form T to more stable forms, thus form T is relatively stabilized.

As water content is decreased to 25%, even when the solution is heated to the boiling point and nucleation is controlled to occur at temperature about 0°C, the trihydrate form

could not be obtained at all, and polymorph II was obtained with a very low possibility (<5%). The increased solubility of acetaminophen in solvent with decreased content of water promotes the solvent mediated polymorph transformation, which may be too fast for the metastable form to be observed. Low water content also limits the interaction of water and acetaminophen molecules, which in turn limits the formation of the trihydate polymorph.

### *2.3.5 Transformation of Form T in Slurry*

When acetaminophen trihydrate crystals are suspended in a 25% ethanol in water slurry, a solvent mediated transformation occurs (Figure 2.7). Principal component analysis was applied to the Raman spectra collected during this transformation. The process can be clearly followed in the scores plot of different principal components (Figure 2.8). At 0°C, form T transforms to form II first, then form II transforms to thermodynamically stable form I. This transformation of form T to form I with form II as an intermediate is observed for the first time. It proves that the system follows the Ostwald's rule of stages, which states the system tends to go to the thermodynamically stable form by crystallizing the least stable polymorph then transforming to the next metastable form until it reaches the thermodynamically stable form. The intermediate stage with polymorph II can only be observed with the right process condition, e.g. low temperature. At higher temperature, the transformation process is too fast for the form II to be observed as intermediate, which might be the reason it was not observed previously by other researchers[9].

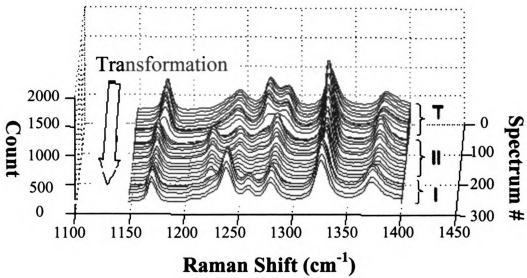


*Figure 2.7. Raman spectra collected during form acetaminophen polymorph T transformation in slurry in 25% ethanol in water at 0℃.*

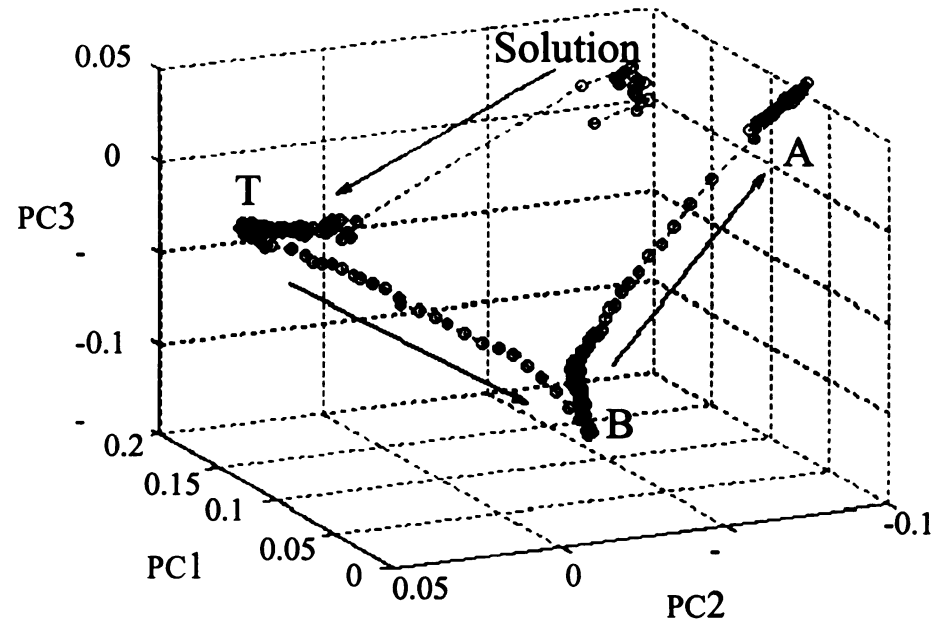


(a)

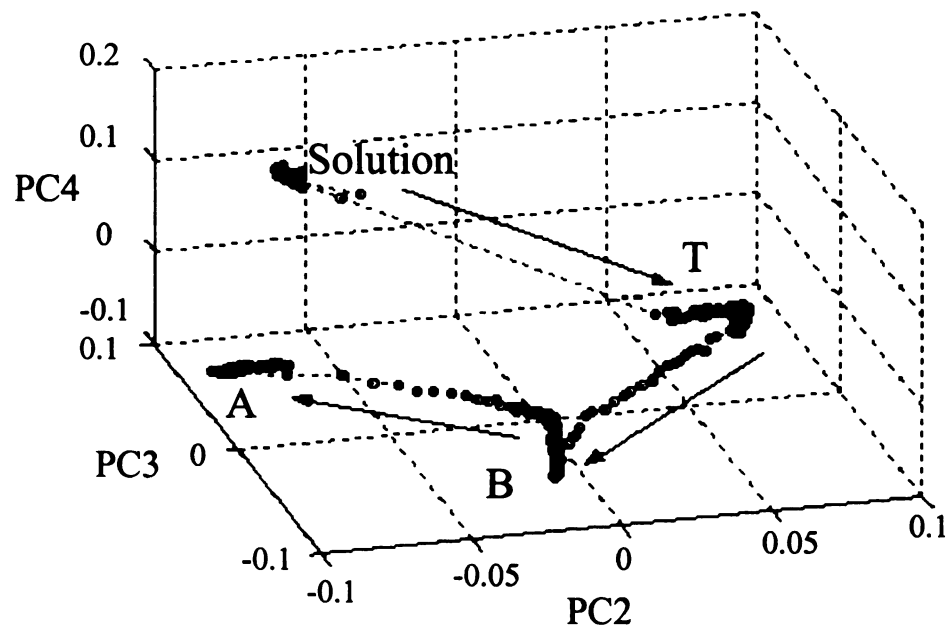


(b)

*Figure 2.8. Scores plots of principal components for acetaminophen polymorph transformation. (a) Spectra in PC1, PC2 and PC3 3-dimensional space; (b) Spectra in PC2, PC3 and PC4 3-diemtional space.*

## 2.4 Conclusions

This study shows that process parameters play a significant role in the crystallization of acetaminophen polymorphs. Thermal history coupled with solvent composition is the primary parameter controlling the polymorph forms. Heating the solution to higher temperature and cooling the solution down at a faster rate both favor the crystallization of metastable polymorphs. Higher water content in solvent mixtures of ethanol and water also favors the trihydrate form T, which has only limited stability at room temperature. Both metastable form T and form II can be reproducibly crystallized from solution by applying proper crystallization process parameters. Although often times neglected in the crystallization of organic substances, it is believed that thermal history can have strong impact on the outcome of polymorph forms.

Raman spectroscopy is also shown to be a convenient tool for on line and *in situ* characterization of polymorph forms in slurry. Coupled with chemometric data analysis methods such as PCA, it is easy to follow a complex polymorph transformation processes without the need of building a calibration model. This would greatly reduce the amount of work needed for method development during kinetic study of polymorph transformation and reduce the project turnover time.

## 2.5 Acknowledgements

The authors wish to thank Kaiser Optical System for a support of the instrument and software used in the study.

## 2.6 References


(1) Rossi, Alessandra; Savioli, Alessandra; Bini, Marcella; Capsoni, Doretta; Massarotti, Vincenzo; Bettini, Ruggero; Gazzaniga, Andrea; Sangalli, Maria Edvige; Giordano, Ferdinando; *Thermochimica acta*, **2003**; 406, 55-67.

(2) Martino, P. Di; Guyot-Hermann, A.-M.; Conflant, P.; Drache, M.; Guyot, J.-C., *International Journal of Pharmaceutics*, **1996**, 128(1,2), 1-8.

(3) Fachaux, J. M.; Hermann, A. M. Guyot; Guyot, J. C.; Conflant, P.; Drache, M.; Huvenne, J. P.; Bouche, R., *Powder Technology*, **1995**, 82(2), 123-128.

(4) Fachaux, J. M.; Hermann, A. M. Guyot; Guyot, J. C.; Conflant, P.; Drache, M.; Huvenne, J. P.; Bouche, R., *Powder Technology*, **1995**, 82(2), 129-133.

(5) Vrcelj, Ranko M.; Clark, Nathan I. B.; Kennedy, Alan R.; Sheen, David B.; Shepherd, Evelyn E. A.; Sherwood, John N., *Journal of Pharmaceutical Sciences*, **2003**, 92(10), 2069-2073.

(6) Fabbiani, Francesca P. A.; Allan, David R.; Dawson, Alice; David, William I. F.; McGregor, Pamela A.; Oswald, Iain D. H.; Parsons, Simon; Pulham, Colin R., *Chemical Communications (Cambridge, United Kingdom)*, **2003**, 24, 3004-3005.

(7) Parkin, Andrew; Parsons, Simon; Pulham, Colin R., *Acta Crystallographica, Section E: Structure Reports Online*, **2002**, E58 (12), 1345-1347.

(8) McGregor, Pamela A.; Allan, David R.; Parsons, Simon; Pulham, Colin R., *Journal of Pharmaceutical Sciences*, **2002**, 91(5), 1308-1311.

(9) Peterson, Matthew L.; McIlroy, David; Shaw, Paul; Mustonen, J. Peter; Oliveira, Mark; Almarsson, Örn., *Crystal Growth & Design*, **2003**, 3(5), 761-765.

(10) Haisa Masao; Kashino Setsuo; Maeda Hironobu, *Acta Crystallography*, **1974**, B30, 2510-2512.

(11) Nichols, Gary; Frampton, Christopher S., *Journal of Pharmaceutical Sciences*. **1998**, *87*, 684-693.

(12) Al-Zoubi, N.; Nikolakakis, I.; Malamataris, S., *Journal of Pharmacy and Pharmacology*, **2001**, 54, 325-333.

(13) Sacchetti, M., *Journal of Thermal Analysis and Calorimetry*, **2001**, 63, 345-350.

(14) Szelagiewicz, M.; Marcolli, C.; Cianferani, S.; Hard, A. P.; Vit, A.; Burkhard, A.; Von Raumer, M.; Hofmeier, U. Ch.; Zilian, A.; Francotte, E.; Schenker, R., *Journal of Thermal Analysis and Calorimetry*, **1999**, 57(1), 23-43.

(15) Martino, P. Di; Conflant, P.; Drache, M.; Huvenne, J.-P., Guyot-Hermann, A.-M.; *Journal of Thermal Analysis,* **1997**, 48, 447-458.

(16) Threlfall, Terry, *Organic Process Research & Development*, **2000**, 4, 384-390.

(17) Beckmann, Wolf, *Trans IchemE*, **1996**, 74 (part A), 750-757.

(18) Hussain, Khalid; Thorsen, Gunnar; Malthe-Sorenssen, Dick, *International Symposium on Industrial Crystallization*, 14th, Cambridge, United Kingdom, Sept., **1999**, 631-643.

# Chapter 3

## IN-SITU MONITOR ACETAMINOPHEN POLYMORPH TRANSFORMATION USING RAMAN AND ATR-FTIR SPECTROSCOPY

Raman and ATR-FTIR spectroscopic methods were used to *in situ* monitor the acetaminophen polymorph crystallization and transformation process. While Raman spectroscopy probes the polymorph form in the solid state, ATR-FTIR measures solution phase concentration at the same time. The relevant kinetic information can be obtained conveniently by such measurements. Under the conditions in this study, acetaminophen polymorph transformation is limited by the crystallization rate of the more stable phase, specifically by crystal growth rate of form II for form T to II transformation, and by nucleation rate of form I for form II to I transformation. As a soft modeling chemometric 'tool', multivariate curve resolution was also demonstrated to be well suited for extracting the crystallization and transformation profile in a complex polymorph system.

### 3.1 Introduction

The significance of polymorphism and polymorph transformation has been realized in pharmaceutical and specialty chemical industries over recent years[1-3]. As different polymorphs have different thermodynamic stability, transformation from a metastable form to a stable form may occur in production processes, thus causing problems with product quality or in process development. Understanding the kinetics of such transformation processes can help to establish production conditions to better control the

desired polymorphic form[4-6]. Solvent mediated polymorph transformation is of practical importance, as solution crystallization is oftentimes the preferred method for material purification and separation. Study of the profile of solid phase polymorph composition and solution phase concentration during transformation can help to identify the kinetic processes that regulate the transformation rate. On line Raman and ATR-FTIR spectroscopic methods are well suited for this type of study. In comparison to common offline analytical techniques such as X-ray powder diffraction (XRPD) and differential scanning calorimetry (DSC), Raman and ATR-FTIR spectroscopy can make measurements in crystallization slurry *in situ*, thus do not require sample preparation. This not only reduces possible sources of error, but also greatly simplifies the measurement procedure[7,8].

On line spectroscopic methods are especially suitable for monitoring complex chemical processes by providing rich information on chemical species. To take advantage of the large amount of information contained in on-line spectroscopy, chemometric analyses are often desirable to extract the relevant information in a simple and efficient way. For example, multivariate curve resolution (MCR) is a particularly useful technique in extracting estimates of pure component spectra and composition profiles from spectral data matrices[9].

Acetaminophen was used as the model compound in this study. Solution crystallization of acetaminophen can produce three forms: Trihydrate form T, orthorhombic form II and monoclinic form I, with form I being the most stable and form T being the least stable form under the conditions of this study. The goal is to develop suitable methods for

probing the kinetic information during acetaminophen polymorph transformation by using on line Raman and ATR-FTIR spectroscopic techniques.

## 3.2 Experimental methods

Acetaminophen (98% pure) was obtained from Aldrich and used as received. Solvents used during crystallization were reagent grade ethanol and distilled, deionized water. Crystallization experiments were carried out in a 1L jacketed crystallizer, equipped with a condenser, a thermocouple and an anchor-type glass stirrer (Figure 2.1). Stirring speed was 500rpm. Two circulators were used to provide heating and cooling fluids, respectively. At the end of heating period, the crystallizer was disconnected from the heating circulator and the heating fluid was emptied out. The crystallizer was then connected with the cooling circulator.

A Hololab 5000 Raman spectrometer from Kaiser Optic Systems was used for *in situ* monitoring the crystallization and transformation process, as well as the solid-state characterization of different polymorphs in slurry. The spectrometer is equipped with a 785nm laser and coupled with an immersion probe through fiber optic cables.

The solution concentration profile during crystallization and transformation was monitored by a ReactIR 1000 FTIR spectrometer from ASI Mettler Toledo. An attenuated total reflection (ATR) probe with diamond as the internal reflection element is attached to the FTIR spectrometer. The system is purged by dry air, and the MCT detector is cooled with liquid $N_2$.

### *3.2.1 Polymorph Crystallization and Transformation of Acetaminophen*

The crystallization of acetaminophen was carried out in 25% (by weight) ethanol in water. The initial concentration of acetaminophen is 9.7g /100g solvent. In order to crystallize the metastable trihydrate polymorph T, the solution was vigorously refluxed at the boiling point for 30 minutes and then rapidly cooled to 0°C at about 6°C/minute. After crystallization occurred at 0°C the slurry was continually stirred until the transformation from form T to stable form I was complete. Both Raman and ATR-FTIR spectra were recorded to *in situ* monitor the crystallization and transformation process after the solution was cooled to 0°C, thus the spectra were collected at isothermal conditions.

### *3.2.2 Spectral Data Analysis*

The Raman spectra collected during crystallization and transformation were subjected to a peak height analysis and a multivariate curve resolution (MCR) analysis. The results from both analyses were compared. The peak height profile at 1237cm-1 after normalized by peak at 1326cm$^{-1}$ was found to be able represent the transformation process. The MCR analysis was performed using the HoloReact software package from Kaiser Optical Systems. MCR[10] analysis begins with principal component analysis (PCA) to transform the original spectra data matrix **D** into a reproduced data matrix **D*** with reduced number of factors (principal components). These factors describe the major variances in data set, but they either are not physically meaningful or are mixed spectra of more than one chemical species. The **D*** matrix is then analyzed by evolutionary factor analysis (EFA) and alternating least square (ALS) method[10]. Some realistic boundary

conditions are applied to ALS analysis, e.g non-negative values for spectra and concentration profiles. Eventually **D*** is transformed to **SC**, which is the product of matrices of individual "pure" spectra **S** (the factor matrix) and of concentration profiles **C** (the score matrix). **D*** and **S** have the same rank or dimension. Thus the advantage of MCR analysis is to provide the concentration profiles of "pure" spectra, which are physically meaningful. Mean centering and normalization were applied to all spectra as data pretreatment.

Solution concentration changes were monitored by ATR-FTIR spectroscopy. A calibration model was developed using partial least square (PLS) regression over the spectral region 1150~1800cm$^{-1}$. The model is then applied to the IR spectra collected during the crystallization and transformation processes. The purpose is to correlate the solution phase concentration change with the polymorph transformation in the solid phase.

### 3.3 Results and Discussion

Raman spectroscopy with an immersion probe can be conveniently used to identify the polymorph form of acetaminophen in the crystallization slurry without any sampling procedure. Raman spectra for solid samples of different acetaminophen polymorphs are shown in Figure 2.2. Significant differences can be observed within the ranges of 1150 ~1300cm-1 and 1530 ~ 1700cm-1. These differences in Raman characteristics reflect different configurations of acetaminophen molecules in the crystalline state caused by intermolecular hydrogen bonding. The slurry of different acetaminophen polymorphs in ethanol and water showed similar spectroscopic characteristics to those of the

corresponding solid sample, thus different polymorphs were identified in the crystallization slurry using Raman.

### *3.3.1 In Situ Monitor Crystallization and Transformation of Acetaminophen Polymorphs by Raman*

When acetaminophen crystals of metastable polymorphs are suspended in a slurry, solvent mediated transformation occurs. Figure 3.1 shows the Raman spectra collected during crystallization and transformation. The system follows the Ostwald's rule of stages with the least stable form T crystallizing out first. It then transforms to the next metastable form II before it transforms to the stable form I. The knowledge of transformation kinetics is important to developing a reliable crystallization process. Raman spectroscopy is a useful tool in such a kinetic study. By following the transformation process, the transformation rate under different crystallization conditions can be measured *in situ.* It is crucial to extract the correct kinetic information by applying proper spectra analysis. For the acetaminophen polymorph transformation process, two types of spectra analysis methods were applied and their results were compared.

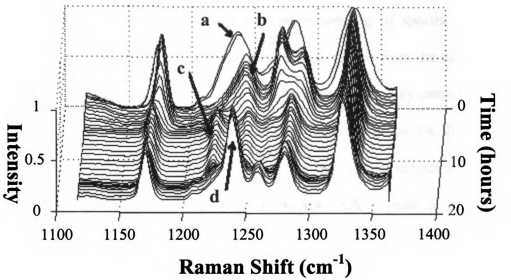


*Figure 3.1 Raman spectra collected during crystallization and transformation of acetaminophen polymorph in 25% ethanol in water at 0℃. a) Solution before crystallization; b) Slurry of form T; c) Slurry of form II; d) Slurry of form I. Peak at 1326cm$^{-1}$ is used for normalization.*

Raman spectra between 1150cm$^{-1}$~1300cm$^{-1}$ were first analyzed by non-chemometric methods. First, a few common spectra pre-processing techniques were applied including base line correction, derivatives of original spectra and normalization of spectra. After the pre-processing of spectra, peak height as well as peak height ratios at different wavenumbers and peak areas under different regions were calculated over the course of crystallization and transformation. Although pre-processing of spectra improves the results to some degree, many transformation profiles extracted from the aforementioned analyses still contain too much noise or have poor shapes, thus they cannot be used for kinetic study. After using the peak at 1326cm$^{-1}$ to normalize the spectra, the peak height at 1237cm$^{-1}$ exhibited a very smooth profile and was used to extract transformation kinetic (Figure 3.2). All three forms of acetaminophen exhibit peaks at 1326cm$^{-1}$ with about the same intensity. Only form I shows a strong peak at 1237cm$^{-1}$, while form T and form II have peaks shifted to different wavenumber, thus exhibit different intensity at 1237cm$^{-1}$. Normalization of the spectra with the peak at 1326cm$^{-1}$ greatly enhances the peak intensity difference at 1237cm$^{-1}$ caused by structural differences in different polymorphs while minimizing the effect of interferences such as baseline shift. Thus, the quality of this analysis is greatly improved and it is possible to use such a simple spectra analysis method to monitor the crystallization and transformation process.

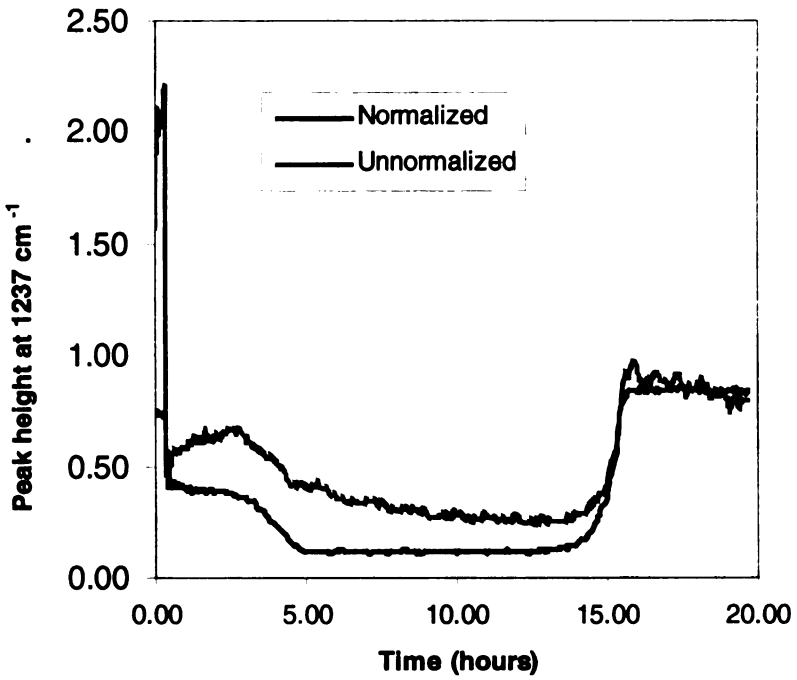


*Figure 3.2 Crystallization and transformation profile represented by peak height at 1237cm-1. For the peak height profile from un-normalized spectra, a factor of 0.001 has been multiplied to bring it to the same scale as the normalized profile.*

Although it was possible to find a good non-chemometric method for spectra analysis in this case, it took a lot of effort in searching and optimizing this method, even though this is a relatively simple system with no more than two components present in the solution at the same time. For a system with more components or with peaks experiencing a high degree of overlapping, this kind of analysis would be very hard if not impossible. As a result, it is often necessary to use chemometric methods to extract relevant information and improve the quality of spectra analysis. MCR is a very useful analysis method, which can extract "pure" component concentration profile from on-line spectra. Figure 3.3 shows the principal components resolved by MCR after the spectra were normalized by the peak at 1326cm$^{-1}$, and figure 3.4 plots the score (i.e. the so called "concentration") profiles of different components during the crystallization and transformation process. The extracted principal component spectra converge very well with the Raman spectra of solid state samples. PC1 peaks at 1177, 1244, 1271 and 1290cm$^{-1}$, which are characteristics in Raman spectrum of trihydrate form T, it has the highest score between a little after 0 and 2 hours when form T is first crystallized out of solution. PC2 peaks at 1168, 1238, 1258 and 1278cm-1, which are due to the thermodynamically stable form I, thus its highest score appears at the end of the process when all the metastable polymorph II has transformed to form I. PC4 features peaks at 1171, 1222, 1247 and 1281cm-1, which belong to the metastable form II, its highest score appears between 5 and 15 hours when form II is the dominant form in slurry. The third principal component PC3 resembles the spectrum of acetaminophen solution in 25% ethanol in water, but with more spectral features resolved. It roughly represents the relative concentration profile during crystallization and transformation. It drops dramatically when nucleation happens

and trihydrate form T crystallizes at the beginning of the experiment, a second and a third drop happen at the transformation from T to II and from II to I respectively due to decrease in solubility of different forms. Compared to the peak height profiling method, much less effort is needed to reach the optimum analysis results using the chemometric method.

Both the peak height and the PC profiles can be used to calculate the polymorph composition changes during the transformation. The results from both approaches agree very well as shown in figure 3.5. Both transformation processes follow the typical polymorph transformation profile with induction, acceleration and decay periods. Nucleation of the more stable form occurs and dominants in the induction period, while crystal growth mainly happens in the acceleration period. It appears that transformation rate from form T to form II is limited by crystal growth rate of form II, while the transformation rate from form II to form I is limited nucleation of the stable form I.

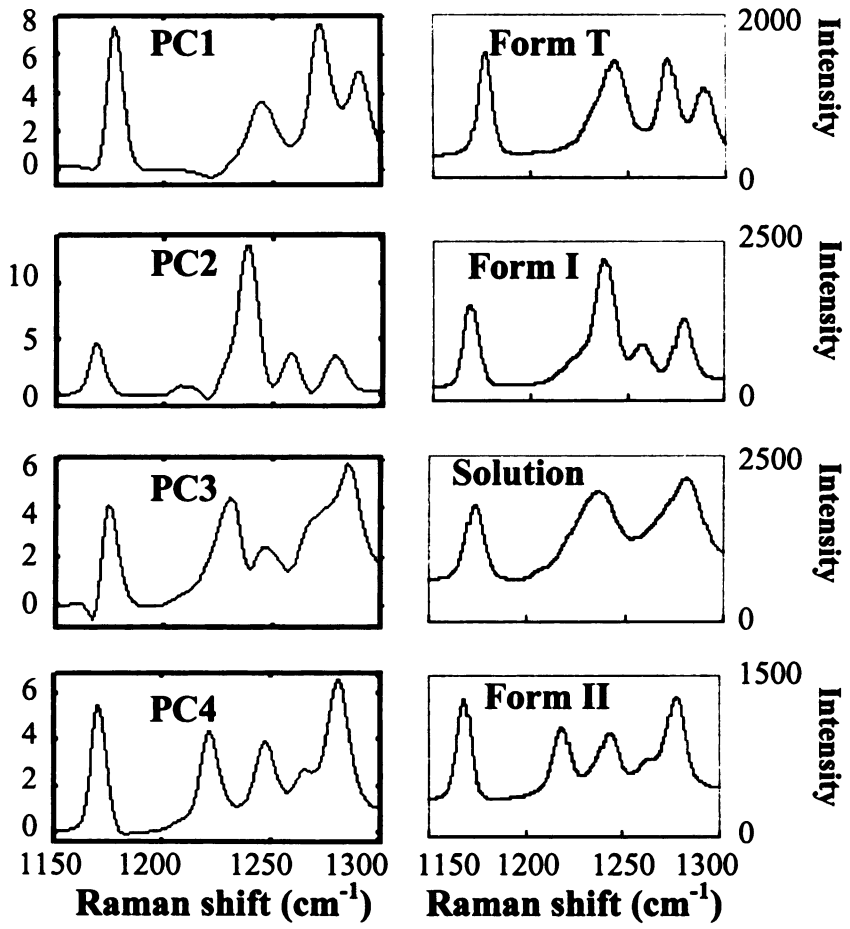


*Figure 3.3. The four pure component spectra extracted from the MCR analysis (left) compared with Raman spectra collected for acetaminophen polymorph or solution (right).*

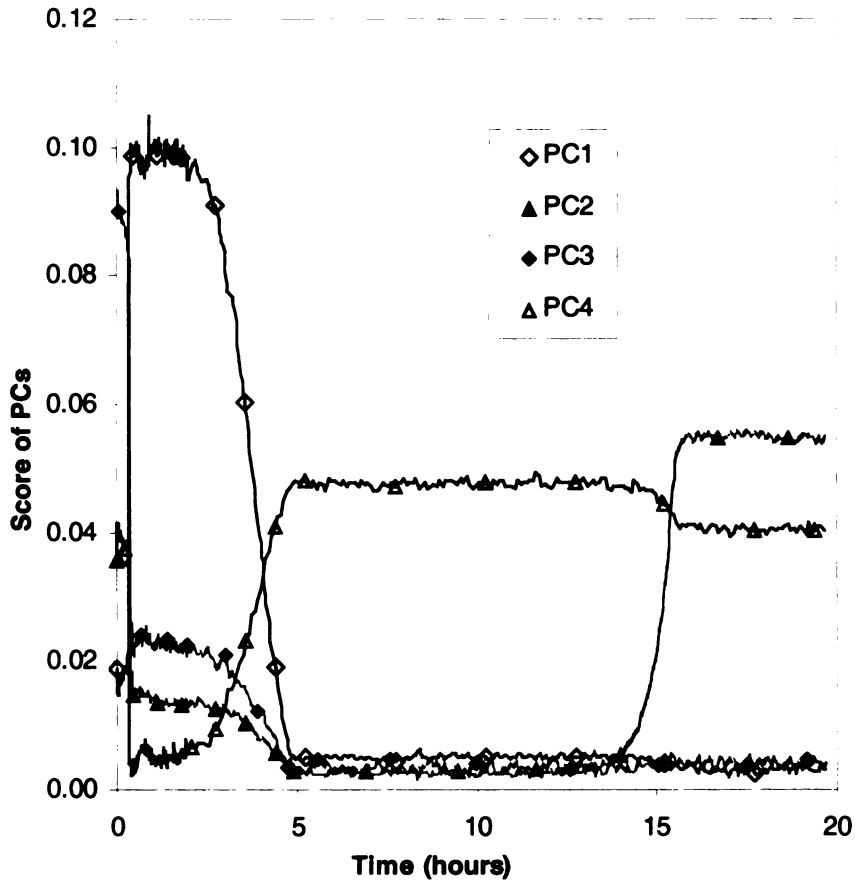


*Figure 3.4 Scores plot for principal components from MCR analysis of acetaminophen polymorph crystallization and transformation.*

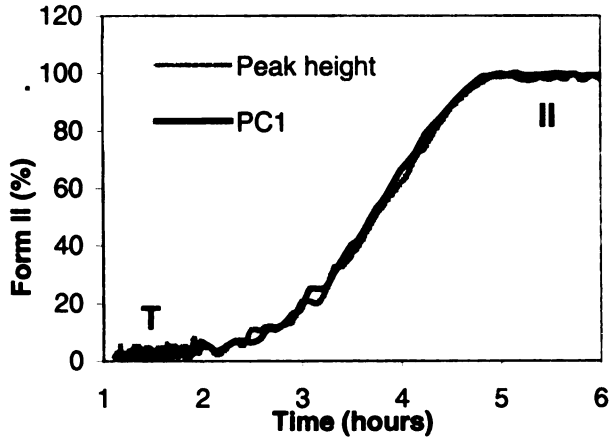


(a)

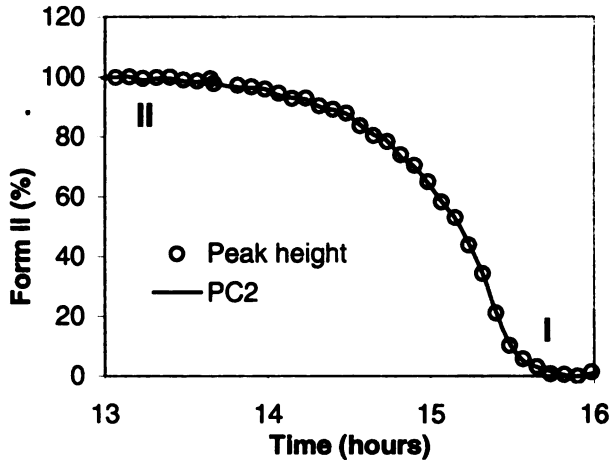


*Figure 3.5 Relative composition profiles calculated from profiles of normalized peak height at 1237cm$^{-1}$, PC1 and PC2 by MCR analysis. (a) Form T to II transformation; (b) Form II to I transformation.*

### *3.3.2 In Situ Monitor Concentration Change During crystallization and Transformation by ATR-FTIR*

In order to characterize the acetaminophen polymorph transformation kinetic processes, the solution phase concentration change was also monitored by ATR-FTIR spectroscopy. ATR is a special sampling technique of FTIR that is capable of measuring the solution phase concentration in slurry without the interference from the solid phase. Another chemometric method, PLS, was used to develop a calibration model using acetaminophen solutions with known concentration. Figure 3.6 shows the region subjected to the PLS analysis. The monitored concentration profile is shown in Figure 3.7. According to Davey and Cardew, the solvent mediated polymorph transformation process consists of continuous dissolution of the less stable form and crystallization of the more stable form. Solution concentration continually drops toward the solubility of the more stable form early in the process for a dissolution-controlled transformation, while it remains close to the solubility of the less stable form until the very end for a crystallization-controlled transformation. It is apparent that both transformation from form T to II and from form II to I are the extreme cases of crystallization-controlled transformation, since the solution concentration stays constant during the transformation process and only starts dropping when the less stable form has all transformed (test by Raman).

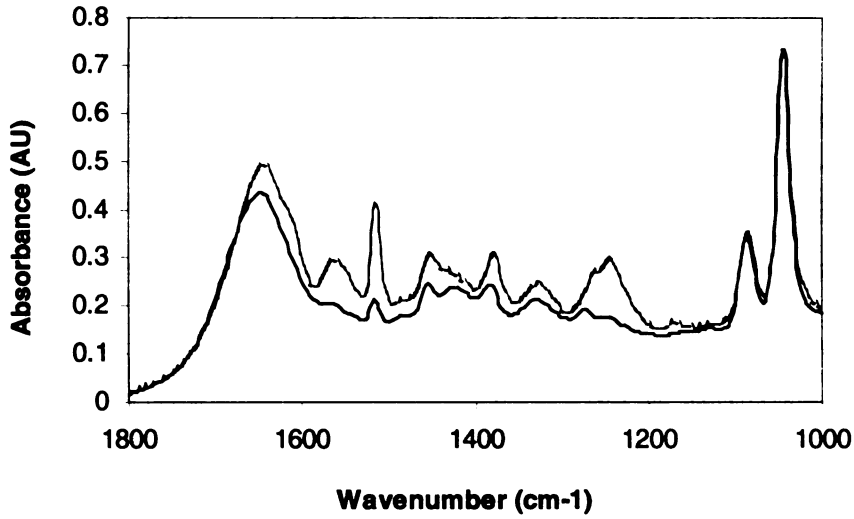


*Figure 3.6 IR spectra of acetaminophen in 25% ethanol in water. The region from 1000 ~1800cm-1 was used to build calibration model by PLS regression.*

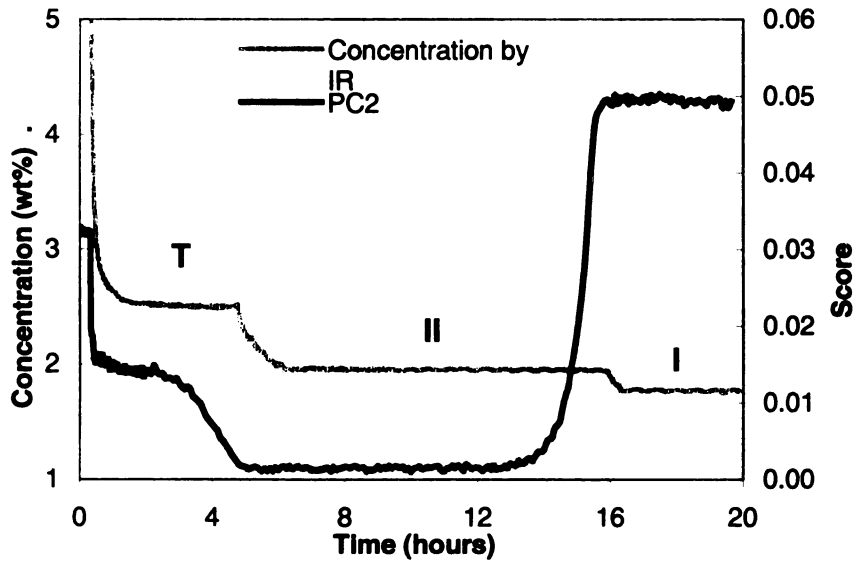


*Figure 3.7. Concentration profile by ATR-FTIR compared with PC2 profile from MCR analysis of Raman spectra.*

## 3.4 Conclusions

Both Raman and ATR-FTIR spectroscopies are suitable for on line monitoring of solvent mediated acetaminophen polymorph transformation processes. These two techniques provide complimentary information about solid phase polymorph form and solution phase concentration respectively, which are important in understanding the solvent mediated transformation pathways and kinetic features of such a process. Under the conditions studied, the concentration profile measured by ATR-FTIR reveals that acetaminophen polymorph transformation rate is controlled by the crystallization rate of the more stable form, while the polymorph composition profiles extracted from Raman spectra identify nucleation and crystal growth are the rate limiting process for form II to I and form T to II transformation, respectively. Applying chemometric analysis methods such as MCR to on line spectral data greatly simplified the method development process for polymorph transformation monitoring.

## 3.5 References


(1) Byrn, S. R., *Solid-state Chemistry of Drugs*, Academic Press: New York, **1982**

(2) Chemburkar, Sanjay R.; et al. *Organic Process Research & Development*, **2000**, 4(5), 413-417.

(3) Vippagunta, S. R.; Brittain, H. G.; Grant, D. J. W., *Advanced Drug Delivery Reviews*, **2001**, 48(1), 3-26.

(4) Rodriguez-Hornedo, Nair; Murphy, Denette., *Journal of Pharmaceutical Sciences*, **1999**, 88(7), 651-660.

(5) Wang, Fang; Wachter, John A.; Antosz, Frederick J.; Berglund, Kris A., *Organic Process Research & Development*, **2000**, 4(5), 391-395.

(6) Starbuck, Cindy; Spartalis, Angela; Wai, Lawrence; Wang, Jian; Fernandez, Paul; Lindemann, Christopher M.; Zhou, George X.; Ge, Zhihong, *Crystal Growth & Design*, **2002**, 2(6), 515-522.

(7) Yu, Lian; Reutzel, Susan M.; Stephenson, Gregory A., *Pharmaceutical Science & Technology Today*, **1998**, 1(3), 118-127.

(8) Head, Teresa; Rydzak, Jim, *American Pharmaceutical Review*, **2003**, 6(1), 78-80, 82-84.

(9) Miller, Charles E., *Journal of Chemometrics*, **2000**, 14: 513-528.

(10) Schoonover, Jon R; Marx, Rob; Zhang, Shuliang, *Applied Spectroscopy*, **2003**, 57, 154A-170A.

# Chapter 4

## ATR-FTIR FOR DETERMINING OPTIMAL COOLING CURVES FOR BATCH CRYSTALLIZATION OF SUCCINIC ACID*

* *Crystal Growth & Design, **2002**, 2, 449-452.*

The temperature profile applied during batch cooling crystallization affects the supersaturation level, which in turn affects the crystal size distribution. It is possible, in principle, to calculate the optimal cooling profile; however, the nucleation and growth kinetics are rarely known to the degree of accuracy necessary for this calculation.. The current study demonstrates an alternative approach to determination of the optimal cooling profile without any prior knowledge of kinetic data or subsequent modeling. An attenuated total reflectance-Fourier transform infrared (ATR-FTIR) spectrometer was used to monitor the supersaturation level during batch cooling crystallization. The ATR-FTIR was interfaced to a LABMAX® automatic reactor system that was used in a feedback mode to control the cooling rate so that supersaturation level remained close to the solubility throughout the cooling process. The resulting temperature profile corresponds to the optimal operating conditions for the maximum in the mean crystal size.

### 4.1 Introduction

Batch crystallization is a widely practiced unit operation in specialty chemical industry such as pharmaceutical and agrochemical industry. An optimized crystallization process

is often required to produce a desired crystal size distribution with good reproducibility from batch to batch.[1,2]. In case of batch cooling crystallization, it is well known that the cooling rate affects supersaturation profile and has strong influence on the crystal size distribution.[3] In order to grow bigger particles, the rate at which supersaturation is generated by cooling should match the rate of desupersaturation by crystal growth throughout the course of the batch cooling crystallization. Nucleation should be suppressed by keeping the supersaturation level close to solubility. However, the determination of the most appropriate cooling profile in industrial crystallization remains a challenge since nucleation and crystal growth kinetic data for a particular system are often not available. Moreover, even when tentative kinetic models are available for a system, the parameters are often highly sensitive to operation conditions such as agitation speed and fail to accurately predict crystallization process when operation conditions change.[4]

In the present work a method to obtain the optimized cooling profile using ATR-FTIR spectroscopy is presented. The method does not require kinetic models thereby reducing possible errors caused by inaccurate kinetic expressions. ATR-FTIR has been shown previously to be an excellent technique for *in situ* monitoring supersaturation in a crystallizing slurry.[5-7] ATR-FTIR was coupled with a LABMAX® automatic reactor system to obtain optimal cooling profiles in a fast, easy and flexible way. The succinic acid-water system was chosen to demonstrate the practical aspects of this approach.

## 4.2 Experimental Section

Succinic acid was purchased from Aldrich. All aqueous solutions of succinic acid were prepared with with deionized water. The schematic of the experimental setup is shown in Figure 4.1. All cooling crystallizations of succinic acid were conducted in the 1-L glass reactor of the Mettler-Toledo LABMAX® System. Two electronic units, the thermostat unit and the controller unit, control the reactor. The thermostat unit controls the reactor and jacket temperature based on the feedback from the temperature sensors in the reactor and in the jacket. Temperature can be controlled either by specifying an endpoint temperature or by keeping a predetermined temperature difference between the reactor and the jacket. The thermostat unit also controls the stirrer speed. The controller unit controls external sensors and devices such as pH electrode, pump and balance, which are not included in this study. *In situ* measurement of supersaturation was performed using ASI-ReactIR1000 spectrometer equipped with an immersion probe equipped with a diamond internal reflection element. The probe was purged with dry air.

The communication between the REACTIR and the LABMAX® is provided by an interface that transmits values such as reactor temperature and supersaturation level. This feature is particularly convenient for the present study since it allows real time feedback control based on the supersaturation value measured by the ReactIR. The LABMAX® can decrease the cooling rate when the supersaturation level is close to the preselected upper limit or increase the cooling rate when the supersaturation level is close to the solubility.

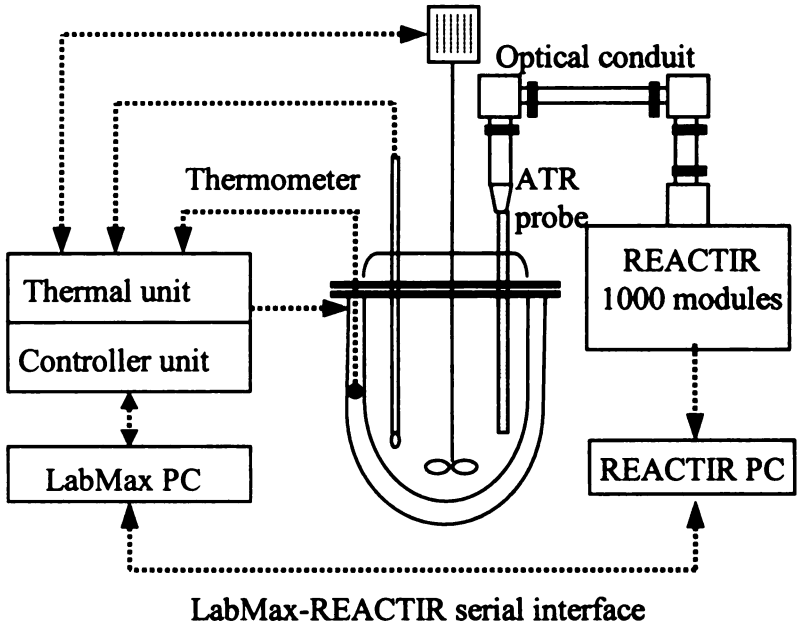


*Figure 4.1 Schematic of the experimental setup: LABMAX automatic reactor coupled with in situ ATR-FTIR probe.*

### *4.2.1 Calibration and Solubility Curve Measurement*

The calibration curve and operating solubility curve can be combined and obtained from a simple experiment described as following. Succinic acid in excess of solubility was mixed with water and kept at temperatures ranging from 10 to 60°C. At each temperature, the slurry was stirred for about 1 hour until equilibrium was reached, then 10 spectra were recorded *in situ*. Different slurry samples were used to make sure the solid concentration does not affect the solution phase IR signal. Spectra were analyzed and appropriate features were used to build the calibration and solubility curve.

### *4.2.2 Determination of Cooling Profiles*

A 19% (w/w) (total weight of the solution was 520g) succinic acid aqueous solution was kept at 60°C for 10 minutes to make sure the solid was dissolved. The solution was cooled at 2°C/minute until it reached the solubility according to the ReactIR reading. Seed crystals were introduced followed by immediate measurement of supersaturation level and temperature. The LABMAX® controlled the cooling rate of the reactor by adjusting the jacket temperature throughout the course of crystallization so that cooling was as fast as possible following the solubility limit closely. After the slurry temperature reached 10°C, the crystallization was ended and the crystals were filtered and dried. The crystal size distribution of the resulted particles was analyzed using a set of Tyler RX-86 sieves.

## 4.3 Results and Discussion

### *4.3.1 Calibration and Solubility Curve*

The common procedure involved in the measurement of supersaturation during crystallization was carried out in two steps.[8-10] A set of solutions with known concentration and temperature were prepared. IR spectra were taken and various IR bands were used to build the calibration curve. As recognized by Lewiner and many others,[4,8] for ATR-FTIR to be used in an industrial context the calibration procedure should be fast, efficient and easy. Since crystallization is operated within the metastable zone, supersaturation level or how far away the solution phase is beyond the solubility limit is the key information for crystallization process control. With these considerations in mind, the band ratioing procedure used by Dunuwila and coworkers.[5-7] was employed. The approach simplifies the calibration and solubility measurement by combining them into one step, requires the minimum amount of measurements, and has good accuracy.

Figure 4.2 shows typical IR spectra of aqueous succinic acid solution at different concentration at 60°C. A number of IR features are available for use in calibration. The band ratioing technique minimized the effects caused by instrumental drift. Such instrumental drift is likely to be associated with IR source instability as well as configuration changes in the optical conduits. Different peak height ratios and peak area ratios were tested and it was determined that peak area ratio (R) of 1806~1675cm-1 over 1671~1494cm-1 gave the best result in terms of reproducibility and accuracy. The reason could be that more features are hidden under the seemingly single peak at 1710cm-1, and the peak area reflects the complexity better than peak intensity at a specific wavelength.

$$R = \frac{Peak\ \ area\ \ under\ \ 1806\ \sim 1675\ cm^{-1}}{Peak\ \ area\ \ under\ \ 1671\ \sim 1494\ cm^{-1}} \tag{4.1}$$

Since this R is a function of both temperature and concentration, it implicitly reflects the supersaturation level during crystallization. No further correlation between this R and the absolute concentration is necessary. Thus R as defined in Equation. 1 was used directly in the calibration and solubility curve development that follows. A PLS calibration was also tried for calibration. Although a higher order of precision could be obtained during one run, this advantage was lost from run to run due to the aforementioned instrumental drift.

Figure 4.3 shows the solubility curve of succinic acid in terms of peak area ratio R. The small error bars substantiate the reproducibility of the approach. The supersaturation level (S) can then be expressed as

$$S = \frac{R(T)}{R^*(T)} \tag{4.2}$$

Where R (T) is the real time peak intensity ratio at temperature T, R*(T) is the peak intensity ratio at solubility at the same temperature T.

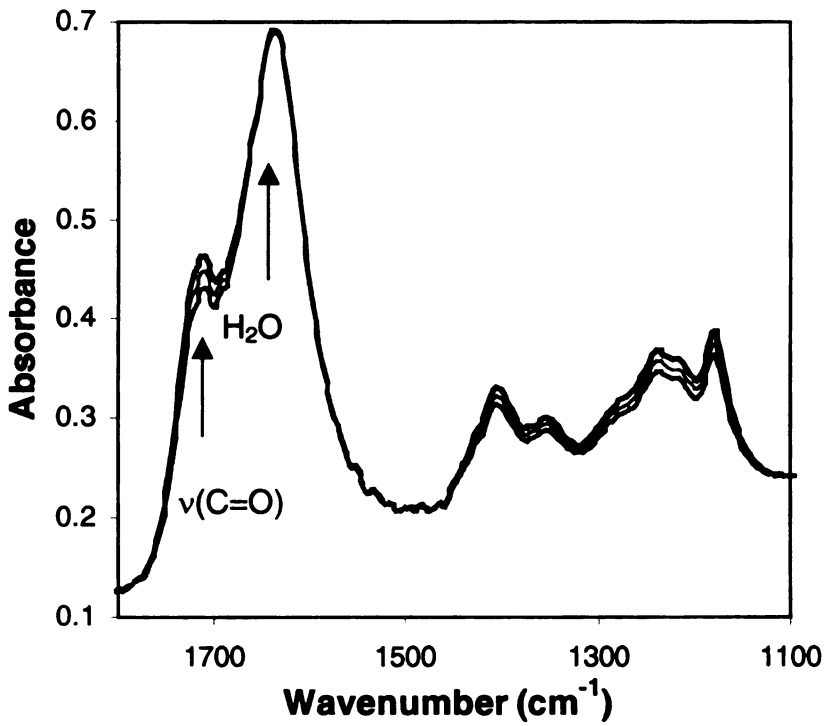


*Figure 4.2 ATR-FTIR spectra of succinic acid aqueous solution at 60°C. The two peaks exploited in peak area ratio are indicated by arrows.*

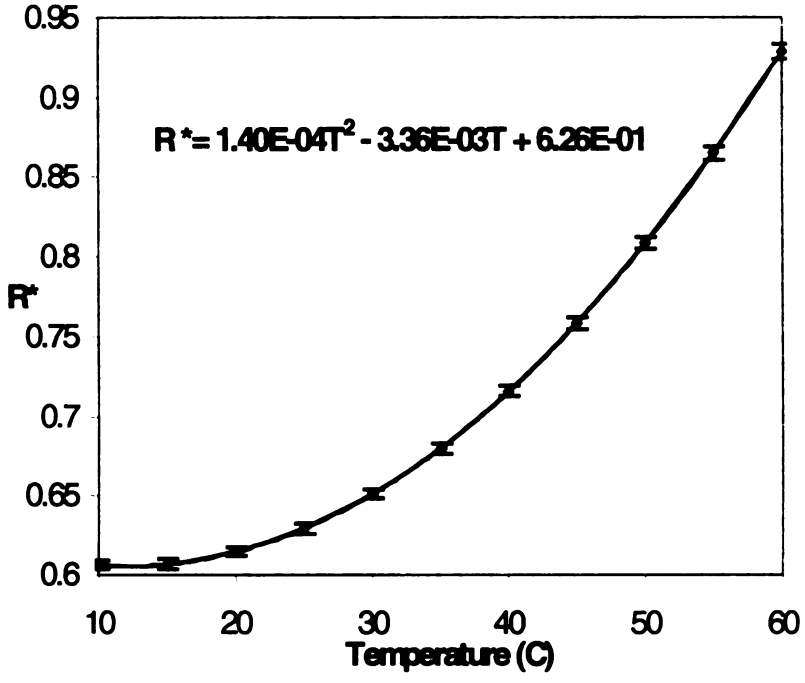


*Figure 4.3 Solubility curve of succinic acid in $H_2O$. R* is solubility represented by ratio of the peak area of the 1806~1675cm$^{-1}$ band to that of the 1671~1494cm$^{-1}$ band in the infrared spectrum.*

### *4.3.2 Determination of Optimal Cooling Profiles*

The optimal cooling profile was chosen based on the criterion to maximize the product weight mean size by suppressing the supersaturation level low enough to encourage crystal growth over nucleation. In the controlled cooling crystallizations of succinic acid studied, the initial solution conditions and other operational parameters were kept constant unless otherwise specified. The values used were 19% (w/w) initial concentration (total weight of solution is 520g), agitation rate of 400rpm, seed size of 355-425μm, and seed mass of 0.5g.

Figure 4.4 shows the effect of seed amount on cooling profile. Faster cooling can be applied with more seeds due to the presence of a greater seed surface area available for crystal growth. Excessive seeding results in a decrease in the mean particle size, which has been also observed by Lewiner et al.[9] While excessive seeding can result in reduced final mean particle due simply the lack of sufficient solute resources in solution to grow, the excess crystals present can also cause secondary nucleation. As noted by Lewiner et al.[9], even under a controlled low level of supersaturation, secondary nucleation is not as effectively suppressed as primary nucleation. Since secondary nucleation depends on magma density, more seeding may promote secondary nucleation and lead to a smaller crystal size distribution.

Figure 4.5 shows that the cooling profile varies with the size of seed applied when the same amount of seed in mass is used. When seed size increases the number of particles decrease as does the overall surface area available for growth. This results in a slower overall mass deposition rate, which requires a slower cooling rate and longer crystallization time.

Agitation rate is another important factor that affects the cooling profile as shown in Figure 4.6. Higher agitation rates improve mass transfer which should increase crystal growth. An agitation rate of 300rpm was not enough to suspend the seeds and product crystals during crystallization. Inhomogeneous slurry conditions reduce the efficiency of seeding and cause severe agglomeration. Comparison of the mean particle size with different agitation rates also reveals that excessive agitation causes more secondary nucleation and reduction in crystal size distribution. The effect of agitation is therefore a compromise between mass transfer, particle suspension, and secondary nucleation.

The cooling profile is also affected by the purity of solution. Acetic acid is a tailor made impurity that reduces the crystal growth rate of succinic acid. One g (2mol%) of acetic acid was added to solution and reduced the crystal growth rate which required the slowing the cooling process significantly in order to maintain constant supersaturation as shown in Figure 4.7. It is known that impurities are often adsorbed selectively on to different crystal faces and retard their growth rate. In an industrial context, crystallization is often operated in the presence many different impurities, hence it is important to be able to develop the optimal cooling profile according to the impurity profile of the raw material. The present approach is capable of identifying the optimal cooling curve when impurities are present. As expected, the crystal size distribution wasn't affected as long as the supersaturation was kept at a constant low level.

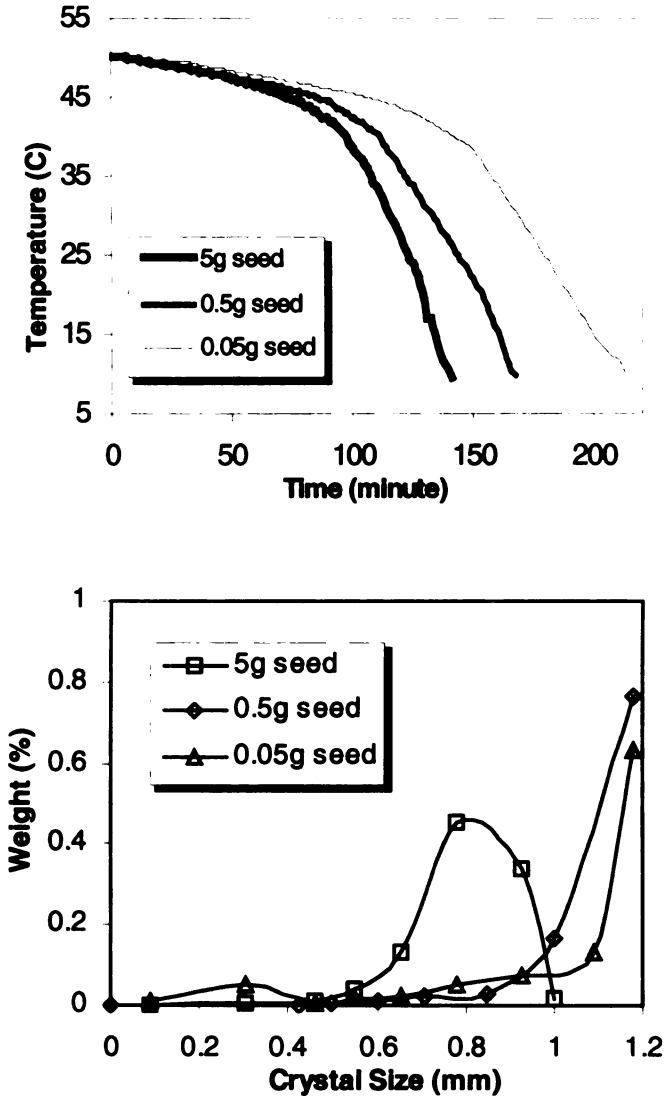


*Figure 4.4 Optimal cooling profiles (top) and CSD (bottom) for succicinic acid crystallization from aqueous solution with different amount of seeding. Initial concentration is 19%(w/w), seed size is 355-425μm, and agitation rate is 400rpm.*

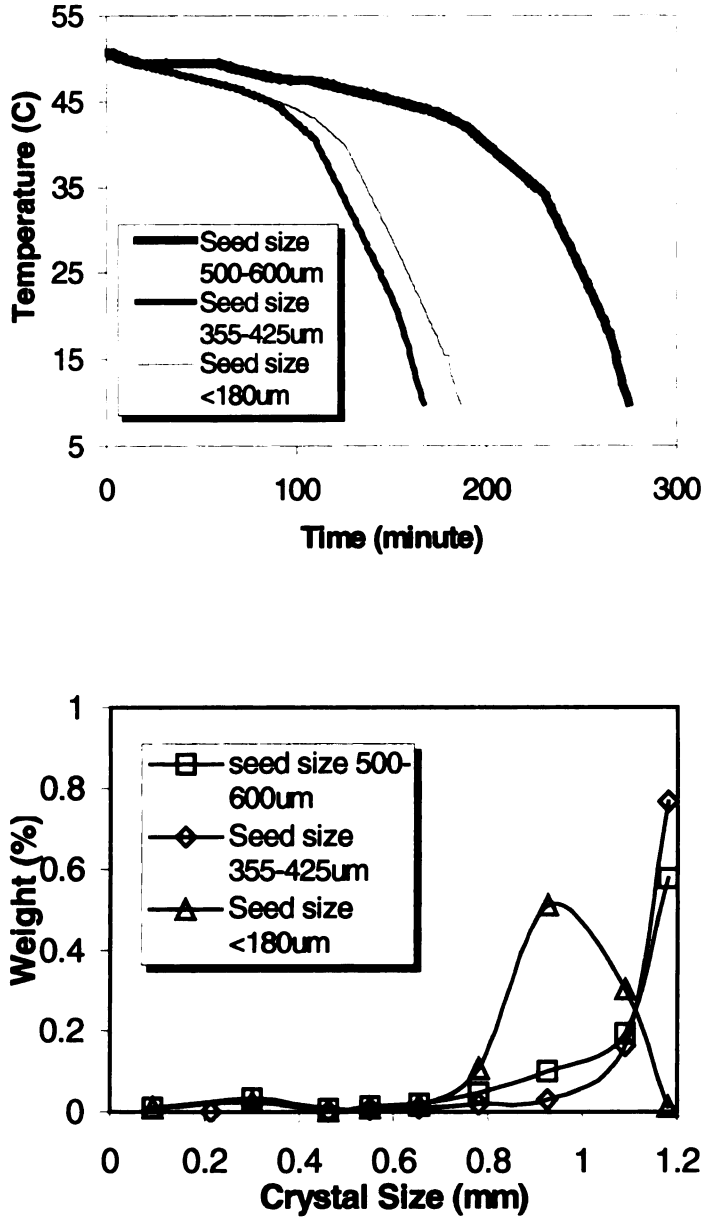


*Figure 4.5 Optimal cooling profile (top) and CSD (bottom) for succicinic acid crystallization from aqueous solution with different seed sizes. Initial concentration is 19% (w/w), seed amount is 5g, and agitation rate is 400rpm.*

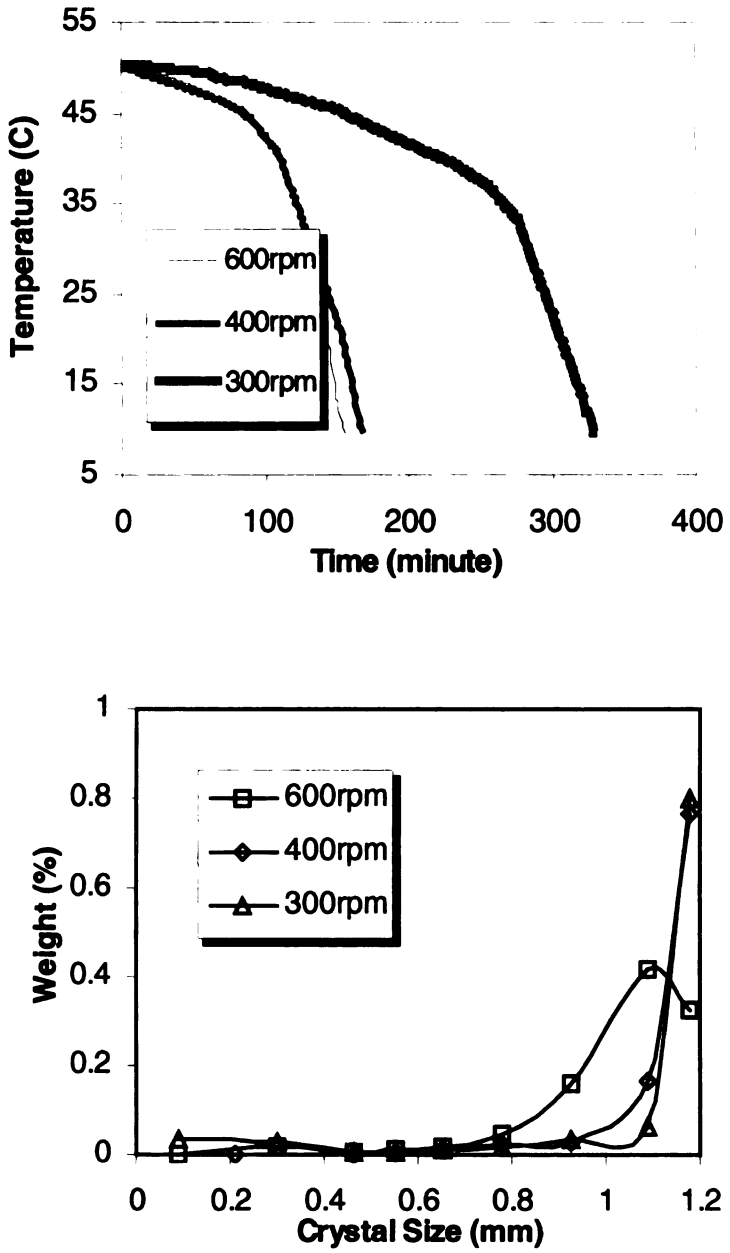


*Figure 4.6 Optimal cooling profile (top) and CSD (top) for succinic acid crystallization from aqueous solution with different agitation speeds. Initial concentration is 19%(w/w), seed amount is 5g, seed size is 355-425μm.*

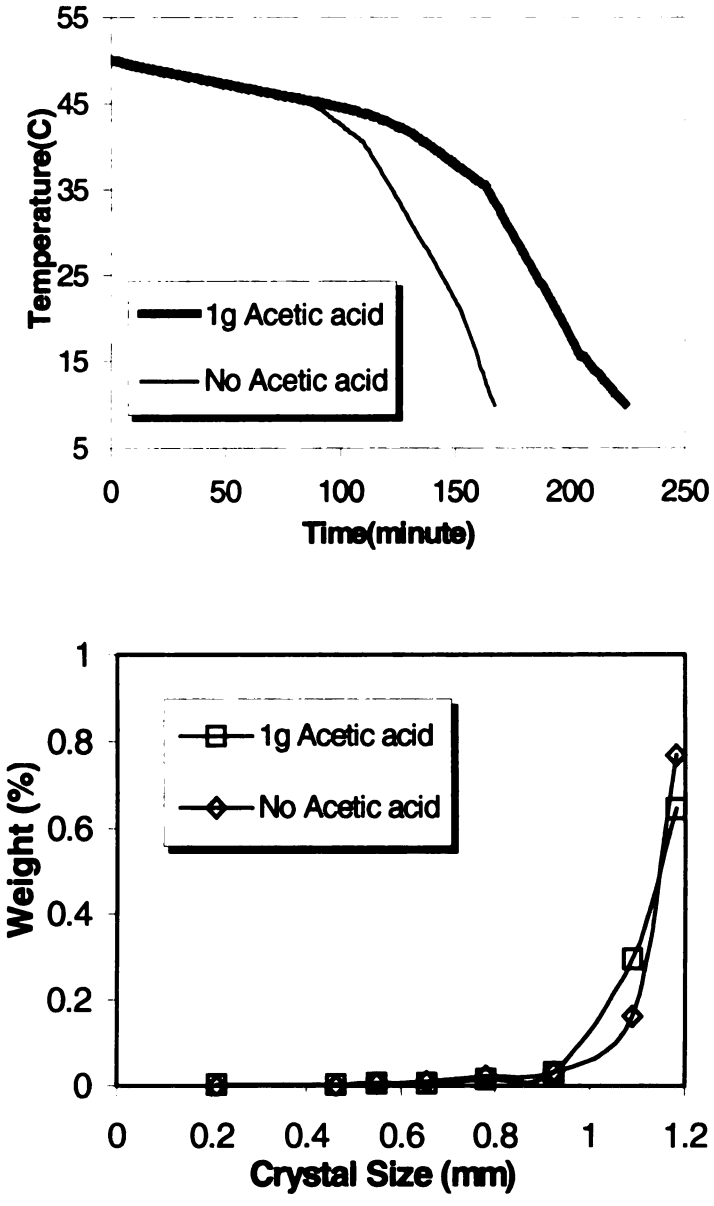


*Figure 4.7 Optimal cooling profile (top) and CSD (bottom) for succicinic acid crystallization from aqueous solution showing the effect of acetic acid present as an impurity (2% mole basis). Initial concentration is 19%(w/w), seed amount is 5g, seed size is 355-425μm, and agitation rate is 400rpm.*

## 4.4 Conclusions

The experimental results for cooling crystallization of succinic acid demonstrate the capability of the ATR-FTIR technique in crystallization process control and design. The calibration procedure is straightforward and efficient, which is preferred by industrial users. By coupling an ATR-FTIR with a LABMAX® automatic reactor system optimal, the optimal cooling curves for crystallization under different operation condition can be easily obtained by *in situ* feedback control of the supersaturation level close to solubility. No single optimal cooling profile works under different operational conditions, and it is critical that the technique used for optimal cooling profile determination must be easy, fast and flexible. The approach presented here does not rely on kinetic models and precludes the error caused by inaccurate kinetic data. Since kinetic data are usually not known in industrial applications, this method is suggested as a simple tool in process design and control of crystallization processes when a cooling policy needs to be determined.

## 4.5 Acknowledgements

The authors wish to thank ASI Mettler-Toledo for a support of the instruments used in the study. Additional support from the Center for New Plant Products and Processes at Michigan State University is also appreciated.

## 4.6 References


(1). Goren, H.; Hammond, R. B.; Lai,x.; Mougin, P.; Roberts, K. J.; Savelli, N.; Thomas, A.; White, G.; Williams, H. L.; Wilkinson, D.; Baker, M.; Dale, D.; Erk, P.; Latham, D.; Merrifield, D.; Oliver, R.; Roberts, D.; Wood, W.; Ford, L.; Hoyle, W., Eds.; Pilot Plants and Scale-up of Chemical Processes II; Special publication 236; Royal Society of Chemistry: Cambrige, 1999; pp40-61.

(2). Tanguy, D.; Marchal, P. *Trans IchemE* **1996**, vol. 74, Part A, 715-722.

(3). Mullin, J. W. *Cyrstallization*, 3rd ed.; Butterworth-Heinemann: Oxford, 1997.

(4). Bohlin, M., Rasmuson, A., C. *Can. J. Chem. Eng.* **1992**, 70, 120-126.

(5). Dunuwila, D. D.; Carroll, L., B.; Berglund, K., A. *J. Cryst. Growth* **1994**, 137, 561-568.

(6). Dunuwila, D. D.; Berglund, K., A. *J. Cryst. Growth* **1997**, 179, 185-193.

(7). Dunuwila, D. D., *An Investigation of the Feasibility of Using in situ ATR FTIR Spectroscopy in the Measurement of Crystallization Phenomena for Research and Development of Batch Crystallization Process*, Dissertation, Department of Chemical Engineering, Michigan State University, 1996.

(8). Lewiner, F.; Fevotte, G.; Klein, J. P.; Puel, F. *Chem. Eng. Sci.* **2001**, 56, 2069-2084.

(9). Lewiner, F.; Fevotte, G.; Klein, J. P.; Puel, F. *J. Cryst. Growth* **2001**, 226, 348-362.

**(10).** Togkalidou, T.; Fujiwara, M. *J. Cryst. Growth* **2001**, 231, 534-543.

# Chapter 5

## STUDY OF THE INHIBITION EFFECT OF FRUCTOSE AND GLUCOSE ON SUCROSE CRYSTALLIZATION*

**Study using Raman spectroscopy was conducted by Javier Falcon.*

The inhibition of sucrose crystallization by non-sucrose sugars is of particular interest to product development in the food industry. To investigate the possible mechanisms of this inhibition, fluorescence and Raman spectroscopic techniques were applied to investigate the thermodynamic and kinetic properties of sucrose solutions with fructose and glucose as impurities. When the overall sugar content is kept the same, both fructose and glucose decrease the viscosity of sucrose solutions, while glucose increases the water activity and fructose decreases the water activity. Fructose takes on an open chain form, a molecular conformation different than the one in crystalline form, at a much higher concentration than glucose does. It is proposed that fructose and glucose inhibit crystallization of sucrose in different ways. It is also demonstrated that fluorescence and Raman spectroscopic techniques can be adapted to monitor and control industrial sucrose crystallizations at high concentration and high temperature.

### 5.1 Introduction

The crystallization of sucrose is important in the processing and storage of food products.[1] While a great deal of research has been performed on bulk crystallization of sucrose that is practiced in the production of sucrose from cane and beets, less attention has been devoted to crystallization conditions that exist during food processing. One of

the main differences in conditions is the intentional addition of non-sucrose sugars (in particular fructose and glucose) to sucrose solutions to inhibit crystallization in many food products.

Impurities are widely known to influence crystallization from solutions for virtually all compounds. While several research groups have studied the effect of fructose and glucose on the crystal growth of sucrose,[2-6] no study has been done on their effect on nucleation, which is an equally important aspect in the crystallization process. Impurities can affect nucleation either thermodynamically or kinetically. Under thermodynamic control, impurities are believed to affect the solubility of the target compound (e.g. the common ion effect). Under kinetic control, impurities can alter mass transfer related physical properties such as viscosity, or they can disrupt the formation of solution aggregates that are the basis for nucleation by assuming molecular conformations different than the one in crystalline form, or by absorbing to the target molecule as "tailor made" impurities. It is also possible that more than one of the aforementioned mechanisms can be operative simultaneously.

In the present work the inhibition of sucrose crystallization by fructose and glucose was studied by fluorescence and Raman spectroscopic methods. These two spectroscopic techniques can be used to investigate the solution properties such as water activity, viscosity and molecular conformation, all of which can affect crystallization processes significantly. Both techniques can be applied to process monitor and quality control at industrial environment. Insights on the mechanisms of sucrose crystallization inhibition are expected to guide new food formulation development.

## 5.2 Experimental Section

The sucrose, glucose and fructose were provided by the Kellogg Company, Battle Creek, MI and used as received. Pyranine and carminic acid were obtained from Sigma. Distilled, deionized water was used in all the measurements. A Fluorolog-2 from Jobin-Yvon Inc. was used for all the steady state fluorescence measurement. A Hololab 1000 series from Kaiser Optical Systems Inc. equipped with 632.8nm laser was used for the collection of Raman spectra. Solution temperatures were regulated using a CN76000 temperature controller (Omega Engineering, Inc., Stamford, CT).

### *5.2.1 Sample Preparation for Steady State Fluorescence Measurements*

Pyranine and carminic acid were chosen as the fluorescence probe molecules. Different amounts of sucrose, glucose, fructose and water were carefully weighted out according to Table 5.1, then 1ml of pyranine or carminic acid stock solution was added to each of the mixture sugar solution to get 20ppm pyranine or 30ppm carminic acid. The sample was briefly heated to the boiling point to dissolve all sugar solids, about 3ml of this clear solution was transferred to a quartz cuvette in a temperature controlled sample holder in the fluorescence spectrometer. Ten to fifteen minutes were allowed for the sample to reach equilibrium temperature before a measurement was carried out. The predetermined temperatures were every 10°C interval between 70°C and 110°C. Each sample was freshly made up at each temperature to minimize the effect of sucrose hydrolysis at high temperatures. A 4 factor experimental design was applied to optimize the number of replicate runs for each sample at each temperature.

**Table 5.1.** Composition of Samples for fluorescence Measurement (Brix represents total sugar percent by weight.)

| BRIX | SUCROSE (g) | FRUCTOSE (g) | GLUCOSE (g) | Water (g) |
|---|---|---|---|---|
| 87 | 47 | 0 | 40 | 12 |
| 87 | 47 | 20 | 20 | 12 |
| 87 | 47 | 40 | 0 | 12 |
| 83.5 | 43.5 | 0 | 40 | 15.5 |
| 83.5 | 43.5 | 20 | 20 | 15.5 |
| 83.5 | 43.5 | 40 | 0 | 15.5 |
| 80 | 40 | 0 | 40 | 19 |
| 80 | 40 | 20 | 20 | 19 |
| 80 | 40 | 40 | 0 | 19 |

### *5.2.2 Steady State Fluorescence Measurement*

Steady state fluorescence spectra were recorded for all the samples in the study of water activity in sucrose solutions. An excitation of 342nm was used for pyranine, with emission spectra collected at 400-650nm. An excitation of 310nm was used for carminic acid, with the emission spectra collected at 350-750nm.

Pyranine was used as the probe molecule in anisotropy measurements. Two polarization films were used before and after the sample chamber. Polarization emission spectra were collected with afore mentioned parameters. Anisotropy (r) was calculated by the peak intensity at 441nm with the films in parallel position ($I_{II}$) and in perpendicular position ($I_{\perp}$) as in Equation 1.

$$r = \frac{I_{II} - I_{\perp}}{I_{II} + 2I_{\perp}} \tag{5.1}$$

Viscosity ($\eta$) is correlated with anisotropy by equation 2.

$$\frac{r_0}{r} = 1 + \frac{R_g T}{\eta V}\tau \tag{5.2}$$

Where $\eta$ is viscosity, T is the temperature of solution, $r_0$ is the anisotropy with no rotation, Rg is the gas constant, V is the volume of rotating unit and $\tau$ is fluorescence lifetime. An increase in viscosity $\eta$ would cause an increase in anisotropy r.

### *5.2.3 Raman Spectra of Pure Sugar Solutions*

Aqueous solutions of glucose, fructose and tagatose were prepared in 100-mL three-necked round bottom flasks in concentrations ranging from 80 to 87 weight percent using increments of 1.75 weight percent. For each specific solution at the specified concentrations Raman spectra were obtained at 70, 80, 90, 100 and 110°C.

Individual, "fresh" solutions were heated to above 110°C in order to dissolve all the crystalline material, using a heating rate of approximately 15 C/min. Once the solutions became clear, the temperature was lowered to 110°C and the solutions were allowed to equilibrate for ten minutes before a Raman spectrum was acquired. Next, the solutions were rapidly cooled to the closest lower temperature, allowed to equilibrate and a Raman spectrum was acquired. This cooling procedure was repeated at all temperatures.

## 5.3 Results and Discussion

### *5.3 1 Emission Properties of Fluorescence Probe Molecules*

Pyranine and carminic acid were used as the fluorescence molecules to probe the water activity in sucrose solutions,[7] and their chemical structures are shown in Figure 5.1. The common characteristic for these two molecules is the equilibrium between protonated form and deprotonated form when dissolved in water, the deprotonated form dominates when there is enough water to interact with the probe molecule, while the protonated form dominates when there isn't enough water to interact with the probe molecule. Their emission properties in sucrose aqueous solutions are shown in Figure 5.2. When excited at 342nm, pyranine emits light at 517nm due to the deprotonated form and at 441nm due

to the protonated form. More water molecules interacting with pyranine results in higher peak intensity at 517nm or lower peak intensity at 441nm. Thus the peak intensity ratio (PIR) between 517nm and 441nm indicates the water activity sensed by pyranine. Similarly, when excited at 310nm, carminic acid emits light at 591nm due to the deprontonated form and at 419nm due to the protonated form. The PIR between 591nm and 419nm indicates the water activity sensed by carminic acid.

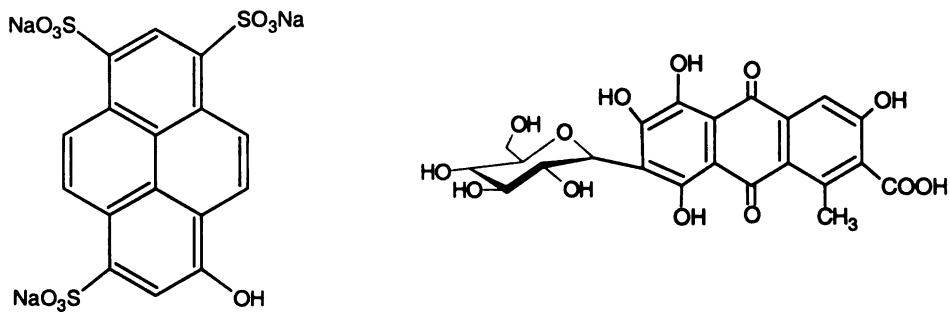


*Figure 5.1 Chemical structures of pyranine (left) and carminic acid (right).*

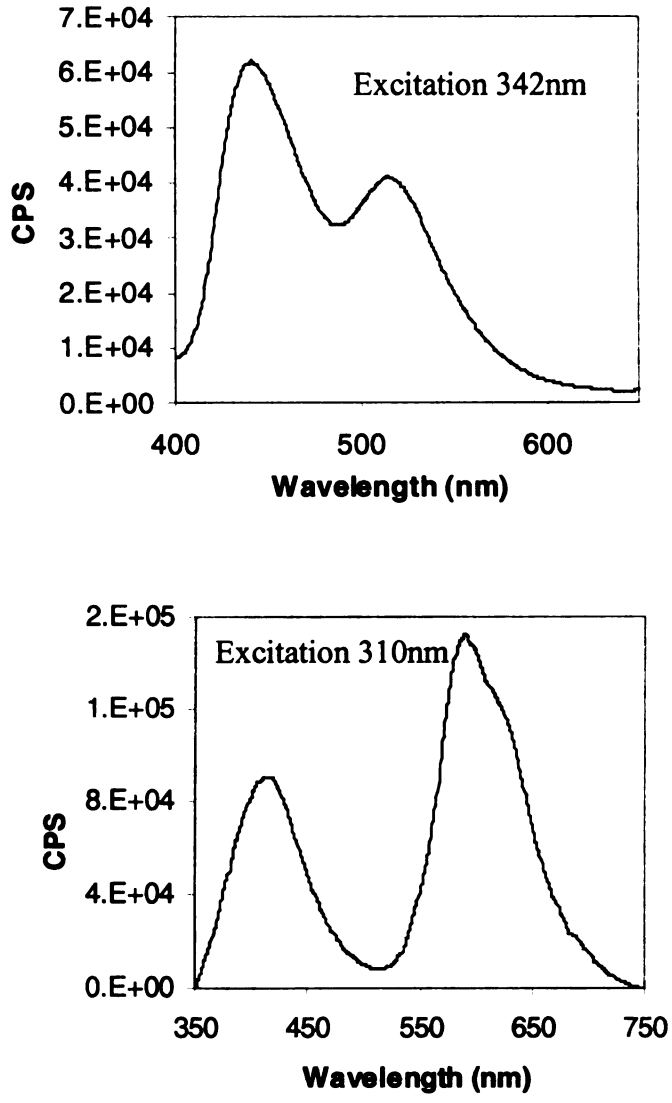


*Figure 5.2 Fluorescence spectrum of 20ppm pyranine (top, peak at 441nm is due to the protonated form, peak at 517nm is due to deprotonated form.) and 30ppm carminic acid (bottom peak at 419nm is due to protonated form, peak at 591nm is due to deprotonated form.) in sucrose solution at 80℃.*

Both pyranine and carminic acid are used to investigate water activity in sucrose solution in similar way, but these two molecules are probing different phases of the sucrose solution. The carminic acid molecule has a glucosyl unit, which renders it the ability to closely interact with sucrose molecules and sense the water availability in the vicinity of sucrose molecules[14]. In contrast, pyranine has no structure similarity with sucrose molecule, thus stays in the bulk water phase in sucrose solution and senses the water availability in bulk water phase.

### *5.3.2 Effect of Glucose and Fructose on Water Activity of Sucrose Solutions*

The coupled effect of glucose and fructose on water activity in sucrose solutions was measured by using pyranine as the probe molecule is shown in Figure 5.3. A decrease in PIR is observed with increasing amount of fructose and decreasing amount of glucose within temperature range 70~110°C and total solid concentration of 80~87%. The decreased PIR indicates a decrease in the amount of free water in bulk water phase. This observation is corroborated by the PIR measurement using carminic acid (Figure 5.4) under the same conditions. With carminic acid as the probe molecule, PIR increases with increased amount of fructose and decreased amount of glucose. Because of the structural similarity between carminic acid and sucrose, it interacts closely with the sucrose. The equilibrium reaction between the protonated and deprontonated carminic acid is affected by the water availability in the vicinity of sucrose instead of in the bulk water phase. Thus increasing PIR for carminic acid indicates that sucrose is highly solvated by water with increasing amount of fructose and decreasing amount of glucose in sucrose solutions.

Figure 5.5 shows the separate effect of fructose and glucose on PIR of pyranine in sucrose solution. Comparing to the pure 80% sucrose solution at 90°C, the PIR of 40% sucrose with 40% fructose binary mixture is decreased, and the PIR of 40% sucrose with 40% glucose is increased.

Combined data in figure 5.3~5.5 confirm that fructose and glucose have opposite effects on water activity in sucrose solutions, fructose decreases water activity and glucose increases water activity. This conclusion is no surprise considering the solubility is in the order of fructose>sucrose>glucose. With fructose in the solution more water molecules are kept in the hydration shell of solute molecules, while with glucose in the solution more water molecules are kept in the bulk water phase. According to crystallization theory, increased water activity corresponds to lower supersaturation, which should leads to the inhibition of nucleation. While this theory may explain the inhibition effect of glucose on sucrose crystallization, it does not explain the inhibition effect of fructose on sucrose crystallization. It appears that fructose and glucose could be working under different mechanisms when inhibiting the crystallization of sucrose. At least it is appropriate to conclude that thermodynamic water activity alone doesn't explain the inhibition effect by both fructose and glucose in sucrose crystallization.

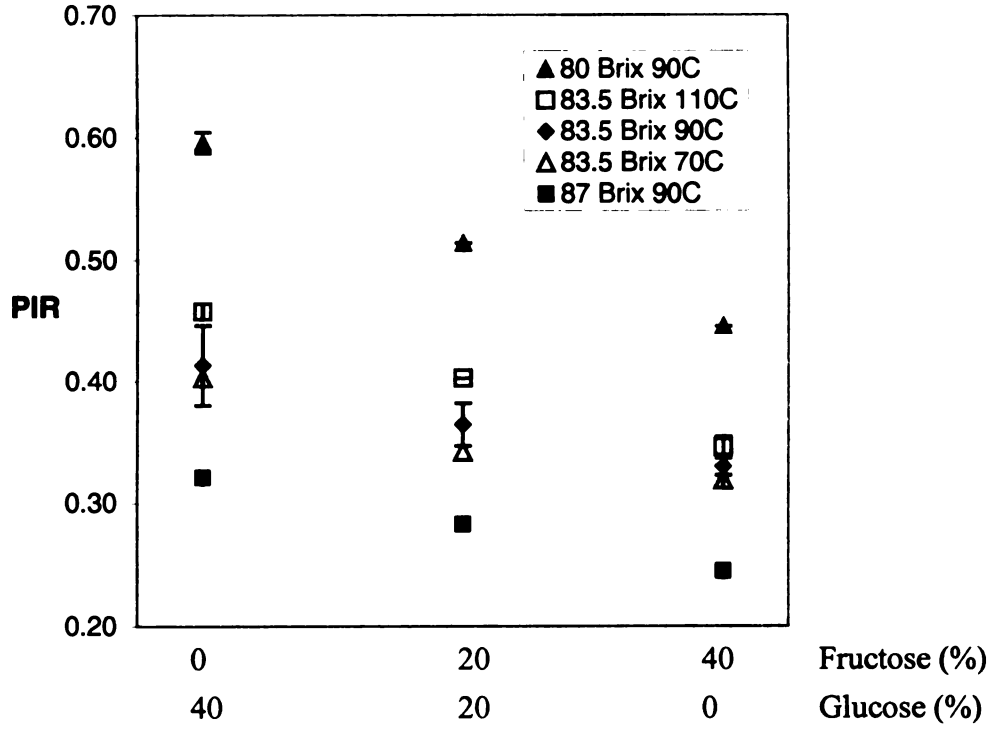


*Figure 5.3 PIR of pyranine in sucrose solutions at different temperature with different amount of fructose and glucose. Brix represents total sugar percent by weight. Data at other compositions and temperatures show the same trend, thus not shown here.*

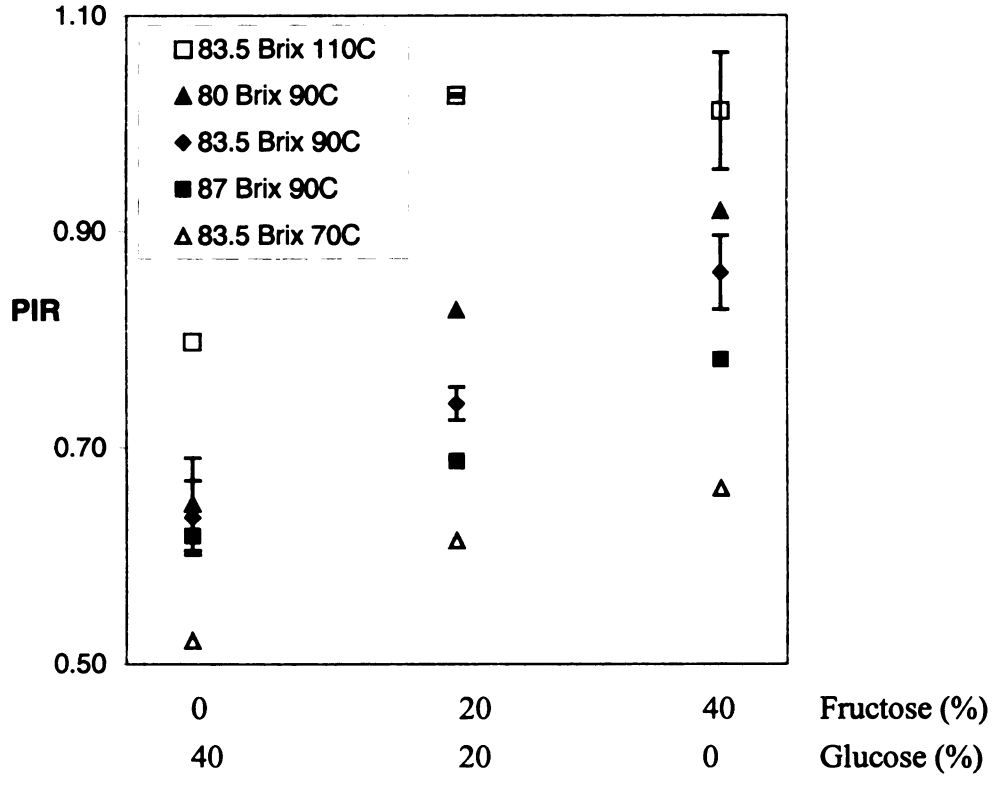


*Figure 5.4 PIR of carminic acid in sucrose solutions at different temperature with different amount of fructose and glucose. Brix represents total sugar percent by weight. Data at other compositions and temperatures show the same trend, thus not shown here.*

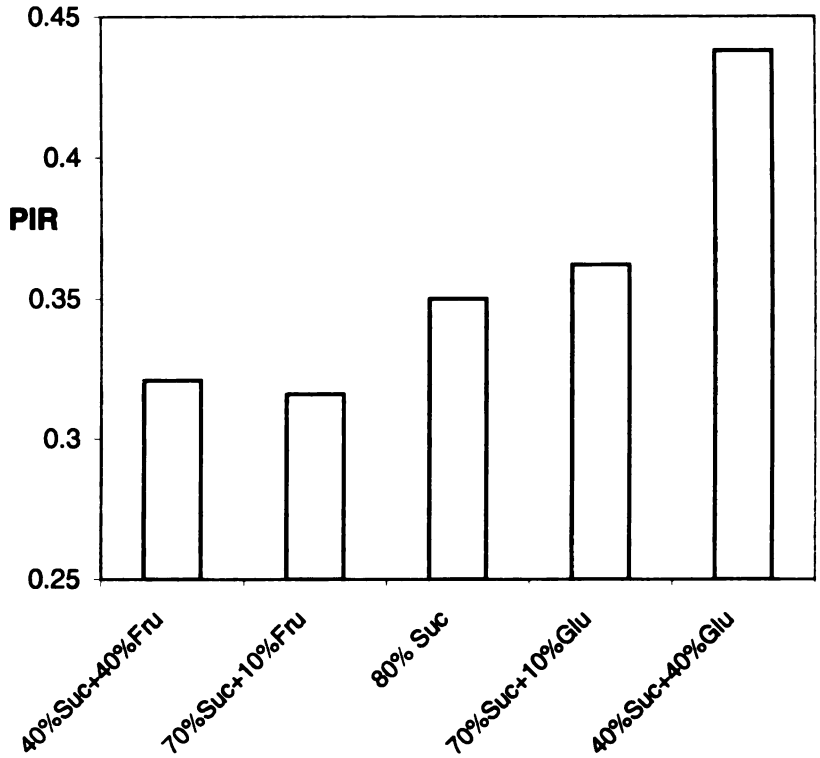


*Figure 5.5 Separate effects of fructose and glucose on the PIR of pyranine in sucrose solution at 90℃ (total sugar content is 80%).*

### *5.3.3 Effect of Glucose and Fructose on Viscosity of Sucrose Solutions*

The coupled effect of increasing fructose concentration and decreasing glucose concentration is shown in figure 5.6. Anisotropy of pyranine in sucrose solution increases with increasing amount of fructose and decreasing amount of glucose. Figure 5.7 shows the separate effect of fructose and glucose in 80% sugar solutions at 90°C. Both fructose and glucose decrease the anisotropy of pyranine in sucrose solution, which indicate that both fructose and glucose decrease the viscosity of sucrose solutions under the condition of this study. Glucose is more effective than fructose.

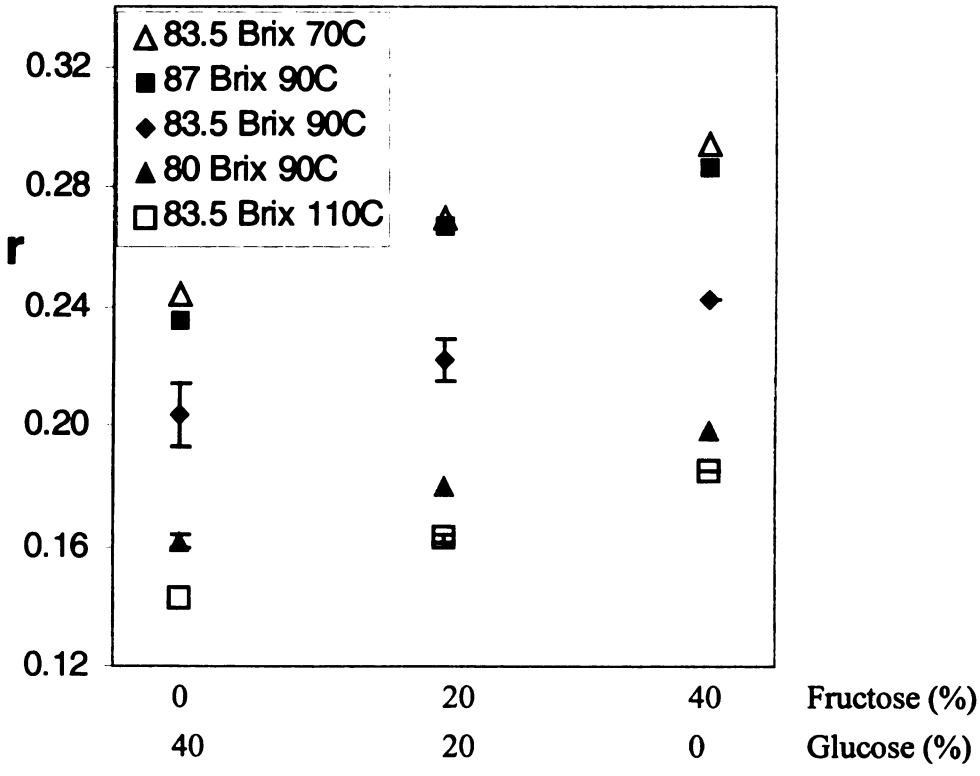


*Figure 5.6 Anisotropy of pyranine in sucrose solutions at different temperature with different amount of fructose and glucose. Brix represents total sugar percent by weight. Data at other compositions and temperatures show the same trend, thus not shown here.*

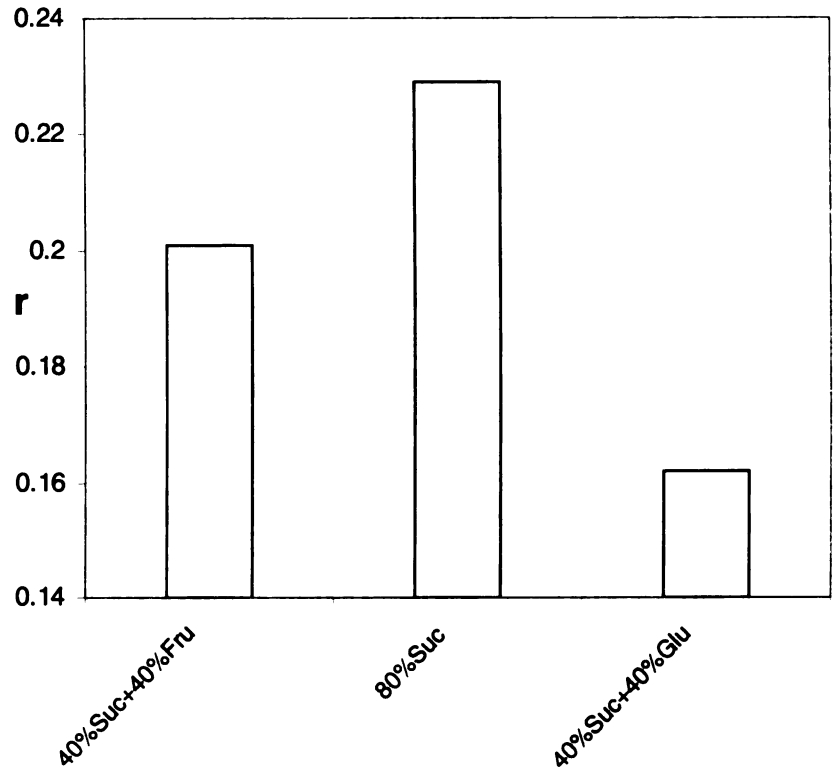


*Figure 5.7 Separate effects of fructose and glucose on the anisotropy r of pyranine in sucrose solution at 90℃ (total sugar content is 80%).*

This conclusion is contradictory to the long held beliefs in industrial sugar crystallization. Fructose has long been considered to increase the viscosity of sucrose and cause inhibition of sucrose crystallization by viscosity effects. Only a handful of studies on the direct viscosity measurement for sucrose/glucose/fructose system can be found in the literature. Zumalacarregui de Cardenas et al.[8] and Smythe[9] found that the viscosity of

sucrose solutions increases with the concentration of glucose and/or fructose. A closer look at their experimental conditions revealed that Zumalacarregui de Cardenas et al. kept the same sucrose/water ratio and added in glucose or fructose, while Smythe kept the same supersaturation level for sucrose and added in invert sugar. In both cases, the overall solid content is increased as glucose and/or fructose is added, which is the real cause for viscosity increase.

Mazurkiewicz et al.[10] showed that the viscosity of solutions with the same mass concentration is in the order of pure disaccharide > disaccharide-monosaccharide mixture > pure monosaccharide. Mathlouthi et al.[11] and Vazquez Una et al.[12] measured the kinematic and intrinsic viscosity of pure solution of sucrose, glucose and fructose. Both groups showed that the viscosity of pure glucose or fructose is always lower than that of the pure sucrose solution at comparative mass concentration. It is worth noting that normally the viscosity of solution has a great dependence on molecular weight when comparing the same type of chemicals species. These literature data proved our conclusion that both fructose and glucose reduce the viscosity of sucrose solutions when the overall solid content is kept the constant.

A reduced viscosity should promote crystallization by increasing the mass transfer efficiency. In fact both glucose and fructose inhibit the crystallization in sucrose solutions despite their reduction effect on viscosity. This observation leads us to believe that viscosity is not the controlling factor in inhibition of sucrose crystallization by fructose or glucose.

### *5.3.4 Molecular Conformation Effect of Glucose and Fructose on Sucrose Solution*

When dissolved in water, fructose and glucose can exist in isomeric forms with molecular conformations different than that in crystalline form. Molecules in these conformations have to go through conformational change in order to be integrated in crystal lattice. This process takes energy and time, and the conditions in industrial sucrose crystallization may not allow this process to occur, thus impede the nucleation and crystal growth.

Raman spectroscopy allows us to probe the molecular structure and conformation of different sugars in solution and make a correlation with the inhibition ability of fructose and glucose. Figure 5.8 and 5.9 shows the Raman spectra of 87% fructose and 87% glucose in water at different temperature. A peak at 1730cm$^{-1}$ is of particular interest to us. It shows up in the fructose solution at high temperature, but not in glucose solution at any temperature. Literature search confirmed that this peak is from the carbonyl group in the open chain form of fructose[13]. While glucose also has the open chain form, its concentration is too low to be detected by Raman spectroscopy. This open chain form can't be integrated into crystalline form, which may play a role in sucrose crystallization inhibition by fructose. The relatively large amount of fructofuranose form due to complex mutarotation in fructose solution may also play a role at slowing down the crystallization process, since only the fructopyranose form can be integrated into the crystal lattice. Raman spectroscopy thus can be used to predict the inhibition ability of sugar by probing their conformations in solution.

Another reducing sugar, tagatose, is expected to be a good inhibitor to sucrose crystallization. The Raman spectra of tagatose (Figure 5.10) also show the peak at 1730cm$^{-1}$, which indicates that the concentration of its open chain form at high

temperature is significant. It is possible that tagatose and fructose inhibit sucrose crystallization by the same mechanism: disrupting the aggregation process by assuming uncrystallizable conformations.

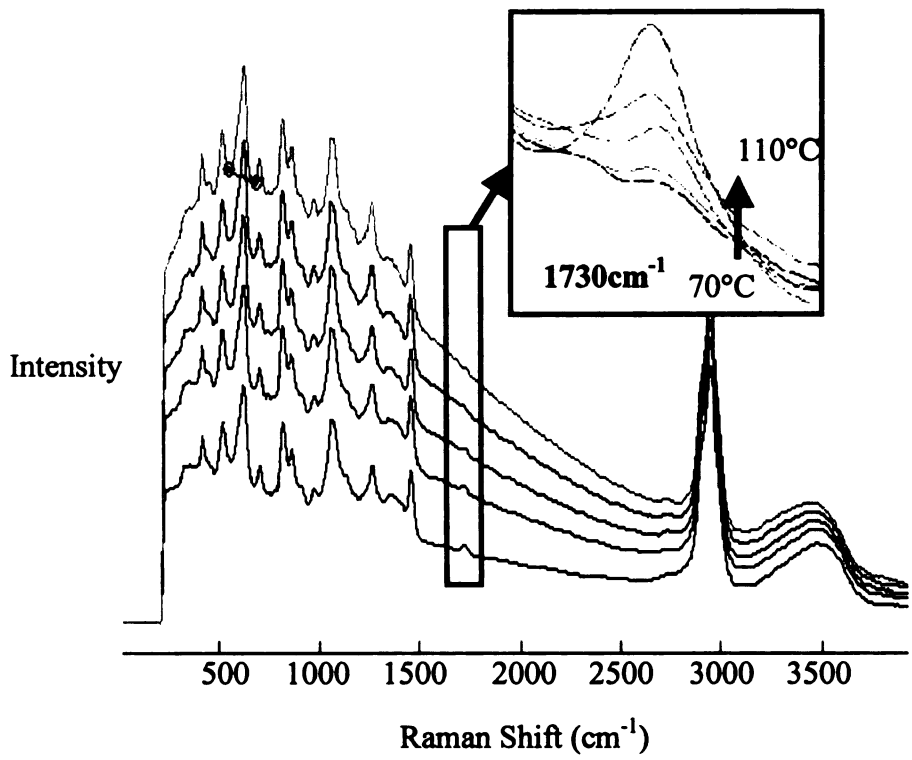


*Figure 5.8 Raman spectra of 87% fructose solutions at different temperature*

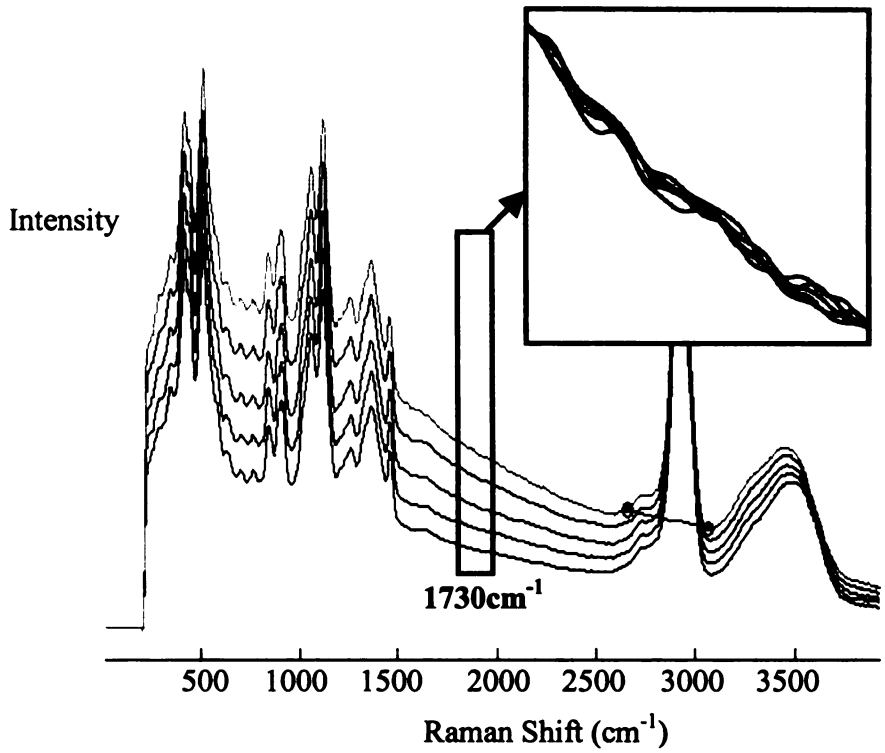


*Figure 5.9 Raman spectra of 87% glucose solutions at different temperature*

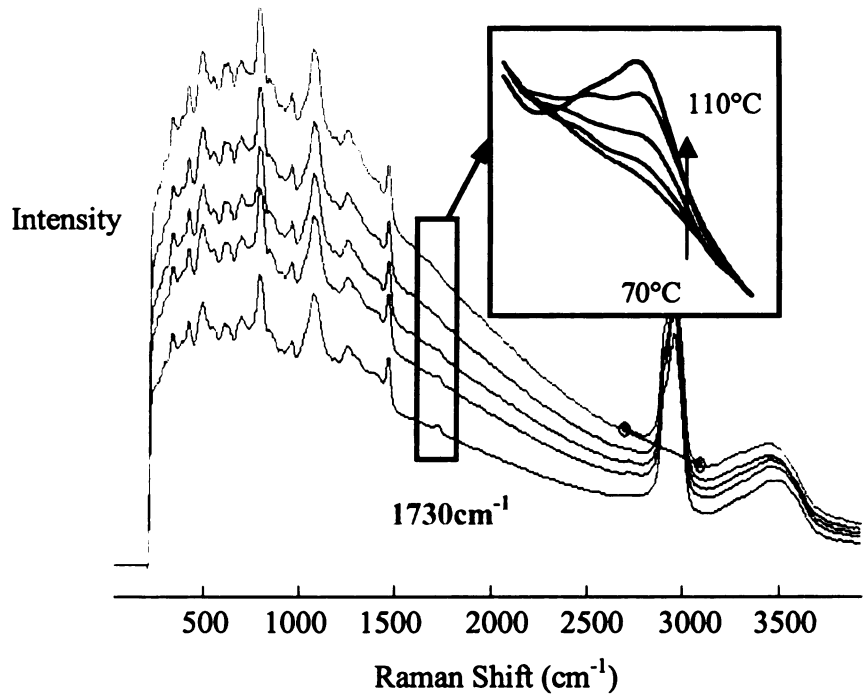


*Figure 5.10 Raman spectra of 87% tagatose solutions at different temperature*

## 5.4 Conclusions

We demonstrated that both fluorescence and Raman spectroscopy can be used to investigate sugar crystallization at conditions relevant to industrial food processing. Fluorescence spectroscopy enables us to probe both thermodynamic and kinetic properties of solutions such as water activity and viscosity on a microscopic scale. Raman provides structural information on a molecular level.

These techniques can be used not only to monitor the sucrose crystallization process, but also to aid the study of the inhibition mechanism by non-sucrose sugars. Our initial study suggests that fructose and glucose may be working under different mechanisms when inhibiting the crystallization of sucrose. Glucose is more effective at increasing the water activity of sucrose solution, thus lowering the driving force for crystallization-supersaturation, while fructose tends to assume molecular conformations different than the one in crystalline form, thus interrupt the aggregation process during nucleation. Contrary to the industrial believe, viscosity may not be a significant factor in inhibiting sucrose crystallization by either fructose or glucose according to this study.

## 5.5 Acknowledgements

The authors wish to thank Kellogg Company for financial support of this study. Tony Gualtieri from Kellogg Company helped with experimental design and data analysis. Help with fluorescence instrumentation from Dr. Gary Blanchard of the Department of Chemistry at Michigan State University is also appreciated.

## 5.6 References


(1). Hartel, R. W. *Crystallization in Foods*, Aspen Publishing: Gaithersburg, **2001.**

(2). Hartel, R. W.; Shastry, A. V. *Critical Review in Food Science and Nutrition*, **1991**, 1(1), 49-112.

(3). Sgaldino, G.; Aquilano, D.; Vaccari, G.; Mantovani, G. *Cryst. Res. Technol.*, **1997**, 32(8), 1057-1065.

(4). Sgaldino, G.; Aquilano, D.; Vaccari, G.; Mantovani, G. *J. Cryst. Growth*, **1998**, 192, 290-299.

(5). Dohl, B.; Follner, H. *Cryst. Res. Technol.*, **1992**, 27(1), 3-12.

(6). Wang, B. G.; Krafczyk, S.; Follner, H. *J. Cryst. Growth*, **2000**, 219, 67-74.

(7). Chakraborty, Reena; Berglund, Kris A. *J. Cryst. Growth*, **1992**, 125(1-2), 81-96.

(8). Zumalacarregui de Cardenas, Lourdes; Ruiz Cruz, Carlos; Guerra Deben, Jorge. *Centro Azucar*, **1988**, 15(3), 57-66.

(9). Smythe, B.M. *Aust. J. Chem.*, **1967**, 20, 1097-111.

(10). Mazurkiewicz, Jozef; Nowotny-Rozanska, Maria. *Polish Journal of Food and Nutrition Sciences*, **1998**, 7(2), 171-180.

(11). Mathlouthi, M.; Hutteau, F.; Angiboust, J. F. *Food Chemistry*, **1996**, 56(3), 215-221.

(12). Vazquez Una, G.; Chenlo Romero, F.; Alvarez Dacosta, E.; Moreira Martinez, R.; Pardo Calvo, P. *J. Chem. Eng. Data*, **1994**, 39, 87-89.

(13). Yaylayan, V. A.; Ismail, A. A. *Journal of Carbohydrate Chemistry,* **1992**, 11(2), 149-58.

(14). Rasimas, J.P.; Berglund, K.A.; Blanchard, G.J., Journal of Physical Chemistry, 1996, 100 (42), 17034-17040.

# Chapter 6

# CONCLUSIONS AND FUTURE WORK

## 6.1 Conclusions

This dissertation focuses on the study of monitoring and control of crystallization processes using spectroscopic methods, including Raman, ATR-FTIR and fluorescence. The goals are to optimize the crystallization process for desired crystal size distribution or polymorph form and to understand the kinetics during various crystallization processes with the help from aforementioned spectroscopic methods.

In chapters 2 and 3, Raman spectroscopy was used as a convenient process development tool for on line and *in situ* characterization of acetaminophen polymorph forms in slurries. Metastable polymorphs of acetaminophen were crystallized reproducibly by pre-heating the solution at higher temperature and cooling the solution down at a faster rate. Higher water content in mixtures of ethanol and water also favors the trihydrate form, which has only limited stability at room temperature. Both Raman and ATR-FTIR spectroscopies were employed to monitor the solvent mediated acetaminophen polymorph transformation process. Complimentary information about solid phase polymorph form and solution phase concentration suggest that crystallization of the more stable form of acetaminophen polymorph is rate limiting during transformation, with nucleation limiting the form II to I transformation and crystal growth limiting the form T to II transformation, respectively.

Applying chemometric data analysis methods such as MCR allowed us to quantitatively follow a complex polymorph transformation processes without the need of building a calibration model.

ATR-FTIR coupled with a LABMAX® automatic reactor system used to optimize cooling curves by *in situ* feedback control of the supersaturation level was discussed in chapter 4. A straightforward and efficient calibration procedure was developed to obtain optimal cooling profiles in an easy, fast and flexible way, which is preferred by industrial users. This approach does not rely on kinetic models and precludes the error caused by inaccurate kinetic data, thus is useful in determining the cooling policy in situations where kinetic data are not available. The succinic acid crystals resulting from the controlled process possess a larger mean size with more uniform size distribution than those from the uncontrolled case.

Fluorescence and Raman spectroscopies were used to investigate sucrose crystallization at conditions relevant to industrial food processing in chapter 5. Water activity and viscosity probed by fluorescence spectroscopy together with molecular structure probed by Raman spectroscopy suggest that fructose and glucose may be working under different mechanisms when inhibiting the crystallization of sucrose. Glucose is more effective at increasing the water activity of sucrose solution, thus lowering the driving force for crystallization-supersaturation, while fructose tends to assume molecular conformations different than the one in crystalline form, thus interrupt the aggregation process during nucleation. Contrary to the industrial believe, viscosity may not be a significant factor in inhibiting sucrose crystallization by either fructose or glucose according to this study.

## 6.2 Future Work

Spectroscopic methods have shown great advantage in on line monitoring and control of crystallization processes. Their potential is yet to be realized in crystallizations in real industrial environment, e.g., the crystallization species may be a more complex polymorphic system, or the spectra may experience more interference from impurities in raw material. Methods developed in this study can be tested in such environment in future studies. Besides the crystallization process monitoring and control, the possibility of using these spectroscopic methods should also be explored for down stream processes such as filtration and drying.

Combined with multivariate curve resolution (MCR), Raman spectroscopic method provided both selectivity and sensitivity for acetaminophen polymorph transformation process analysis. One possible study is to test the reproducibility of such analysis. With good reproducibility, these type of methods can be used in real time monitoring and quantitative analysis.

The mechanisms of controlling acetaminophen polymorph crystallization were proposed in chapter 2. More experiments need to be carried out to confirm how thermal history and solvent composition affect the crystallization process. Other analytical techniques such as solution NMR or photon correlation spectroscopy (PCS) may be used to measure solution structure change after different thermal treatments.

# APPENDICES

Table A.1. Data for figure 2.5. Solubility curve of acetaminophen form I in ethanol/H2O mixture solvent.

| | | | | | | |
|---|---|---|---|---|---|---|
| Temperature ( C ) | 0 | 10 | 20 | 30 | 40 | 50 |
| Solubility in 0% ethanol (wt%) | 0.7 | 0.9 | 1.3 | 1.7 | 2.4 | 3.3 |
| Temperature ( C ) | 0 | 10 | 25 | 30 | 41 | 50 |
| Solubility in 25% ethanol (wt%) | 2.4 | 4.0 | 6.1 | 7.6 | 11.8 | 16.8 |
| Temperature ( C ) | 0 | 10 | 20 | 30 | 41 | 50 |
| Solubility in 50% ethanol (wt%) | 7.5 | 10.6 | 14.4 | 18.7 | 25 | 30.5 |
| Temperature ( C ) | 0 | 10 | 20 | 30 | 42 | 49 |
| Solubility in 75% ethanol (wt%) | 14.3 | 15.9 | 19.7 | 25.4 | 32.3 | 36.1 |
| Temperature ( C ) | 0 | 10 | 20 | 30 | 40 | 50 |
| Solubility in 100% ethanol (wt%) | 9.6 | 10.7 | 13.3 | 16.9 | 21.6 | 25.7 |

Table A.2. Data for Figure 2.6. Solubility curve of acetaminophen polymorphs in ethanol:H2O=1:3..

| Temperature ( C ) | Solubility for I (wt%) | Standard error | Solubility for II (wt%) | Standard error | Solubility for T (wt%) | Standard error |
|---|---|---|---|---|---|---|
| -10 | 1.01 | 0.017 | 1.20 | 0.082 | 1.12 | 0.044 |
| -5 | 1.34 | 0.023 | 1.55 | 0.077 | 1.75 | 0.038 |
| 0 | 1.79 | 0.011 | 2.06 | 0.041 | 2.50 | 0.132 |
| 5 | 2.28 | 0.026 | 2.75 | 0.03 | 3.80 | 0.076 |
| 10 | 2.94 | 0.025 | 3.47 | 0.007 | N/A | N/A |

Table A.3. Data for Figure 3.2. Crystallization and transformation profile represented by peak height at 1237cm$^{-1}$. For the peak height profile from un-normalized spectra, a factor of 0.001 has been multiplied to bring it to the same scale as the normalized profile.

| Time (Hour) | Peak Height at 1237cm-1 Normalized | Peak Height at 1237cm-1 un-normalized (x0.001) | Time (Hour) | Peak Height at 1237cm-1 Normalized | Peak Height at 1237cm-1 un-normalized (x0.001) |
|---|---|---|---|---|---|
| 0.00 | 0.75 | 1.57 | 6.15 | 0.12 | 0.35 |
| 0.07 | 0.75 | 2.09 | 6.48 | 0.11 | 0.33 |
| 0.13 | 0.74 | 1.99 | 6.82 | 0.12 | 0.34 |
| 0.20 | 0.74 | 2.02 | 7.40 | 0.11 | 0.32 |
| 0.32 | 0.72 | 1.91 | 7.73 | 0.11 | 0.31 |
| 0.38 | 0.44 | 0.56 | 8.07 | 0.12 | 0.30 |
| 0.45 | 0.41 | 0.45 | 8.65 | 0.11 | 0.30 |
| 0.57 | 0.42 | 0.56 | 8.98 | 0.12 | 0.28 |
| 0.63 | 0.41 | 0.56 | 9.32 | 0.12 | 0.27 |
| 0.70 | 0.42 | 0.58 | 9.90 | 0.11 | 0.29 |
| 0.82 | 0.42 | 0.58 | 10.23 | 0.12 | 0.26 |
| 0.88 | 0.40 | 0.57 | 10.57 | 0.12 | 0.26 |
| 0.95 | 0.41 | 0.58 | 11.15 | 0.12 | 0.27 |
| 1.07 | 0.40 | 0.61 | 11.48 | 0.12 | 0.26 |
| 1.13 | 0.40 | 0.61 | 11.82 | 0.12 | 0.25 |
| 1.20 | 0.39 | 0.61 | 12.40 | 0.11 | 0.24 |
| 1.32 | 0.38 | 0.61 | 12.73 | 0.12 | 0.25 |
| 1.38 | 0.39 | 0.62 | 13.07 | 0.13 | 0.25 |
| 1.45 | 0.38 | 0.63 | 13.65 | 0.13 | 0.27 |
| 1.57 | 0.39 | 0.61 | 13.98 | 0.15 | 0.28 |
| 1.63 | 0.39 | 0.66 | 14.32 | 0.19 | 0.30 |
| 1.70 | 0.38 | 0.64 | 14.90 | 0.34 | 0.39 |
| 1.82 | 0.39 | 0.61 | 15.23 | 0.53 | 0.55 |
| 1.88 | 0.39 | 0.61 | 15.57 | 0.80 | 0.91 |
| 1.95 | 0.39 | 0.63 | 16.15 | 0.86 | 0.87 |
| 2.40 | 0.38 | 0.66 | 16.48 | 0.85 | 0.88 |
| 2.73 | 0.36 | 0.66 | 16.82 | 0.84 | 0.88 |
| 3.07 | 0.34 | 0.62 | 17.40 | 0.85 | 0.91 |
| 3.65 | 0.28 | 0.54 | 17.73 | 0.85 | 0.86 |
| 3.98 | 0.23 | 0.51 | 18.07 | 0.83 | 0.85 |
| 4.32 | 0.19 | 0.45 | 18.65 | 0.84 | 0.82 |
| 4.90 | 0.12 | 0.41 | 18.98 | 0.84 | 0.80 |
| 5.23 | 0.12 | 0.41 | 19.32 | 0.84 | 0.78 |
| 5.57 | 0.12 | 0.40 | 19.65 | 0.84 | 0.80 |

Table A.4. Data for Figure 3.4. Scores for principal components from MCR analysis of acetaminophen polymorph crystallization and transformation.

| Time (Hours) | PC1 | PC2 | PC3 | PC4 | Time (Hours) | PC1 | PC2 | PC3 | PC4 |
|---|---|---|---|---|---|---|---|---|---|
| 0.00 | 1.87E-02 | 3.55E-02 | 9.33E-02 | 3.64E-02 | 6.07 | 5.38E-03 | 2.87E-03 | 2.43E-03 | 4.81E-02 |
| 0.07 | 1.62E-02 | 3.57E-02 | 8.99E-02 | 4.06E-02 | 6.40 | 4.95E-03 | 2.63E-03 | 2.97E-03 | 4.73E-02 |
| 0.13 | 1.67E-02 | 3.56E-02 | 8.93E-02 | 3.98E-02 | 6.73 | 5.08E-03 | 2.71E-03 | 2.83E-03 | 4.73E-02 |
| 0.20 | 1.88E-02 | 3.52E-02 | 8.74E-02 | 3.77E-02 | 7.07 | 4.64E-03 | 2.46E-03 | 3.54E-03 | 4.73E-02 |
| 0.27 | 1.93E-02 | 3.54E-02 | 8.61E-02 | 3.88E-02 | 7.40 | 4.89E-03 | 2.77E-03 | 2.66E-03 | 4.77E-02 |
| 0.33 | 8.99E-02 | 1.99E-02 | 2.90E-02 | 6.89E-03 | 7.73 | 4.52E-03 | 2.51E-03 | 2.86E-03 | 4.71E-02 |
| 0.40 | 1.01E-01 | 1.72E-02 | 2.12E-02 | 4.10E-03 | 8.07 | 5.03E-03 | 2.86E-03 | 2.50E-03 | 4.76E-02 |
| 0.47 | 9.88E-02 | 1.46E-02 | 2.29E-02 | 4.73E-03 | 8.40 | 6.14E-03 | 2.73E-03 | 2.97E-03 | 4.68E-02 |
| 0.53 | 1.01E-01 | 1.55E-02 | 2.29E-02 | 3.65E-03 | 8.73 | 4.62E-03 | 2.48E-03 | 4.20E-03 | 4.71E-02 |
| 0.60 | 1.00E-01 | 1.56E-02 | 2.41E-02 | 5.87E-03 | 9.07 | 4.76E-03 | 2.58E-03 | 4.12E-03 | 4.71E-02 |
| 0.67 | 9.73E-02 | 1.44E-02 | 2.32E-02 | 6.78E-03 | 9.40 | 5.58E-03 | 2.73E-03 | 2.06E-03 | 4.79E-02 |
| 0.73 | 9.83E-02 | 1.44E-02 | 2.37E-02 | 6.73E-03 | 9.73 | 5.54E-03 | 2.89E-03 | 1.76E-03 | 4.86E-02 |
| 0.80 | 9.52E-02 | 1.43E-02 | 2.57E-02 | 5.64E-03 | 10.07 | 5.26E-03 | 2.59E-03 | 3.53E-03 | 4.77E-02 |
| 0.87 | 9.71E-02 | 1.43E-02 | 2.42E-02 | 6.17E-03 | 10.40 | 4.94E-03 | 2.64E-03 | 4.52E-03 | 4.68E-02 |
| 0.93 | 9.90E-02 | 1.44E-02 | 2.27E-02 | 6.35E-03 | 10.73 | 5.33E-03 | 2.97E-03 | 2.48E-03 | 4.81E-02 |
| 1.00 | 1.00E-01 | 1.44E-02 | 2.31E-02 | 5.45E-03 | 11.07 | 4.91E-03 | 2.60E-03 | 3.93E-03 | 4.70E-02 |
| 1.07 | 9.96E-02 | 1.39E-02 | 2.35E-02 | 3.89E-03 | 11.40 | 5.47E-03 | 3.06E-03 | 1.99E-03 | 4.78E-02 |
| 1.13 | 9.87E-02 | 1.36E-02 | 2.45E-02 | 5.04E-03 | 11.73 | 5.60E-03 | 2.99E-03 | 1.78E-03 | 4.87E-02 |
| 1.20 | 9.98E-02 | 1.35E-02 | 2.31E-02 | 4.44E-03 | 12.07 | 4.95E-03 | 2.63E-03 | 4.72E-03 | 4.68E-02 |
| 1.27 | 9.86E-02 | 1.35E-02 | 2.28E-02 | 4.22E-03 | 12.40 | 5.21E-03 | 2.57E-03 | 3.29E-03 | 4.78E-02 |
| 1.33 | 9.71E-02 | 1.33E-02 | 2.27E-02 | 6.03E-03 | 12.73 | 5.01E-03 | 2.73E-03 | 3.04E-03 | 4.79E-02 |
| 1.40 | 9.97E-02 | 1.31E-02 | 2.35E-02 | 4.16E-03 | 13.07 | 5.15E-03 | 3.21E-03 | 3.65E-03 | 4.73E-02 |
| 1.47 | 9.95E-02 | 1.35E-02 | 2.38E-02 | 4.82E-03 | 13.40 | 5.10E-03 | 3.43E-03 | 2.69E-03 | 4.78E-02 |
| 1.53 | 1.00E-01 | 1.35E-02 | 2.32E-02 | 4.58E-03 | 13.73 | 5.18E-03 | 4.31E-03 | 4.34E-03 | 4.66E-02 |
| 1.60 | 1.00E-01 | 1.35E-02 | 2.14E-02 | 4.41E-03 | 14.07 | 4.61E-03 | 6.34E-03 | 2.92E-03 | 4.72E-02 |
| 1.67 | 9.90E-02 | 1.30E-02 | 2.16E-02 | 5.29E-03 | 14.40 | 5.16E-03 | 8.83E-03 | 2.82E-03 | 4.81E-02 |
| 1.73 | 9.90E-02 | 1.28E-02 | 2.28E-02 | 5.35E-03 | 14.73 | 4.66E-03 | 1.43E-02 | 4.11E-03 | 4.67E-02 |
| 1.80 | 9.83E-02 | 1.32E-02 | 2.15E-02 | 5.53E-03 | 15.07 | 4.52E-03 | 2.47E-02 | 3.86E-03 | 4.48E-02 |
| 1.87 | 9.74E-02 | 1.38E-02 | 2.25E-02 | 5.50E-03 | 15.40 | 3.02E-03 | 4.38E-02 | 5.64E-03 | 4.32E-02 |
| 1.93 | 9.73E-02 | 1.29E-02 | 2.18E-02 | 5.71E-03 | 15.73 | 3.20E-03 | 5.40E-02 | 3.71E-03 | 4.13E-02 |
| 2.07 | 9.64E-02 | 1.34E-02 | 2.23E-02 | 6.47E-03 | 16.07 | 3.43E-03 | 5.42E-02 | 3.79E-03 | 4.13E-02 |
| 2.40 | 9.45E-02 | 1.31E-02 | 2.09E-02 | 7.21E-03 | 16.40 | 2.69E-03 | 5.49E-02 | 4.28E-03 | 4.01E-02 |
| 2.73 | 9.08E-02 | 1.26E-02 | 1.85E-02 | 9.24E-03 | 16.73 | 3.12E-03 | 5.47E-02 | 4.55E-03 | 4.00E-02 |
| 3.07 | 7.74E-02 | 1.19E-02 | 1.77E-02 | 1.57E-02 | 17.07 | 2.79E-03 | 5.53E-02 | 4.23E-03 | 3.93E-02 |
| 3.40 | 6.72E-02 | 1.09E-02 | 1.61E-02 | 1.96E-02 | 17.40 | 3.90E-03 | 5.51E-02 | 2.32E-03 | 4.12E-02 |
| 3.73 | 5.05E-02 | 9.26E-03 | 1.29E-02 | 2.73E-02 | 17.73 | 2.53E-03 | 5.54E-02 | 3.47E-03 | 4.04E-02 |
| 4.07 | 3.41E-02 | 7.49E-03 | 1.10E-02 | 3.33E-02 | 18.07 | 2.62E-03 | 5.47E-02 | 4.78E-03 | 3.98E-02 |
| 4.40 | 1.89E-02 | 5.50E-03 | 7.75E-03 | 4.08E-02 | 18.40 | 3.14E-03 | 5.48E-02 | 3.32E-03 | 4.05E-02 |
| 4.73 | 7.69E-03 | 3.51E-03 | 3.59E-03 | 4.66E-02 | 18.73 | 3.21E-03 | 5.47E-02 | 4.17E-03 | 4.02E-02 |
| 5.07 | 4.90E-03 | 2.61E-03 | 3.05E-03 | 4.79E-02 | 19.07 | 3.42E-03 | 5.50E-02 | 3.48E-03 | 4.06E-02 |
| 5.40 | 4.80E-03 | 2.62E-03 | 4.05E-03 | 4.73E-02 | 19.40 | 2.77E-03 | 5.38E-02 | 4.36E-03 | 4.05E-02 |
| 5.73 | 4.80E-03 | 2.62E-03 | 3.35E-03 | 4.76E-02 | 19.65 | 3.13E-03 | 5.46E-02 | 3.90E-03 | 4.02E-02 |

Table A.5. Data for Figure 3.5. Relative composition of form II calculated from profiles of normalized peak height at 1237cm$^{-1}$, PC1 and PC2 by MCR analysis during form T to II transformation (left) and form II to I transformation (right).

| Time (hours) | By peak height (%) | By PC1 (%) | Time (Hours) | By peak height (%) | By PC2 (%) |
|---|---|---|---|---|---|
| 1.12 | 0.0 | 1.5 | 12.98 | 99.7 | 99.7 |
| 1.17 | 4.6 | 0.2 | 13.07 | 99.8 | 99.8 |
| 1.22 | 0.4 | 0.4 | 13.15 | 100.0 | 100.0 |
| 1.27 | 0.2 | 2.6 | 13.23 | 99.4 | 98.9 |
| 1.32 | 2.9 | 1.9 | 13.32 | 99.7 | 99.4 |
| 1.37 | 2.6 | 0.3 | 13.40 | 99.9 | 99.4 |
| 1.42 | 2.7 | 0.0 | 13.48 | 98.9 | 98.5 |
| 1.47 | 3.6 | 1.6 | 13.57 | 98.5 | 98.3 |
| 1.52 | 0.1 | 2.5 | 13.65 | 99.3 | 98.7 |
| 1.57 | 1.3 | 3.9 | 13.67 | 97.6 | 97.7 |
| 1.62 | 1.8 | 3.6 | 13.82 | 97.2 | 96.5 |
| 1.67 | 2.8 | 2.3 | 13.90 | 96.6 | 96.3 |
| 1.72 | 4.4 | 3.0 | 13.98 | 95.9 | 95.8 |
| 1.77 | 3.2 | 2.5 | 14.07 | 94.5 | 93.8 |
| 1.82 | 0.8 | 2.9 | 14.15 | 92.8 | 92.9 |
| 1.87 | 3.8 | 3.8 | 14.23 | 92.9 | 92.4 |
| 1.92 | 7.0 | 4.2 | 14.32 | 90.3 | 90.0 |
| 1.97 | 2.4 | 5.6 | 14.40 | 89.1 | 89.0 |
| 2.15 | 1.4 | 3.3 | 14.48 | 87.8 | 87.6 |
| 2.48 | 10.3 | 6.4 | 14.57 | 83.6 | 83.9 |
| 2.73 | 11.1 | 10.9 | 14.65 | 80.3 | 80.7 |
| 2.98 | 19.4 | 17.9 | 14.73 | 78.2 | 78.5 |
| 3.23 | 23.5 | 25.6 | 14.82 | 73.9 | 73.3 |
| 3.48 | 35.8 | 39.8 | 14.90 | 70.4 | 69.8 |
| 3.73 | 50.3 | 52.4 | 14.98 | 64.9 | 64.5 |
| 3.98 | 60.8 | 65.8 | 15.07 | 58.2 | 58.4 |
| 4.23 | 73.9 | 78.6 | 15.15 | 52.9 | 52.5 |
| 4.48 | 87.3 | 88.1 | 15.23 | 43.7 | 44.3 |
| 4.73 | 95.1 | 96.7 | 15.32 | 34.2 | 34.2 |
| 4.98 | 98.6 | 100.0 | 15.40 | 21.0 | 21.5 |
| 5.23 | 97.3 | 99.6 | 15.48 | 10.2 | 10.8 |
| 5.48 | 97.7 | 99.9 | 15.57 | 5.6 | 5.1 |
| 5.73 | 100.0 | 99.7 | 15.65 | 3.1 | 3.0 |
| 5.98 | 98.4 | 99.4 | 15.73 | 0.7 | 1.7 |
| | | | 15.82 | 0.5 | 0.4 |
| | | | 15.90 | 0.0 | 0.0 |
| | | | 15.98 | 1.4 | 0.9 |

Table A.6. Data for Figure 3.7. Concentration profile by ATR-FTIR compared with PC2 profile from MCR analysis of Raman spectra.

| Time (hours) | PC2 | Time (hours) | Concentration (wt%) |
|---|---|---|---|
| 0.00 | 0.0325 | 0.00 | 5.40 |
| 0.10 | 0.0324 | 0.33 | 5.31 |
| 0.20 | 0.0322 | 0.42 | 3.58 |
| 0.32 | 0.0320 | 0.50 | 3.06 |
| 0.33 | 0.0199 | 0.58 | 2.88 |
| 0.42 | 0.0166 | 0.67 | 2.79 |
| 0.58 | 0.0158 | 0.75 | 2.73 |
| 0.75 | 0.0152 | 0.83 | 2.69 |
| 0.88 | 0.0152 | 0.88 | 2.66 |
| 1.08 | 0.0145 | 1.00 | 2.64 |
| 1.25 | 0.0144 | 1.08 | 2.61 |
| 1.50 | 0.0143 | 1.17 | 2.58 |
| 1.83 | 0.0142 | 1.25 | 2.57 |
| 2.07 | 0.0141 | 1.33 | 2.55 |
| 2.40 | 0.0138 | 1.42 | 2.55 |
| 2.57 | 0.0132 | 1.50 | 2.54 |
| 2.73 | 0.0132 | 1.58 | 2.53 |
| 2.90 | 0.0131 | 1.67 | 2.53 |
| 3.07 | 0.0121 | 1.75 | 2.52 |
| 3.23 | 0.0120 | 1.83 | 2.52 |
| 3.40 | 0.0109 | 1.92 | 2.53 |
| 3.57 | 0.0101 | 2.00 | 2.52 |
| 3.73 | 0.0089 | 2.08 | 2.53 |
| 3.90 | 0.0077 | 2.17 | 2.51 |
| 4.07 | 0.0068 | 2.25 | 2.53 |
| 4.23 | 0.0055 | 3.00 | 2.52 |
| 4.40 | 0.0045 | 3.50 | 2.49 |
| 4.57 | 0.0033 | 4.00 | 2.51 |
| 4.73 | 0.0023 | 4.50 | 2.49 |
| 4.90 | 0.0017 | 4.75 | 2.45 |
| 5.57 | 0.0013 | 4.83 | 2.38 |
| 6.57 | 0.0017 | 4.92 | 2.32 |
| 7.57 | 0.0011 | 5.00 | 2.26 |
| 8.57 | 0.0015 | 5.25 | 2.18 |
| 9.57 | 0.0017 | 5.50 | 2.11 |
| 10.57 | 0.0016 | 5.75 | 2.03 |
| 11.57 | 0.0012 | 6.00 | 2.01 |
| 12.57 | 0.0013 | 6.25 | 1.95 |
| 12.65 | 0.0014 | 6.50 | 1.97 |
| 12.73 | 0.0015 | 6.75 | 1.95 |

Table A.6 (contd.). Data for Figure 3.7. Concentration profile by ATR-FTIR compared with PC2 profile from MCR analysis of Raman spectra.

| Time (hours) | PC2 | Time (hours) | Concentration (wt%) |
|---|---|---|---|
| 12.82 | 0.0017 | 7.75 | 1.95 |
| 12.90 | 0.0015 | 8.75 | 1.96 |
| 12.98 | 0.0020 | 9.75 | 1.94 |
| 13.23 | 0.0024 | 10.75 | 1.95 |
| 13.48 | 0.0026 | 11.75 | 1.96 |
| 13.73 | 0.0030 | 12.75 | 1.96 |
| 13.98 | 0.0038 | 13.75 | 1.94 |
| 14.23 | 0.0055 | 14.75 | 1.95 |
| 14.48 | 0.0078 | 15.83 | 1.95 |
| 14.73 | 0.0121 | 16.00 | 1.89 |
| 14.98 | 0.0188 | 16.08 | 1.86 |
| 15.23 | 0.0284 | 16.17 | 1.83 |
| 15.48 | 0.0444 | 16.25 | 1.82 |
| 15.90 | 0.0495 | 16.50 | 1.77 |
| 16.32 | 0.0498 | 17.00 | 1.77 |
| 16.40 | 0.0496 | 18.00 | 1.78 |
| 17.40 | 0.0498 | 19.00 | 1.77 |
| 18.40 | 0.0494 | 20.00 | 1.77 |
| 19.40 | 0.0485 | | |
| 19.65 | 0.0493 | | |

Table A.7. Data for Figure 4.3. Solubility curve of succinic acid in $H_2O$. R* is solubility represented by ratio of the peak area of the 1806~1675cm$^{-1}$ band to that of the 1671~1494cm$^{-1}$ band in the infrared spectrum.

| Temperature ( C ) | Solubility R* | Standand error |
|---|---|---|
| 10 | 0.606 | 0.0030 |
| 15 | 0.607 | 0.0029 |
| 20 | 0.615 | 0.0030 |
| 25 | 0.629 | 0.0030 |
| 30 | 0.651 | 0.0031 |
| 35 | 0.680 | 0.0032 |
| 40 | 0.716 | 0.0033 |
| 45 | 0.758 | 0.0035 |
| 50 | 0.808 | 0.0038 |
| 55 | 0.865 | 0.0042 |
| 60 | 0.929 | 0.0047 |

Table A.8. Data for Figure 4.4. Optimal cooling profiles for succicinic acid crystallization with different amount of seeding. Initial concentration is 19%(w/w), seed size is 355-425μm, and agitation rate is 400rpm.

| Time | Temperature ( °C ) | | |
|---|---|---|---|
| (minutes) | 0.05g seed | 0.5g seed | 5g seed |
| 1 | 50.2 | 50.2 | 50.2 |
| 11 | 49.6 | 49.7 | 49.8 |
| 21 | 49.5 | 49.1 | 49.2 |
| 31 | 49.5 | 48.6 | 48.7 |
| 41 | 48.8 | 48.0 | 48.0 |
| 51 | 48.3 | 47.5 | 47.3 |
| 61 | 47.8 | 47.0 | 46.4 |
| 71 | 47.2 | 46.3 | 45.3 |
| 81 | 46.7 | 45.5 | 44.0 |
| 86 | 46.3 | 45.0 | 43.0 |
| 91 | 46.0 | 44.3 | 42.0 |
| 96 | 45.7 | 43.3 | 40.5 |
| 101 | 45.4 | 42.3 | 38.3 |
| 106 | 45.0 | 41.3 | 36.0 |
| 111 | 44.6 | 40.0 | 33.0 |
| 116 | 44.1 | 37.8 | 29.8 |
| 121 | 43.5 | 35.5 | 26.6 |
| 126 | 42.9 | 33.3 | 23.1 |
| 131 | 42.2 | 31.0 | 17.1 |
| 136 | 41.2 | 28.7 | 13.0 |
| 141 | 40.2 | 26.3 | 9.5 |
| 146 | 39.3 | 24.0 | |
| 151 | 38.1 | 21.5 | |
| 156 | 35.8 | 18.4 | |
| 161 | 33.6 | 14.5 | |
| 166 | 31.3 | 10.5 | |
| 171 | 29.0 | | |
| 176 | 26.7 | | |
| 181 | 24.3 | | |
| 186 | 21.9 | | |
| 191 | 19.5 | | |
| 196 | 17.0 | | |
| 201 | 14.5 | | |
| 206 | 12.7 | | |
| 211 | 11.4 | | |
| 214 | 9.7 | | |

Table A.9. Data for Figure 4.5. Optimal cooling profiles for succicinic acid crystallization with different seed sizes. Initial concentration is 19% (w/w), seed amount is 5g, and agitation rate is 400rpm.

| Time (minutes) | Temperature ( °C ) | | |
|---|---|---|---|
| | Seed size 500-600um | Seed size 355-425um | seed size <180um |
| 1 | 50.7 | 50.2 | 50.3 |
| 11 | 50.0 | 49.7 | 49.7 |
| 21 | 49.5 | 49.1 | 49.3 |
| 31 | 49.5 | 48.6 | 48.7 |
| 41 | 49.5 | 48.0 | 48.1 |
| 51 | 49.5 | 47.5 | 47.5 |
| 61 | 49.3 | 47.0 | 47.0 |
| 71 | 48.7 | 46.3 | 46.3 |
| 81 | 48.2 | 45.5 | 45.7 |
| 91 | 47.7 | 44.3 | 44.9 |
| 101 | 47.5 | 42.3 | 44.1 |
| 111 | 47.3 | 40.0 | 42.8 |
| 121 | 46.8 | 35.5 | 40.8 |
| 126 | 46.5 | 33.3 | 39.8 |
| 131 | 46.3 | 31.0 | 37.6 |
| 136 | 46.0 | 28.7 | 35.4 |
| 141 | 45.7 | 26.3 | 33.1 |
| 146 | 45.4 | 24.0 | 30.8 |
| 151 | 45.1 | 21.5 | 28.5 |
| 156 | 44.8 | 18.4 | 26.1 |
| 161 | 44.5 | 14.5 | 23.7 |
| 166 | 44.3 | 10.5 | 21.4 |
| 171 | 43.9 | | 19.0 |
| 176 | 43.5 | | 16.5 |
| 181 | 43.0 | | 13.6 |
| 186 | 42.5 | | 10.1 |
| 191 | 41.8 | | |
| 201 | 39.8 | | |
| 211 | 37.9 | | |
| 221 | 36.0 | | |
| 231 | 34.0 | | |
| 241 | 29.4 | | |
| 251 | 24.6 | | |
| 261 | 19.8 | | |
| 271 | 12.7 | | |
| 275 | 9.9 | | |

Table A.10. Data for Figure 4.6. Optimal cooling profiles for succicinic acid crystallization with different agitation speeds. Initial concentration is 19%(w/w), seed amount is 5g, seed size is 355-425μm.

| Time (minutes) | Tempersture (°C) | | |
|---|---|---|---|
| | 300rpm | 400rpm | 600rpm |
| 1 | 50.2 | 50.2 | 50.2 |
| 11 | 50.4 | 49.7 | 50.0 |
| 21 | 50.2 | 49.1 | 49.7 |
| 31 | 50.0 | 48.6 | 49.2 |
| 41 | 49.8 | 48.0 | 48.6 |
| 51 | 49.7 | 47.5 | 48.0 |
| 61 | 49.5 | 47.0 | 47.3 |
| 71 | 48.8 | 46.3 | 46.4 |
| 81 | 48.6 | 45.5 | 45.3 |
| 91 | 48.3 | 44.3 | 44.0 |
| 101 | 47.8 | 42.3 | 42.0 |
| 111 | 47.3 | 40.0 | 40.0 |
| 121 | 46.8 | 35.5 | 35.4 |
| 131 | 46.3 | 31.0 | 30.6 |
| 141 | 45.9 | 26.3 | 23.8 |
| 151 | 45.5 | 21.5 | 12.2 |
| 161 | 44.5 | 14.5 | |
| 166 | 44.2 | 10.5 | |
| 171 | 43.8 | | |
| 181 | 43.0 | | |
| 191 | 42.3 | | |
| 201 | 41.6 | | |
| 211 | 40.9 | | |
| 221 | 40.2 | | |
| 231 | 39.5 | | |
| 241 | 38.5 | | |
| 251 | 37.5 | | |
| 261 | 36.0 | | |
| 271 | 34.2 | | |
| 281 | 31.2 | | |
| 291 | 26.8 | | |
| 301 | 22.3 | | |
| 311 | 17.9 | | |
| 321 | 13.7 | | |
| 329 | 9.6 | | |

Table A.11. Data for Figure 4.7. Optimal cooling profiles for succicinic acid crystallization showing the effect of acetic acid present as an impurity (2% mole basis). Initial concentration is 19%(w/w), seed amount is 5g, seed size is 355-425μm, and agitation rate is 400rpm.

| Time (minutes) | Temperature (°C) | |
|---|---|---|
| | With acetic acid | Without acetic acid |
| 1 | 50.0 | 50.2 |
| 11 | 49.3 | 49.7 |
| 21 | 48.8 | 49.1 |
| 31 | 48.3 | 48.6 |
| 41 | 47.7 | 48.0 |
| 51 | 47.2 | 47.5 |
| 61 | 46.7 | 47.0 |
| 71 | 46.1 | 46.3 |
| 81 | 45.6 | 45.5 |
| 91 | 45.1 | 44.3 |
| 96 | 44.8 | 43.3 |
| 101 | 44.5 | 42.3 |
| 106 | 44.2 | 41.3 |
| 111 | 43.8 | 40.0 |
| 116 | 43.4 | 37.8 |
| 121 | 42.8 | 35.5 |
| 126 | 42.2 | 33.3 |
| 131 | 41.6 | 31.0 |
| 136 | 40.6 | 28.7 |
| 141 | 39.6 | 26.3 |
| 146 | 38.7 | 24.0 |
| 151 | 37.7 | 21.5 |
| 156 | 36.8 | 18.4 |
| 161 | 35.8 | 14.5 |
| 166 | 33.9 | 10.5 |
| 171 | 31.7 | |
| 176 | 29.4 | |
| 181 | 27.0 | |
| 186 | 24.6 | |
| 191 | 22.2 | |
| 196 | 19.8 | |
| 201 | 17.4 | |
| 211 | 13.9 | |
| 216 | 12.4 | |
| 224 | 10.0 | |

Table A.12. Data for Figure 4.4. CSD of succicinic acid with different amount of seeding. Initial concentration is 19%(w/w), seed size is 355-425μm, and agitation rate is 400rpm.

| Sieve # | Crystal size range (mm) | Median crystal size (mm) | CSD (wt%) | | |
|---|---|---|---|---|---|
| | | | 5g seed | 0.5g seed | 0.05g seed |
| 16 | >1.18 | 1.18 | 0 | 76.6 | 63.1 |
| 18 | 1~1.18 | 1.09 | 1.7 | 16.4 | 13.1 |
| 20 | 0.85~1 | 0.925 | 33.7 | 3.1 | 7.6 |
| 25 | 0.71~0.85 | 0.78 | 45.1 | 2.1 | 5.4 |
| 30 | 0.6~0.71 | 0.655 | 13.4 | 0.9 | 2.4 |
| 35 | 0.5~0.6 | 0.55 | 41.3 | 0.5 | 1.5 |
| 40 | 0.425~0.5 | 0.463 | 12.4 | 0.1 | 0.8 |
| 80 | 0.18~0.425 | 0.303 | 0.6 | 0.1 | 5.1 |
| Pan | 0~0.425 | 0.09 | 0 | 0 | 1 |

Table A.13. Data for Figure 4.5. CSD of succicinic acid with different seed sizes. Initial concentration is 19% (w/w), seed amount is 5g, and agitation rate is 400rpm.

| Sieve # | Crystal size range (mm) | Median crystal size (mm) | CSD (wt%) | | |
|---|---|---|---|---|---|
| | | | seed size 500-600um | seed size 355-425um | seed size <180um |
| 16 | >1.18 | 1.18 | 57.9 | 76.6 | 1.2 |
| 18 | 1~1.18 | 1.09 | 19.2 | 16.4 | 30.2 |
| 20 | 0.85~1 | 0.925 | 10.1 | 3.1 | 51.3 |
| 25 | 0.71~0.85 | 0.78 | 4.8 | 2.1 | 10.7 |
| 30 | 0.6~0.71 | 0.655 | 2 | 0.9 | 1.6 |
| 35 | 0.5~0.6 | 0.55 | 1.2 | 0.5 | 1.2 |
| 40 | 0.425~0.5 | 0.463 | 0.7 | 0.1 | 0.5 |
| 80 | 0.18~0.425 | 0.303 | 3.4 | 0.1 | 2.4 |
| Pan | 0~0.425 | 0.09 | 0.9 | 0 | 1 |

Table A.14. Data for Figure 4.6. CSD of succicinic acid with different agitation speeds. Initial concentration is 19%(w/w), seed amount is 5g, seed size is 355-425μm.

| Sieve # | Crystal size range (mm) | Median crystal size (mm) | CSD (wt%) | | |
|---|---|---|---|---|---|
| | | | 600rpm | 400rpm | 300rpm |
| 16 | >1.18 | 1.18 | 32.6 | 76.6 | 80 |
| 18 | 1~1.18 | 1.09 | 41.5 | 16.4 | 6.5 |
| 20 | 0.85~1 | 0.925 | 16 | 3.1 | 3.2 |
| 25 | 0.71~0.85 | 0.78 | 4.7 | 2.1 | 2 |
| 30 | 0.6~0.71 | 0.655 | 1.7 | 0.9 | 0.9 |
| 35 | 0.5~0.6 | 0.55 | 1 | 0.5 | 0.7 |
| 40 | 0.425~0.5 | 0.463 | 0.4 | 0.1 | 0.5 |
| 80 | 0.18~0.425 | 0.303 | 1.7 | 0.1 | 3 |
| Pan | 0~0.425 | 0.09 | 0.2 | 0 | 3.4 |

Table A.15. Data for Figure 4.7. CSD of succicinic acid showing the effect of acetic acid present as an impurity (2% mole basis). Initial concentration is 19%(w/w), seed amount is 5g, seed size is 355-425μm, and agitation rate is 400rpm.

| Sieve # | Crystal size range (mm) | Median crystal size (mm) | CSD (wt%) | |
|---|---|---|---|---|
| | | | With acetic acid | Witout acetic acid |
| 16 | >1.18 | 1.18 | 64.2 | 76.6 |
| 18 | 1~1.18 | 1.09 | 29.5 | 16.4 |
| 20 | 0.85~1 | 0.925 | 3.2 | 3.1 |
| 25 | 0.71~0.85 | 0.78 | 1.4 | 2.1 |
| 30 | 0.6~0.71 | 0.655 | 0.6 | 0.9 |
| 35 | 0.5~0.6 | 0.55 | 0.6 | 0.5 |
| 40 | 0.425~0.5 | 0.463 | 0.2 | 0.1 |
| Pan | 0~0.425 | 0.2125 | 0.2 | 0.1 |

Table A.16 Data for Figure 5.3. Peak intensity ratio (PIR) at 517nm over 441nm of pyranine in sucrose solutions at different temperature with different amount of fructose and glucose. Brix represents total sugar percent by weight.

| RUN # | Fructose (wt%) | Glucose (wt%) | Sucrose (wt%) | BRIX | Temperature (°C) | Peak intensity ratio PIR |
|---|---|---|---|---|---|---|
| 1 | 0 | 40 | 47 | 87 | 110 | 0.349 |
| 2 | 20 | 20 | 40 | 80 | 110 | 0.533 |
| 3 | 0 | 40 | 43.5 | 83.5 | 90 | 0.437 |
| 4 | 40 | 0 | 40 | 80 | 90 | 0.446 |
| 5 | 20 | 20 | 40 | 80 | 70 | 0.475 |
| 6 | 20 | 20 | 43.5 | 83.5 | 90 | 0.352 |
| 7 | 0 | 40 | 47 | 87 | 70 | 0.315 |
| 8 | 0 | 40 | 47 | 87 | 110 | 0.342 |
| 9 | 20 | 20 | 40 | 80 | 70 | 0.471 |
| 10 | 20 | 20 | 43.5 | 83.5 | 110 | 0.403 |
| 11 | 20 | 20 | 40 | 80 | 90 | 0.514 |
| 12 | 40 | 0 | 47 | 87 | 90 | 0.245 |
| 13 | 40 | 0 | 47 | 87 | 110 | 0.299 |
| 14 | 20 | 20 | 43.5 | 83.5 | 90 | 0.377 |
| 15 | 20 | 20 | 47 | 87 | 70 | 0.246 |
| 16 | 40 | 0 | 43.5 | 83.5 | 70 | 0.319 |
| 17 | 40 | 0 | 43.5 | 83.5 | 90 | 0.335 |
| 18 | 0 | 40 | 40 | 80 | 90 | 0.590 |
| 19 | 30 | 10 | 41.75 | 81.75 | 80 | 0.396 |
| 20 | 0 | 40 | 41.75 | 81.75 | 80 | 0.508 |
| 21 | 30 | 10 | 45.25 | 85.25 | 100 | 0.336 |
| 22 | 20 | 20 | 43.5 | 83.5 | 70 | 0.342 |
| 23 | 30 | 10 | 41.75 | 81.75 | 100 | 0.428 |
| 24 | 20 | 20 | 47 | 87 | 110 | 0.367 |
| 25 | 40 | 0 | 47 | 87 | 70 | 0.239 |
| 26 | 0 | 40 | 40 | 80 | 110 | 0.605 |
| 27 | 0 | 40 | 40 | 80 | 110 | 0.619 |
| 28 | 40 | 0 | 47 | 87 | 70 | 0.242 |
| 29 | 0 | 40 | 40 | 80 | 110 | 0.553 |
| 30 | 0 | 40 | 40 | 80 | 70 | 0.552 |
| 31 | 20 | 20 | 47 | 87 | 90 | 0.283 |
| 32 | 20 | 20 | 47 | 87 | 70 | 0.263 |
| 33 | 0 | 40 | 47 | 87 | 90 | 0.321 |
| 34 | 20 | 20 | 40 | 80 | 70 | 0.481 |
| 35 | 0 | 40 | 40 | 80 | 70 | 0.549 |
| 36 | 30 | 10 | 45.25 | 85.25 | 80 | 0.299 |
| 37 | 20 | 20 | 40 | 80 | 110 | 0.536 |
| 38 | 40 | 0 | 40 | 80 | 110 | 0.473 |

Table A.16 (contd) Data for Figure 5.3. Peak intensity ratio (PIR) at 517nm over 441nm of pyranine in sucrose solutions at different temperature with different amount of fructose and glucose. Brix represents total sugar percent by weight.

| RUN # | Fructose (wt%) | Glucose (wt%) | Sucrose (wt%) | BRIX | Temperature (°C) | Peak intensity ratio PIR |
|---|---|---|---|---|---|---|
| 39 | 0 | 40 | 47 | 87 | 70 | 0.286 |
| 40 | 0 | 40 | 47 | 87 | 110 | 0.310 |
| 41 | 0 | 40 | 43.5 | 83.5 | 110 | 0.458 |
| 42 | 40 | 0 | 40 | 80 | 70 | 0.417 |
| 43 | 40 | 0 | 40 | 80 | 70 | 0.416 |
| 44 | 0 | 40 | 47 | 87 | 70 | 0.287 |
| 45 | 20 | 20 | 43.5 | 83.5 | 110 | 0.403 |
| 46 | 20 | 20 | 47 | 87 | 70 | 0.272 |
| 47 | 0 | 40 | 43.5 | 83.5 | 70 | 0.403 |
| 48 | 0 | 40 | 40 | 80 | 90 | 0.602 |
| 49 | 40 | 0 | 40 | 80 | 70 | 0.379 |
| 50 | 40 | 0 | 43.5 | 83.5 | 110 | 0.352 |
| 51 | 40 | 0 | 43.5 | 83.5 | 110 | 0.340 |
| 52 | 0 | 40 | 43.5 | 83.5 | 90 | 0.390 |
| 53 | 40 | 0 | 43.5 | 83.5 | 90 | 0.325 |
| 54 | 40 | 0 | 40 | 80 | 110 | 0.469 |
| 55 | 40 | 0 | 47 | 87 | 70 | 0.225 |
| 56 | 40 | 0 | 40 | 80 | 110 | 0.483 |
| 57 | 40 | 0 | 47 | 87 | 110 | 0.340 |
| 58 | 20 | 20 | 47 | 87 | 110 | 0.308 |
| 59 | 0 | 40 | 40 | 80 | 70 | 0.550 |
| 60 | 40 | 0 | 47 | 87 | 110 | 0.328 |

Table A.17 Data for Figure 5.4. Peak intensity ratio (PIR) at 591nm over 419nm of carminic acid in sucrose solutions at different temperature with different amount of fructose and glucose. Brix represents total sugar percent by weight.

| RUN # | Fructose (wt%) | Glucose (wt%) | Sucrose (wt%) | BRIX | Temperature (°C) | Peak intensity ratio PIR |
|---|---|---|---|---|---|---|
| 1 | 0 | 40 | 47 | 87 | 110 | 0.773 |
| 2 | 20 | 20 | 40 | 80 | 110 | 1.242 |
| 3 | 0 | 40 | 43.5 | 83.5 | 90 | 0.673 |
| 4 | 40 | 0 | 40 | 80 | 90 | 0.918 |
| 5 | 20 | 20 | 40 | 80 | 70 | 0.628 |
| 6 | 20 | 20 | 43.5 | 83.5 | 90 | 0.730 |
| 7 | 0 | 40 | 47 | 87 | 70 | 0.554 |
| 8 | 0 | 40 | 47 | 87 | 110 | 0.856 |
| 9 | 20 | 20 | 40 | 80 | 70 | 0.717 |
| 10 | 20 | 20 | 43.5 | 83.5 | 110 | 1.027 |
| 11 | 20 | 20 | 40 | 80 | 90 | 0.827 |
| 12 | 40 | 0 | 47 | 87 | 90 | 0.781 |
| 13 | 40 | 0 | 47 | 87 | 110 | 0.936 |
| 14 | 20 | 20 | 43.5 | 83.5 | 90 | 0.751 |
| 15 | 20 | 20 | 47 | 87 | 70 | 0.643 |
| 16 | 40 | 0 | 43.5 | 83.5 | 70 | 0.662 |
| 17 | 40 | 0 | 43.5 | 83.5 | 90 | 0.838 |
| 18 | 0 | 40 | 40 | 80 | 90 | 0.678 |
| 19 | 30 | 10 | 41.75 | 81.75 | 80 | 0.779 |
| 20 | 0 | 40 | 41.75 | 81.75 | 80 | 0.683 |
| 21 | 30 | 10 | 45.25 | 85.25 | 100 | 0.934 |
| 22 | 20 | 20 | 43.5 | 83.5 | 70 | 0.614 |
| 23 | 30 | 10 | 41.75 | 81.75 | 100 | 0.941 |
| 24 | 20 | 20 | 47 | 87 | 110 | 0.974 |
| 25 | 40 | 0 | 47 | 87 | 70 | 0.601 |
| 26 | 0 | 40 | 40 | 80 | 110 | 0.859 |
| 27 | 0 | 40 | 40 | 80 | 110 | 0.864 |
| 28 | 40 | 0 | 47 | 87 | 70 | 0.606 |
| 29 | 0 | 40 | 40 | 80 | 110 | 0.688 |
| 30 | 0 | 40 | 40 | 80 | 70 | 0.586 |
| 31 | 20 | 20 | 47 | 87 | 90 | 0.687 |
| 32 | 20 | 20 | 47 | 87 | 70 | 0.558 |
| 33 | 0 | 40 | 47 | 87 | 90 | 0.618 |
| 34 | 20 | 20 | 40 | 80 | 70 | 0.638 |
| 35 | 0 | 40 | 40 | 80 | 70 | 0.547 |
| 36 | 30 | 10 | 45.25 | 85.25 | 80 | 0.721 |
| 37 | 20 | 20 | 40 | 80 | 110 | 1.084 |
| 38 | 40 | 0 | 40 | 80 | 110 | 1.050 |

Table A.17(contd) Data for Figure 5.4. Peak intensity ratio (PIR) at 591nm over 419nm of carminic acid in sucrose solutions at different temperature with different amount of fructose and glucose. Brix represents total sugar percent by weight.

| RUN # | Fructose (wt%) | Glucose (wt%) | Sucrose (wt%) | BRIX | Temperature (°C) | Peak intensity ratio PIR |
|---|---|---|---|---|---|---|
| 39 | 0 | 40 | 47 | 87 | 70 | 0.566 |
| 40 | 0 | 40 | 47 | 87 | 110 | 0.744 |
| 41 | 0 | 40 | 43.5 | 83.5 | 110 | 0.798 |
| 42 | 40 | 0 | 40 | 80 | 70 | 0.720 |
| 43 | 40 | 0 | 40 | 80 | 70 | 0.646 |
| 44 | 0 | 40 | 47 | 87 | 70 | 0.585 |
| 45 | 20 | 20 | 43.5 | 83.5 | 110 | 1.025 |
| 46 | 20 | 20 | 47 | 87 | 70 | 0.576 |
| 47 | 0 | 40 | 43.5 | 83.5 | 70 | 0.522 |
| 48 | 0 | 40 | 40 | 80 | 90 | 0.617 |
| 49 | 40 | 0 | 40 | 80 | 70 | 0.749 |
| 50 | 40 | 0 | 43.5 | 83.5 | 110 | 1.049 |
| 51 | 40 | 0 | 43.5 | 83.5 | 110 | 0.973 |
| 52 | 0 | 40 | 43.5 | 83.5 | 90 | 0.606 |
| 53 | 40 | 0 | 43.5 | 83.5 | 90 | 0.886 |
| 54 | 40 | 0 | 40 | 80 | 110 | 1.062 |
| 55 | 40 | 0 | 47 | 87 | 70 | 0.668 |
| 56 | 40 | 0 | 40 | 80 | 110 | 1.182 |
| 57 | 40 | 0 | 47 | 87 | 110 | 0.836 |
| 58 | 20 | 20 | 47 | 87 | 110 | 1.015 |
| 59 | 0 | 40 | 40 | 80 | 70 | 0.576 |
| 60 | 40 | 0 | 47 | 87 | 110 | 0.780 |
| r2* | 20 | 20 | 40 | 80 | 110 | 1.059 |
| r9* | 20 | 20 | 40 | 80 | 70 | 0.590 |
| r13* | 40 | 0 | 47 | 87 | 110 | 0.758 |
| r15* | 20 | 20 | 47 | 87 | 70 | 0.544 |
| r29* | 0 | 40 | 40 | 80 | 110 | 0.705 |
| r37* | 20 | 20 | 40 | 80 | 110 | 0.986 |
| r52* | 0 | 40 | 43.5 | 83.5 | 90 | 0.627 |
| r55* | 40 | 0 | 47 | 87 | 70 | 0.584 |
| r57* | 40 | 0 | 47 | 87 | 110 | 0.988 |

*runs are repeated in addition to the original experiemtal design

Table A.18 Data for Figure 5.6. Anisotropy of pyranine in sucrose solutions at different temperature with different amount of fructose and glucose. Brix represents total sugar percent by weight.

| RUN # | Fructose (wt%) | Glucose (wt%) | Sucrose (wt%) | BRIX | Temperature (°C) | Anisotropy r |
|---|---|---|---|---|---|---|
| 1 | 0 | 40 | 47 | 87 | 110 | 0.176 |
| 2 | 20 | 20 | 40 | 80 | 110 | 0.133 |
| 3 | 0 | 40 | 43.5 | 83.5 | 90 | 0.196 |
| 4 | 40 | 0 | 40 | 80 | 90 | 0.198 |
| 5 | 20 | 20 | 40 | 80 | 70 | 0.238 |
| 6 | 20 | 20 | 43.5 | 83.5 | 90 | 0.227 |
| 7 | 0 | 40 | 47 | 87 | 70 | 0.270 |
| 8 | 0 | 40 | 47 | 87 | 110 | 0.180 |
| 9 | 20 | 20 | 40 | 80 | 70 | 0.237 |
| 10 | 20 | 20 | 43.5 | 83.5 | 110 | 0.162 |
| 11 | 20 | 20 | 40 | 80 | 90 | 0.180 |
| 12 | 40 | 0 | 47 | 87 | 90 | 0.286 |
| 13 | 40 | 0 | 47 | 87 | 110 | 0.225 |
| 14 | 20 | 20 | 43.5 | 83.5 | 90 | 0.217 |
| 15 | 20 | 20 | 47 | 87 | 70 | 0.302 |
| 16 | 40 | 0 | 43.5 | 83.5 | 70 | 0.294 |
| 17 | 40 | 0 | 43.5 | 83.5 | 90 | 0.242 |
| 18 | 0 | 40 | 40 | 80 | 90 | 0.163 |
| 19 | 30 | 10 | 41.75 | 81.75 | 80 | 0.234 |
| 20 | 0 | 40 | 41.75 | 81.75 | 80 | 0.198 |
| 21 | 30 | 10 | 45.25 | 85.25 | 100 | 0.221 |
| 22 | 20 | 20 | 43.5 | 83.5 | 70 | 0.270 |
| 23 | 30 | 10 | 41.75 | 81.75 | 100 | 0.178 |
| 24 | 20 | 20 | 47 | 87 | 110 | 0.206 |
| 25 | 40 | 0 | 47 | 87 | 70 | 0.321 |
| 26 | 0 | 40 | 40 | 80 | 110 | 0.122 |
| 27 | 0 | 40 | 40 | 80 | 110 | 0.120 |
| 28 | 40 | 0 | 47 | 87 | 70 | 0.323 |
| 29 | 0 | 40 | 40 | 80 | 110 | 0.128 |
| 30 | 0 | 40 | 40 | 80 | 70 | 0.211 |
| 31 | 20 | 20 | 47 | 87 | 90 | 0.267 |
| 32 | 20 | 20 | 47 | 87 | 70 | 0.304 |
| 33 | 0 | 40 | 47 | 87 | 90 | 0.235 |
| 34 | 20 | 20 | 40 | 80 | 70 | 0.235 |
| 35 | 0 | 40 | 40 | 80 | 70 | 0.209 |
| 36 | 30 | 10 | 45.25 | 85.25 | 80 | 0.272 |
| 37 | 20 | 20 | 40 | 80 | 110 | 0.133 |
| 38 | 40 | 0 | 40 | 80 | 110 | 0.150 |

Table A.18 (contd) Data for Figure 5.6. Anisotropy of pyranine in sucrose solutions at different temperature with different amount of fructose and glucose. Brix represents total sugar percent by weight.

| RUN # | Fructose (wt%) | Glucose (wt%) | Sucrose (wt%) | BRIX | Temperature (°C) | Anisotropy r |
|---|---|---|---|---|---|---|
| 39 | 0 | 40 | 47 | 87 | 70 | 0.275 |
| 40 | 0 | 40 | 47 | 87 | 110 | 0.194 |
| 41 | 0 | 40 | 43.5 | 83.5 | 110 | 0.143 |
| 42 | 40 | 0 | 40 | 80 | 70 | 0.256 |
| 43 | 40 | 0 | 40 | 80 | 70 | 0.254 |
| 44 | 0 | 40 | 47 | 87 | 70 | 0.274 |
| 45 | 20 | 20 | 43.5 | 83.5 | 110 | 0.164 |
| 46 | 20 | 20 | 47 | 87 | 70 | 0.304 |
| 47 | 0 | 40 | 43.5 | 83.5 | 70 | 0.244 |
| 48 | 0 | 40 | 40 | 80 | 90 | 0.160 |
| 49 | 40 | 0 | 40 | 80 | 70 | 0.265 |
| 50 | 40 | 0 | 43.5 | 83.5 | 110 | 0.185 |
| 51 | 40 | 0 | 43.5 | 83.5 | 110 | 0.185 |
| 52 | 0 | 40 | 43.5 | 83.5 | 90 | 0.211 |
| 53 | 40 | 0 | 43.5 | 83.5 | 90 | 0.242 |
| 54 | 40 | 0 | 40 | 80 | 110 | 0.148 |
| 55 | 40 | 0 | 47 | 87 | 70 | 0.326 |
| 56 | 40 | 0 | 40 | 80 | 110 | 0.145 |
| 57 | 40 | 0 | 47 | 87 | 110 | 0.233 |
| 58 | 20 | 20 | 47 | 87 | 110 | 0.204 |
| 59 | 0 | 40 | 40 | 80 | 70 | 0.206 |
| 60 | 40 | 0 | 47 | 87 | 110 | 0.225 |